Microneedles for painless transdermal immunotherapeutic applications

Hamed Amani, Mohammad-Ali Shahbazi, Carmine D'Amico, Flavia Fontana, Samin Abbaszadeh, Hélder A. Santos

PII: S0168-3659(20)30743-4

DOI: https://doi.org/10.1016/j.jconrel.2020.12.019

Reference: COREL 10717

To appear in: *Journal of Controlled Release*

Received date: 27 September 2020

Revised date: 11 December 2020

Accepted date: 14 December 2020

Please cite this article as: H. Amani, M.-A. Shahbazi, C. D'Amico, et al., Microneedles for painless transdermal immunotherapeutic applications, *Journal of Controlled Release* (2020), https://doi.org/10.1016/j.jconrel.2020.12.019

Microneedles for Painless Transdermal Immunotherapeutic Applications

Hamed Amani[a,b], Mohammad-Ali Shahbazi[a,c]*, Carmine D'Amico[a], Flavia Fontana[a], Samin Abbaszadeh[d] and Hélder A. Santos[a,e]*

[a] Drug Research Program, Division of Pharmaceutical Chemistry and Technology, Faculty of Pharmacy, University of Helsinki, Helsinki FI-00014, Finland

[b] Department of Medical Nanotechnology, Faculty of Advanced Technologies in Medicine, Iran University of Medical Science, Tehran, Iran

[c] Zanjan Pharmaceutical Nanotechnology Research Center (ZPNRC), Zanjan University of Medical Sciences, 45139-56184 Zanjan, Iran

[d] Department of Pharmacology, School of Medicine, Zanjan University of Medical Sciences, Zanjan, Iran

[e] Helsinki Institute of Life Science (HiLIFE), University of Helsinki, FI-00014 Helsinki, Finland.

Correspondence to:

m.a.shahbazi@helsinki.fi, helder.santos@helsinki.fi

Keywords: Microneedles; Cancer therapy; Vaccination; Autoimmune disease; Allergy; Infection

Abstract

Immunotherapy has recently garnered plenty of attention to improve the clinical outcomes in the treatment of various diseases. However, owing to the dynamic nature of the immune system, this approach has often been challenged by concerns regarding the lack of adequate long-term responses in patients. The development of microneedles (MNs) has resulted in the improvement and expansion of immuno-reprogramming strategies due to the housing of high accumulation of dendritic cells, macrophages, lymphocytes, and mast cells in the dermis layer of the skin. In addition, MNs possess many outstanding properties, such as the ability for the painless traverse of the stratum corneum, minimal invasiveness, facile fabrication, excellent biocompatibility, convenient administration, and bypassing first-pass metabolism that allows direct translocation of therapeutics into the systematic circulation. These advantages make MNs excellent candidates for the delivery of immunological biomolecules to the dermal antigen-presenting cells in the skin with the aim of vaccinating or treating different diseases, such as cancer and autoimmune disorders, with minimal invasiveness and side effects. This review discusses the recent advances in engineered MNs and tackles limitations relevant to traditional immunotherapy of various hard-to-treat diseases.

1. Introduction

Microneedles (MNs) are needle-like structures with microscale diameter and lengths up to 1 mm that can penetrate into the stratum corneum (10–40 μm in thickness), and enter the epidermis/dermis layers without touching blood vessels and pain-sensing neurons, while the administration is easy enough to avoid the need for professional training [1-3]. Therefore, MNs have garnered great attention for transdermal immunotherapy since they can bypass the stratum corneum layer and directly deliver antibodies, allergens, and therapeutic antigens into the skin, painless and with minimal invasiveness [4, 5]. All types of MNs can promote the delivery of immunostimulatory or immunosuppressive payloads into the immune cell-rich microenvironment of the dermis layer [6, 7], while controlling the dosage and improving the consistency of therapeutic response is achievable [8-11].

Immunotherapy has been proposed as a promising strategy to manage or fight different diseases through the activation or suppression of the patient's immune system [12]. The controlled modulation of the immune system is an important issue that should be taken into account during the design of novel immune-formulations, in order to achieve desired therapeutic effects without off-target responses [13]. For example, in the case of cancer and infectious diseases, immunomodulators should activate immune cells and elicit stimulatory responses. In contrast, in the context of allergies, autoimmune disorders, transplantation, and wound healing, immunomodulators are applied to hinder the activation of immune cells in hyperactive biological environments to accelerate treatment or tissue regeneration [14, 15]. Therefore, immunotherapy can be achieved by various approaches, including immune-modifying agents (e.g., cytokines and vaccines), oncolytic viruses, adoptive cell therapy, immune checkpoint inhibitors, etc. [16, 17]. The approaches can be used for either passive therapy, which refers to the use of cytokines,

antibodies, and immune cells in patients to trigger anti-tumor action without generating immunological memory, or active immunotherapy by triggering the immune system of the patient to create a long-lasting antigen-specific response. Nevertheless, there are still significant limitations to overcome, such as off-target toxicity, tissue heterogeneity, and insufficient durability, demonstrating the necessity for further investigations of advanced immunotherapeutic formulations due to the unpredictable efficacy, weak immunogenicity, and reduced tissue infiltration of the current formulations [18]. The successful implementation of immunotherapies and breakthroughs in clinical practice by new techniques and formulations depends on an adequate dose of immunomodulators, suitable delivery technique, and the right location of their infusion [19, 20]. It is well-known that both the antigen type and the route by which antibodies, therapeutic antigens, and allergens are delivered to the desired region strongly influence the resulting immune response [21]. For example, the initiation of a T-helper 2 (Th2)-based immune response against the allergen results in the maintenance or exacerbation of allergic inflammation in patients. In contrast, initiation of a Th1 type immune response against the allergen and viruses might create beneficial effects [22, 23].

In this review, we discuss the recent progress in the development of MNs for immunotherapy of hard-to-treat and chronic diseases to achieve the highest efficiency with minimal side effects. First, we discuss recent advancements of MNs for immunotherapy of cancer, followed by autoimmune diseases, allergies, inflammatory diseases, as well as discussing vaccination against viral and bacterial diseases (Scheme 1). We summarize the outlooks on the trajectory of recent MN developments, highlighting the unanswered challenges and future trends of MNs for immunotherapeutic applications.

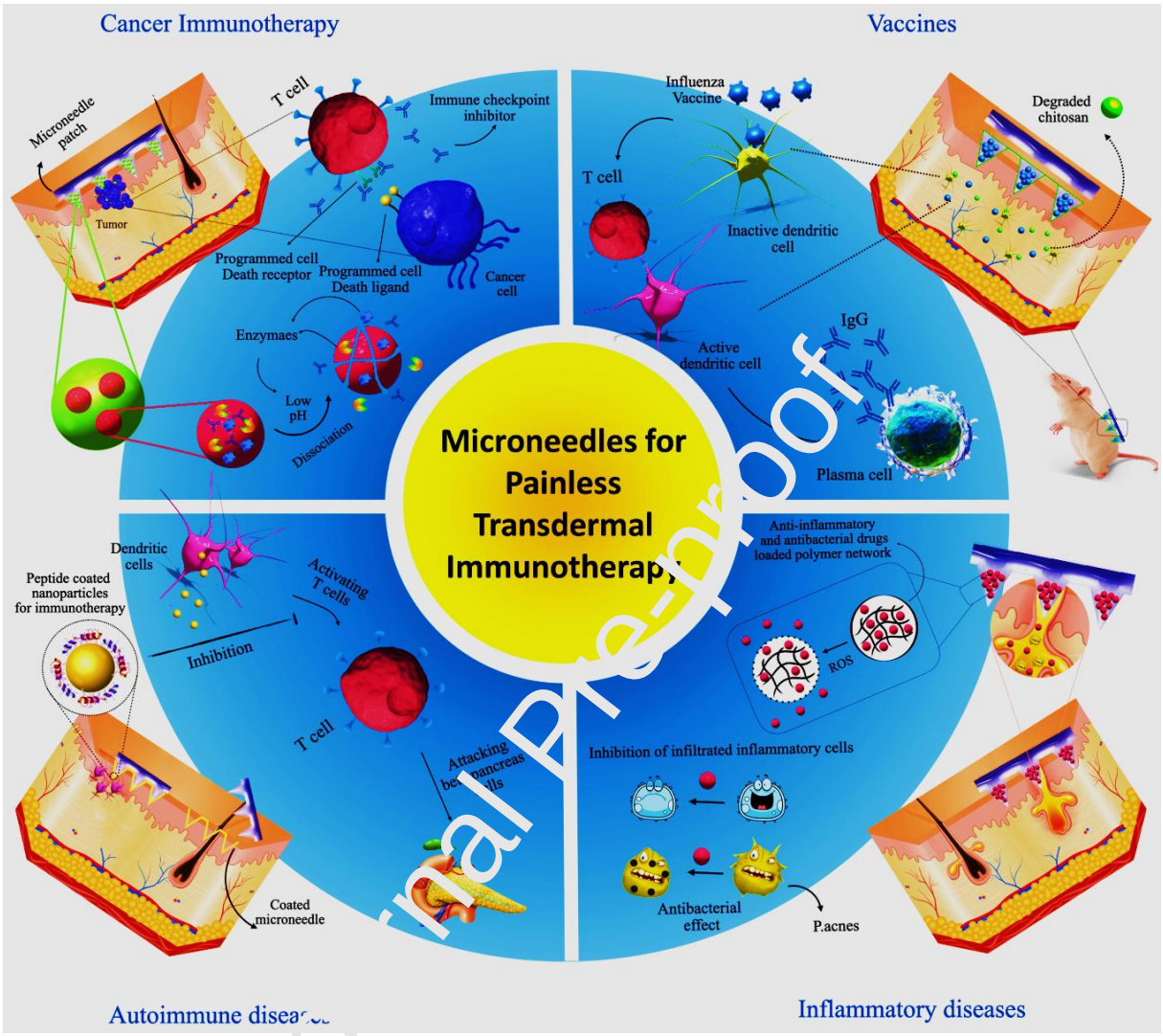

Scheme 1. Different strategies employed by MNs to treat or vaccinate various immune-related diseases.

2. Physicochemical features of materials used in immunotherapeutic MNs

Various types of materials have received substantial attention for MN design to induce programmed immune responses by contributing to sustained release of immunotherapeutic agents, safe transportation of vaccines to the skin, or programmed in situ T cell expansion [24].

Moreover, using biomaterials within the structure of MNs can trigger a series of pathways for recruitment or reprogramming of immune cells, which results in more localized immune responses in comparison with systemic methods [25]. Successful immunotherapy by MNs strongly depends on the physiochemical properties of materials that are used to fabricate these needles. The most common materials include silicon [26, 27], metals [28, 29], glasses [30], ceramics [31], and polymers [32], which their mechanical strength, porosity, charge, and molecular weight can highly affect antigen stability, antigen or vaccine loading into the MNs or even control the kinetics of vaccine transportation in vivo [33]. For example, Kathuria *et al*. showed that the dissolution rate of polyvinylpyrrolidone (PVP)-based dissolvable MN patches can be tuned by the incorporation of hydroxypropyl methylcellulose (HPMC) and methylcellulose (MC) with different molecular weights as dissolution modifier [34]. The PVP MNs showed a rapid dissolution profile within 0.75 h, while incorporating HPMC with high molecular weight (K100LV, or K100M) into their structure resulted in dissolution profiles ranging from 2-2.5 h. Likewise, incorporating low molecular weight HPMCs (E3LV, or E15LV) into the structure of the PVP MNs resulted in dissolution time of higher than 16 h.

Moreover, fabrication methods of MNs can strongly affect the cost-effectiveness of immunotherapy. For example, although micromolding is the most common fabrication technique for dissolving MNs, its efficiency for immunotherapy has been often challenged by concerns regarding noticeable antigen wastage in this method and lack of cost-saving for manufacturers [35]. In addition, the selection of a suitable material that contributes to the localization of antigen within the needles is a substantial issue that needs much attention to optimize immunotherapy of various diseases by MNs. For example, Prausnitz et al. improved the localization of active therapeutic molecules to the needles through casting a highly concentrated

polymer solution that was able to increase viscosity or contribute to the incorporation of an air bubble at the base of the MN to hamper diffusion of therapeutic molecules into the backing [36]. A summary of materials used in the structure of MNs towards immunotherapy, as well as a comparison of their advantages and disadvantages, are shown in **Table 1**.

Table 1. A summary of various materials used into the structure of MNs towards immunotherapy, as well as a comparison of their advantages and limitations.

Category	Material	Fabrication methods	Advantages	Limitations	Ref.
Silicon MNs	Silicon	Wet etch technology	- Ability for coating of the viable virus in a dry form around the shaft of needles - Elimination of cold chain storage	----	[37]
	Silicon	Wet etch technology	- Successful delivery of liquid vaccinia virus Ankara (MVA) vaccine - Eliminating the skin inflammatory response	-----	[38]
	Silicon	Wet etch technology	Decreasing the anti-vector antibody response	------	[39]
	Silicon	-Photolithography -Thin-film deposition - Microelectromechanical systems (MEMS)	Easily fabrication using existing MEMS technologies	Easy breaking and subsequent creation of biohazardous waste	[40]
	Silicon	-----	- Capability of surface decoration of silicon with pH-sensitive groups towards burst release of antigen within 15s	Suitability for delivering only ovalbumin (OVA) antigen (no for all the antigens)	[41]
	Silicon	------	------	-Lack of FDA approval for silicon - Requiring extensive processing and clean-room facilities for fabricating silicon MNs	[42]
Metal MNs	- Stainless steel - Titanium	- Micromachining - Laser ablation -Photochemical etching	Adequate mechanical strength for penetration into the skin	Possibility of creating a potential biohazardous waste	[40]
	Stainless steel	----------	Capability for creating the nano-patterning on the surface of stainless MNs	Poor coating efficiency of DNA-based immunotherapeutic agents owing to low hydrophilic nature of stainless steel	[43]
	Stainless steel	Laser cutting	Cost-effective and FDA approval for stainless MNs	-----	[44]

	Titanium	Lithographic masking followed by wet etching	Facile adsorption of Vaccine to the titanium surface via electrostatic/hydrophobic interactions due to high dielectric constant (ε ~ 114) and isoelectric point (3.5–6.7) of titanium oxide	------	[45]
Ceramic MNs	Alpha calcium sulfate hemihydrate	Micromolding process	Higher mechanical strength and better stability at high temperature and humidity than most polymeric MNs	Possibility of contamination during production and risk of microbial spoilage	[46]
	- β-Tricalcium phosphate ($Ca_3(PO_4)_2$) - Monocalcium phosphate monohydrate ($Ca(H_2PO_4)_2 \cdot H_2O$) - Calcium sulfate alpha hemihydrates ($CaSO_4 \cdot 0.5H_2O$)	Micromolding process	Capability for controlling drug release by changing the bulk surface area, porosity and resorbability of the ceramics	Low drug loading capability	[47]
	Al_2O_3	Micromolding process	Capability for creating nanoporous MNs for both delivery of substances, and the extraction of compounds	----	[48]
	- Alumina - Alpha calcium sulfate hemihydrate	- Micromolding process - Sintering technique	- Good in vivo resorbability (micromolding process) - Adjustable porosity	Non-resorbability of sintered ceramic MNs	[49]
	Alumina	- Sintering technique	good mechanical strength in comparison with monocrystalline silicon	Poor loading efficiency for thermo-labile medications into sintered ceramic MNs due to the high temperature treatment during the fabrication process	[50]
	polyvinylpyrrolidone (PVP)	Soft lithography	Highly water solubility, high tensile strength, and FDA approval of PVP	-----	[51]
	PVP	Micromolding process	safely clearance of PVP via the kidneys within a few days	----	[52]
	PVP	Micromolding process	Low likelihood of RNase contamination of PVP	-Poor solubility of mRNA vaccine in	[53]

				concentrated PVP solutions - Inhibitory effect of concentrated PVP solutions on mRNA transfection due to steric hindrance.	
	PVP	In situ micromolding process	Good mechanical strength of PVP due to the presence of a ring in the chemical backbone structure of the vinyl pyrrolidone monomer		[32]
dissolvable Polymeric MNs	PVP	Micromolding process	-----	Possibility for the DNA vaccine degradation in PVP matrices	[54]
	PVP/ dextran	two-step molding process	the adjuvant effects of PVP and dextran	-----	[55]
	hyaluronan	Micromolding process	FDA approval and biodegradability of hyaluronan	Possibility for insoluble particle formation and entrapment of vaccine antigens into them during MN preparation	[56]
	chitosan	Micromolding process	- Excellent biodegradability - Noncytotoxicity - Ability of chitosan for improving both humoral and cell-mediated immune responses - creating an antigen depot by the viscous chitosan solution	- Requiring supporting arrays for insertion owing to weak mechanical strength of chitosan	[57]
	Gantrez	Micromolding process	Highly water solubility and biodegradability of Gantrez	----	[58]
	Trehalose and sodium carboxymethyl cellulose (CMC)	Theraject's microneedle technology	-------	The difficulty of analysis of the samples by single radial immunodiffusion (SRID) with increasing the viscosity of Trehalose and sodium carboxymethyl cellulose	[59]
	Trehalose and CMC		- FDA approval for both trehalose and CMC - Increasing antigen stability by trehalose - water-solubility and mechanical strength of CMC	-------	[60]

	CMC and amylopectin	Micromolding process	---	Producing deformed microneedles with weak mechanical strength at high viscosity of CMC	[61]
	Sodium Alginate	Micromold casting technique	- Adjuvant properties of sodium alginate - Good biocompatibility and biodegradability - Utilizing sodium alginate as a permeation enhancer	----	[62]
	Sodium Alginate	Spin-casting approach	----	Less physical robustness than biodegradable polylactic-co-glycolic acid MN	[63]
	Silk fibroin /poly(acrylic acid)	Micromolding process	- Good Biocompatibility and Biodegradability of silk fibroin - Simple one-step process for loading antigens in silk protein matrices - Facile stabilization of immunotherapeutic agents and vaccines in silk at room temperature for more than two months - Rapid dissolution of PPA in the skin - Sustained vaccine release from silk protein matrices (over 1–2 weeks)	- The high brittleness of silk fibroin	[33]
	poly(lactide-coglycolide) (PLGA)/PPA	Micromolding process	- Rapid dissolution of PPA in the skin - Adjustable sustained release of encapsulated vaccines based on the PLGA molecular weight	- Complexity of the vaccine loading process in PLGA polymer	[64]
	Carboxymethylcellulose and trehalose as coating	Dip-coating	- Improving antigen stability during drying by trehalose disaccharide - Improving the retention of Hemagglutination activity of influenza vaccine after drying by trehalose	Loss of Hemagglutination (HA) activity at high concentrations of CMC (1wt%)	[24]
	Carboxymethylcellulose and trehalose as coating	Dip-coating	---	Increasing trehalose crystallization and vaccine separation from the trehalose crystal matrix during crystallization result in	[65]

				denaturation of antigenic proteins	
Coated MNs	Carboxymethylcellulose and trehalose as coating	Dip-coating	Reducing virus aggregation at 3% concentration of trehalose	Reduced delivery efficiency of the inactivated virus at a high concentration of trehalose	[66]
	Poly(o-nitrobenzyl-methacrylate-comethylmethacrylate-copoly(ethylene-glycol)-methacrylate) (PNMP)/ polyelectrolyte multilayers as coating	Layer by layer assembly	- Ability for the preparation of bioresponsive MNs due to photo-sensitive and pH-responsive properties of PNMP polymer - Delivery of antigens in a sustained manner after photoswitching PNMP polymer through ultraviolet irradiation (254 nm, 2.25 mW cm^{-2}) for 15 min during coating	The need for reformulation of vaccine components for their coating	[67]

3. Trend of material development in the clinical trials of MN technology

MNs are still under development for the translation of immunotherapeutic molecules into the clinical trial phase. The solid and hollow MNs fabricated from silicon and metals have dominated the clinical trial setup for transportation of immunotherapeutic molecules [68, 69]. Although coated silicon MNs were used for the first time to create immunization, most of MNs in clinical trial have polymeric structure [2]. It has been reported that Soluvia™ microinjection system and MicronJet™, hollow MNs device made of silicon, are the two most widely used MN devices for intradermal vaccine delivery in clinical trials [2]. In a clinical trial study by Icardi *et al*., intradermal vaccine delivery using Soluvia™ microinjection system in children, adults <60 years, and elderly people demonstrated well tolerability without safety issues [70]. Likewise, using MicronJet™ for the delivery of inactivated polio vaccine (IPV) to in 6–14 week-old infants demonstrated promising outcomes [71]. A 60% reduction in the standard IPV dose without

decreasing in antibody titers was found after using MicronJetTM injection in human immunodeficiency virus (HIV)-infected patients compared to intramuscular (IM) injection [72]. Although above-mentioned studies show that silicon or metal MNs might possess beneficial effects on clinical trial outcomes, their clinical translation has been often challenged by concerns regarding lack of FDA approval for silicon and producing biohazardous sharp wastes by metals [73]. Currently, polymers are accelerating into the clinic for MN fabrication due to increasing interest in biocompatible systems [74]. Phase 1 of the clinical trial studies have shown that using biocompatible and dissolvable polymeric MNs for influenza vaccination was well tolerated and generated robust antibody responses compared to IM injection [75]. Hirobe *et al*. reported that using a self-dissolving MN (MicroHyala; MH) made of hyaluronic acid (HA) and collagen in 20 healthy volunteers enrolled in a clinical study effectively increased antibody titer in comparison with transcutaneous immunization (TCI) without any severe adverse reactions [76][77]. Likewise, a clinical trials study showed that dissolvable polymeric MNs composed of 50% (w/w) polyvinyl alcohol (molecular weight 31 kDa) and 50% (w/w) sucrose did not create pain or swelling in the skin, and only mild erythema localized to the injection site was found after administration [78]. Considering the above examples, we estimate that in the near future we will observe a high interest in the design and fabrication of biocompatible and dissolvable polymeric MN systems for immunotherapeutic applications.

4. Cancer immunotherapy by MN patches

Various types of MNs, including solid removable, coated, dissolving, hollow, and hydrogel-forming ones, have been proposed (Figure 1) [9, 79], in order to overcome the challenges and

drawbacks of cancer immunotherapy by other approaches that have hindered their clinical translation.

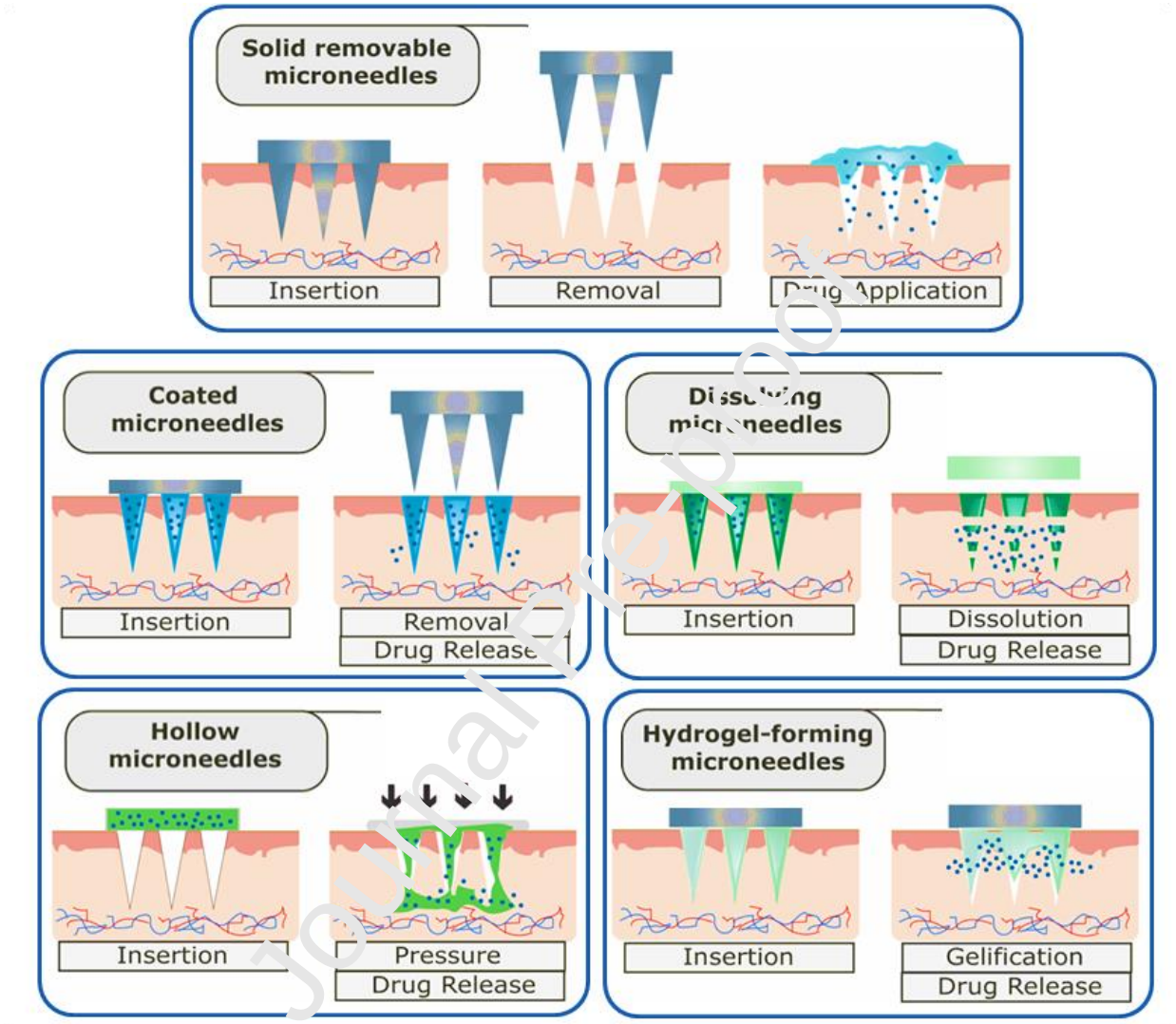

Figure 1. Different types of MNs used for the delivery of immunotherapeutic agents and mechanisms of action for the controlled release of payloads. Solid MNs: immunotherapeutic agents are able to pass via the micro-channels created by MN. Coated MNs: immunotherapeutic agents are able to mix with interstitial fluids and then their delivery occurs through diffusion. Dissolving MNs: dissolution and diffusion of immunotherapeutic agents occur into the body along with other components within the structure of MNs. Hollow MNs: immunotherapeutic agents are able to pass through the MNs. Hydrogel-forming MNs: immunotherapeutic agents are able to diffuse into the body after insertion and the swelling of MNs. Adapted with permission from ref.[79]; Copyright 2018, Elsevier B.V.

In general, current limitations include inadequate infiltration of lymphocytes during the evolution of tumoral immune escape, the presence of immune checkpoints in the tumor site, the high cost of immune checkpoint inhibitors, and the possible development of dosage-related autoimmune side effects through off-target binding of therapeutic agents to healthy tissues [80-83]. In this section, the discussion is subdivided based on the biological pathways and biological molecules used for MN-mediated cancer immunotherapy.

4.1. Design of MNs for immune checkpoint inhibition

Tumor cells possess several mechanisms to conceal themselves as "healthy cells" and prevent their detection and digestion by the immune system. These mechanisms have been summarized in the review by Liu et al.[84]. Although immune checkpoint molecules display powerful roles in the prevention of autoimmunity and tissue damage following the immune reaction in the pathogenic infection, dysregulating their expression in cancer tissue results in innate- and adaptive immune resistance of tumor [85]. Generally, the programmed cell death protein 1 (PD1), indoleamine 2,3-dioxygenase (IDO), and the cytotoxic T-lymphocyte-associated antigen 4 (CTLA4) are the three most important immune checkpoint molecules that are involved in the regulation of T-cell function and are extensively used to modulate antitumor immunity [86].

4.1.1. Design of MNs for cancer immunotherapy by IDO blockade

IDO is an enzyme with the ability to degrade essential amino acid, tryptophan, in an independent process of normal tryptophan homeostasis. IDO is highly expressed in both tumor cells and stromal cells and contributes to the establishment of peripheral tolerance to tumor antigens. IDO give power to tumor cells to escape from T-cell-dependent immune attack and improve tumor

survival and outgrowth through the creation of pathogenic inflammatory states [87]. Although photothermal therapy (PTT) has been reported to be a promising approach for the treatment of metastatic tumors through alteration of immune response with the help of releasing neoantigens and damage-associated molecular patterns, the upregulation of IDO by mild heating limits effective immunotherapeutic outcome. PTT can increase interferon-γ (IFN-γ) secretion and subsequently enhance the IDO expression in tumor cells and antigen-presenting cells (APCs) [88]. High expression levels of IDO suppresses APCs activation and decline their antigen-presenting efficacy [89]. IDO is able to catalyze the degradation of tryptophan into kynurenine, which, in turn, gives rise to impairment of $CD8^+$ T cells activation and inhibition of their antitumor ability via increased activity of regulatory T cells (Tregs) [90, 91]. To address these limitations of PPT, Chen et al. engineered an ingenious core-shell structure MN (CSMNs) array that was able to synergistically boost robust immune response through intralesional co-delivery of a photosensitizer and IDO blocking agent [92]. They loaded 1-methyl-tryptophan (1-MT) into the cross-linked PVP and poly (vinyl alcohol) gel as the MN core and encapsulated photosensitizer indocyanine green into chitosan nanoparticles (ICG-NPs), followed by concentrating on the tip shell of MNs. The in vivo experiments in the lung metastatic tumor model showed that treatment with 1-MT@ICG-NPs-MN+L (laser irradiation) resulted in 1.8-fold higher percentage of $CD8^+$ T cells in the primary tumors than blank group (Figure 2A and 2B). The immunofluorescence staining demonstrated that that treatment with 1-MT@ICG-NPs-MN+L significantly increased the amount of $CD8^+$ T cells in the lung slices whereas markedly reduced the expressions of IFN-γ in the metastatic nodules compared to the blank group (Figure 2C and 2D). Likewise, H&E staining and terminal deoxynucleotidyl transferase dUTP nick-end labeling staining demonstrated that apoptosis and proliferation inhibition of the cancer cells were

higher in 1-MT@ICG-NPs-MN+L group as compared to other groups (Figure 2E and 2F). Immunohistochemistry staining further confirmed that the anti-metastatic effect of 1-MT@ICG-NPs-MN+L was associated with significantly reduced levels of IDO enzyme compared to other groups (Figure 2G). Generally, the results of this study showed that 1-MT@ICG-NPs-MN+L could exert good anti-metastatic effect through the activation of robust immune response in the tumor microenvironment (TME) using synergistic immunotherapy.

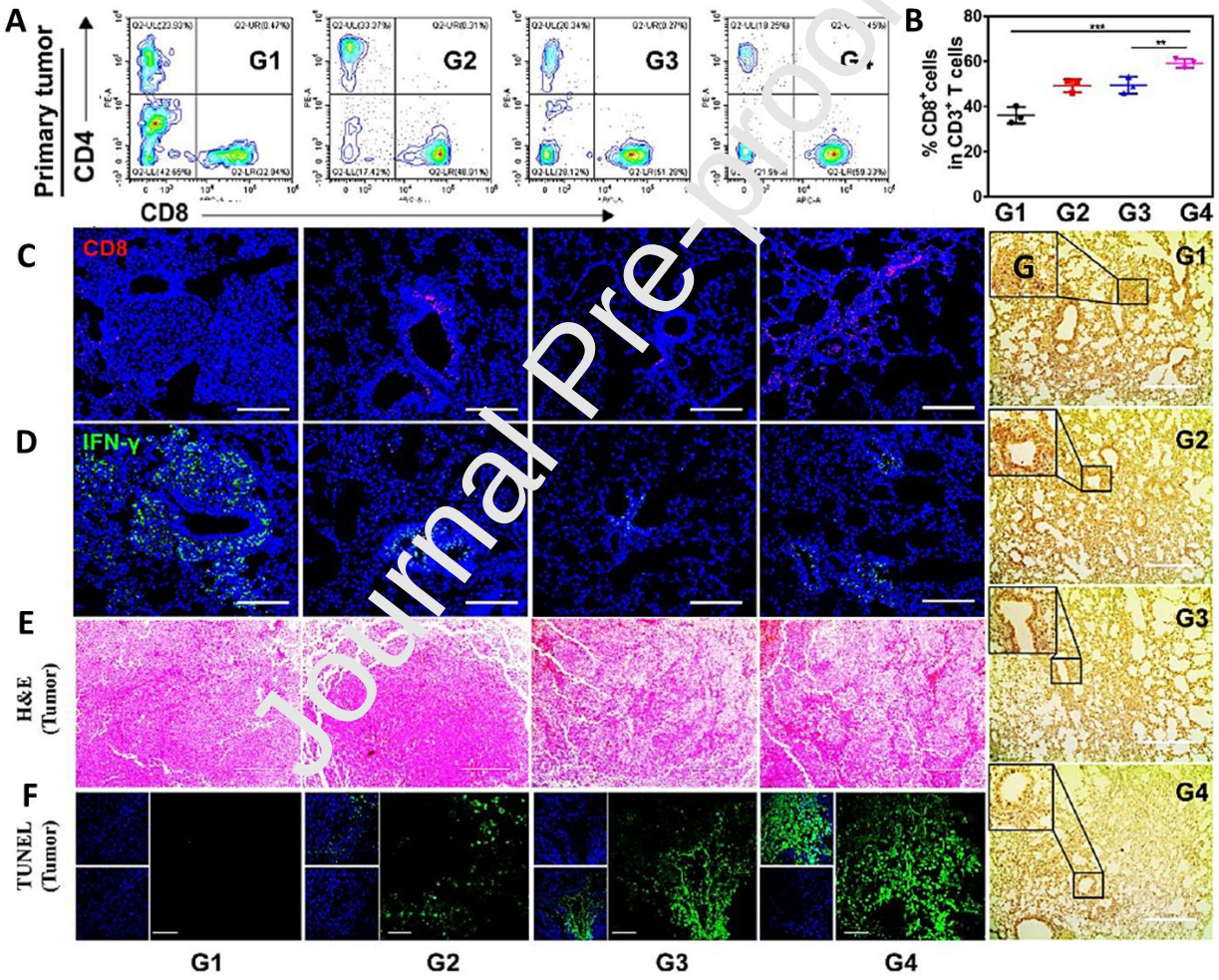

Figure 2. The immune response of CSMNs on a lung metastatic B16 tumor model. **A)** Flow cytometric assay of $CD4^+$ and $CD8^+$ T cell infiltration in primary tumors. **B)** Quantitative analysis of $CD8^+$ T cell infiltration in primary tumors. Immunofluorescence staining of **C)** $CD8^+$ T cells (red) and **D)** IFN-γ (green) in metastatic lung nodules. **E)** Histological assessment of primary tumors (Scale bar: 400 μm). **F)** TUNEL staining of the primary tumors (Scale bar: 50 μm). **G)** Immunohistochemistry staining for evaluation of IDO expression in the metastatic lung

nodules of the B16 tumors after various treatments (Scale bar: 200 μm). (G1) Blank, (G2) 1-MT-MN, (G3) ICG-NPs-MN+L, (G4) 1-MT@ICG-NPs-MN+L. L= (laser irradiation) in G3 and G4 groups (* P<0.05, ** P<0.01, *** P<0.001). Reproduced with permission from ref.[92]; Copyright 2020, American Chemical Society.

4.1.2. Design of MNs for cancer immunotherapy by PD-L1 blockade

The interplay between programmed cell death receptor 1 (PD-1), present on the surface of activated anti-tumor cytotoxic T-cells, and PD ligand one (PD-L1), found on the surface of tumor cells, results in facilitating tumor immune escape. Indeed, the interaction between PD-1 and PD-L1 results in the initiation of apoptosis in the tumor-specific cytotoxic T-cell, annealing their antitumoral immune effects [93-95]. Immune checkpoint inhibitors against PD-1, such as nivolumab, are routinely employed for the treatment of metastatic melanoma [96]. Nevertheless, as an expensive therapeutic option, this drug cannot bring optimal results in up to 80% of patients due to the presence or development of resistance mechanisms or the instauration of off-site immunotoxicity derived from the systemic administration of the medicines [96, 97]. To address these limitations, a biodegradable MN was designed to target the PD-1 pathway by delivering a checkpoint blockade antibody against melanoma locally in the TME [98]. In this study, Wang et al. embedded the anti-PD-1 antibodies (aPD1) and glucose oxidase (GOx)/catalase (CAT) enzymatic system within pH-sensitive nanoparticles composed of ketal modified dextran and then loaded it into HA-based MNs (Figure 3A and 3B) [98]. Various microscopic methods (scanning electron microscope (SEM) and fluorescence) confirmed the distribution of the loaded pH-sensitive NPs at the tips of the MNs (Figure 3C–3E). In vivo experiments demonstrated that the MNs were capable of penetrating the TME to a depth of approximately 200 μm (Figure 3F–3H). The MN patch used in this study showed a sustained release profile and improved retention of aPD1 into the TME. The release profile was modulated

by the CAT enzymatic system: the enzymes convert glucose into gluconic acid, decreasing the pH in their immediate surrounding, dissolving the NPs and releasing the antibody. The MN patch elicited a robust immune response against B16F10 mouse melanoma in comparison to free aPD1, completely eradicating the tumors in some of the animals treated. Their results showed that treatment with this aPD1 patch resulted in the survival of 40% of mice after 40 days, while all the mice treated with free aPD1 or a MN patch without the CAT enzyme died within 30 days after treatment due to tumor relapsing.

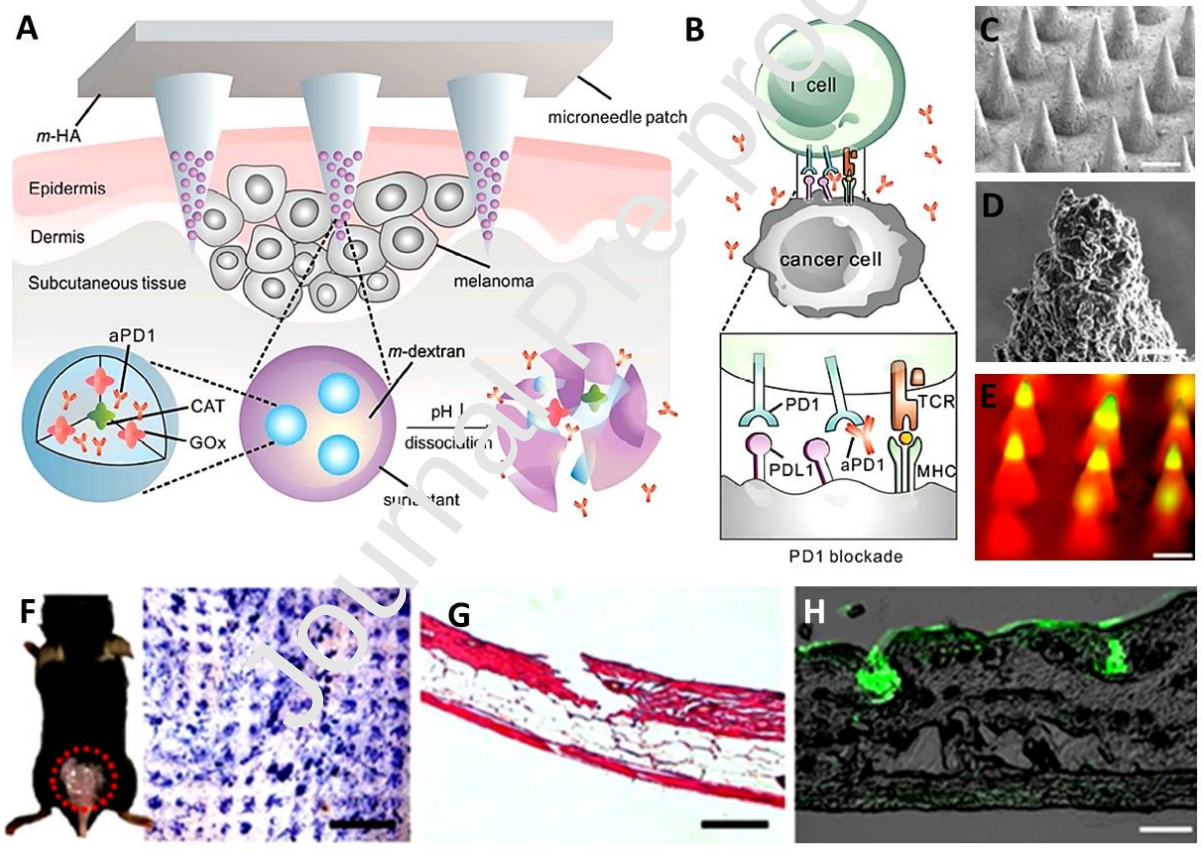

Figure 3. Innovative self-degradable MN patch for the sustained and smart release of aPD1 towards cancer immunotherapy in a B16F10 mouse melanoma model. **A)** Schematic depiction of HA-based MNs loaded with pH-sensitive NPs (ketal modified dextran containing aPD1/GOx/CAT) and the fate of NPs at the tumor site after insertion into the skin. The release of aPD1 was based on the enzyme-mediated conversion of blood glucose to gluconic acid and subsequent gradual dissociation of NPs. **B)** The blockade of PD-1 by aPD1 and subsequent activation of the immune system to fight skin tumor cells. **C)** SEM image of a MN patch (scale bar 200 μm). **D)** SEM images at a higher magnification that confirmed the loading of pH-

sensitive NPs into MNs (scale bar 5 μm). **E**) Fluorescence imaging of MNs containing FITC-antibody loaded NPs (scale bar 200 μm). **F)** Desired region for the insertion of MNs on the mouse skin (red dashed line) and proof of effective delivery by trypan blue staining (scale bar 1 mm). **G)** H&E stain of mouse skin region penetrated by MN (scale bar 200 μm). **H)** Merged fluorescence and bright field image demonstrating the presence of FITC-antibody loaded MN in mouse skin after insertion (green: aPD1) (scale bar 200 μm). Reproduced with permission from ref.[98]; Copyright 2016, American Chemical Society.

In another study, a transdermal hollow structured MN array (MNA) patch was designed to enable cold atmospheric plasma (CAP)-mediated aPD-L1 therapy [99]. The application of CAP improved the transportation of the payload into the TME by the MN patch. Furthermore, CAP was channeled to the tumor, inducing the death of cancer cells and the release of tumor-associated antigens, which resulted in the significant maturation of dendritic cells (DCs) and presentation of the antigens to T-cells in the draining lymph nodes. The release of tumor-associated antigens combined with the simultaneous release of aPD-L1 antibody controlled the tumor growth in both primary tumors and distant tumors, demonstrating the effective priming of a systemic antitumoral immune response. Since the therapeutic potential of various approaches might be undermined due to the diversity, complexity, and heterogeneity of tumors, MNs can provide a paradigm shift for combination therapy to enhance treatment efficacy [100]. For example, Yanqi et al. developed a transcutaneous delivery platform for aPD1. The technology combined nanocapsules of HA modified with 1-MT, an inhibitor of IDO, embedded within MNs [101]. The IDO enzyme is responsible for maintaining DCs in an immature state, suppressing antigen-specific T cell proliferation by increasing their sensitivity to apoptosis [102]. Furthermore, this enzyme has been correlated with an increased number of anti-inflammatory Tregs [103]. The TME is characterized by the overexpression of hyaluronidase, which controls the release of aPD1 through the enzymatic digestion of HA-based MNs. In vivo experiments on a B16.F10 mouse model of melanoma showed that the MNs induced a significant increase in the amount of T-cell, and, in particular, in $CD8^+$ cytotoxic T-cells, while reducing the number of

Tregs in the TME. However, the authors did not evaluate whether the increased presence of cytotoxic T-cells is correlated with an increase in the number of antigen-specific cytotoxic T-cells.

Despite all the advantages of MNs as innovative formulations, they suffer from several disadvantages towards the effective delivery of immune checkpoint inhibitors. The limitations include low drug loading capacity owing to the small volume of their microstructures and the inability of simultaneous multi-drug loading due to the specific interaction of drug-matrix [104, 105]. To overcome some of these disadvantages, Yang et al. fabricated a highly drug-concentrated hybrid core-shell MN (CSMN) system to facilitate the co-delivery of checkpoint inhibitors, 1-MT and aPD-L1, into the TME (Figure 4A and 4B) [106]. The author firstly synthesized the shell of CSMN by pipetting sodium alginate and chitosan solution onto the surface of a polydimethylsiloxane (PDMS) mold, followed by the addition of aPD-L1. In the next step, an aqueous solution containing 25% (w/v) PVP K30 with 15 mg/mL 1-MT and 15% (w/v) PVA was added on the surface of the molds to create the core (Figure 4C). This fabrication method resulted in the concentration of aPD-L1 in the tips of MNs and increased protein loading, which was mainly attributed to electrostatic interactions between polymers and proteins and to hydrogen-bond interaction between 1-MT and the polymeric matrix of MN. The developed patch possessed adequate mechanical strength to penetrate into the corium layer of rat skin to the depth of 700 μm (Figure 4D). In vitro experiments showed a complete release of the cargo and the degradation of chitosan shell after 48 h. Additionally, in vivo experiments in a B16 subcutaneous melanoma mice model demonstrated that the CSMN system better inhibited the tumor growth, owing to the longer local retention time of inhibitors compared to the intra-tumor injection route. The highest infiltration of T lymphocytes, such as cytotoxic T lymphocytes ($CD3^+$ $CD8^+$) was

found in the tumor site of mice treated with the aPD-L1/1-MT CS-CSMN in comparison with blank CS-CSMN control (Figure 4E and 4F).

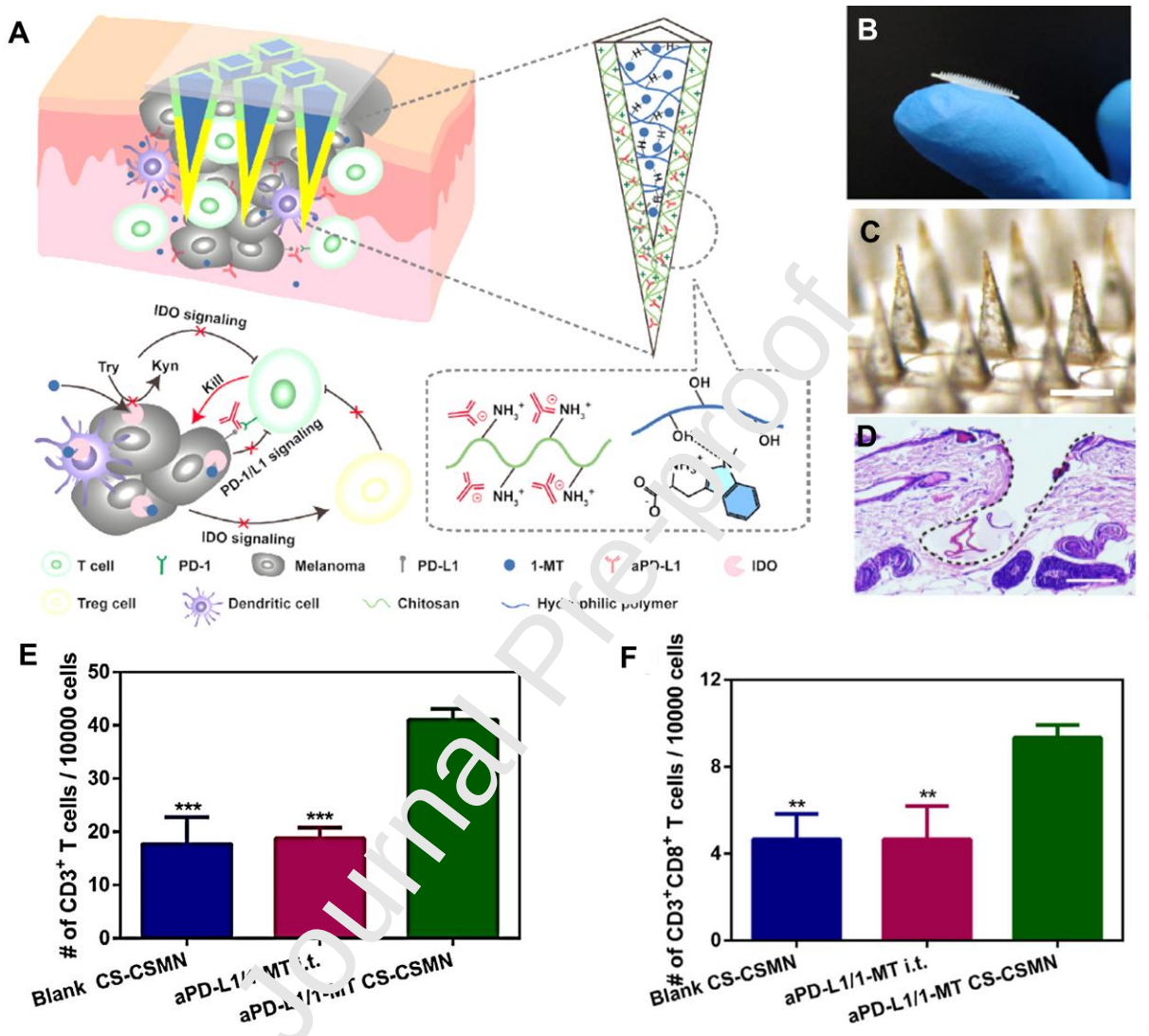

Figure 4. A highly drug-concentrated hybrid CSMN system for co-delivery of checkpoint inhibitors, including 1-MT and aPD-L1 and cancer immunotherapy in a B16 subcutaneous melanoma mice model. **A)** Schematic representation of CSMN-assisted co-delivery of aPD-L1 and 1-MT for the treatment of melanoma. **B)** A representative photograph of the CS-CSMN patch. **C)** Bright-field image of CS-CSMN (scale bar 500 μm). **D)** H&E staining image of rat skin after insertion of CS-CSMN patch (scale bar 100 μm). The numbers of **E)** $CD3^+$ T cells and **F)** $CD3^+$ $CD8^+$ T cells per 10,000 of cells in tumor tissue after the removal of red blood cells at12 days after treatment. Data are expressed as Mean ±SD (n = 3 animals per group). ** P<0.0 and *** P<0.001 *versus* the aPD-L1/1-MT CS-CSMN group. Reproduced with permission from ref.[106]; Copyright 2020, Acta Materialia Inc. Published by Elsevier Ltd.

In another interesting example, Lan *et al*. developed a MN patch loaded with pH-responsive tumor-targeted lipid NPs, which provide the possibility of local delivery of aPD-1 and cisplatin (CDDP) to create a synergistic immuno-chemotherapy [107]. They firstly synthesized the aPD-1/CDDP@NPs using a reverse-phase microemulsion technique. Then, aPD-1/CDDP@NPs were further encapsulated into dissolving MNs made of PVP using the molding method (Figure 5A). Lipid coated NPs were able to facilitate drug release and tumor-targeting. The *in vivo* experiments showed that MN group cause the most notable tumor regression (strongest effect on reducing tumor volume and tumor weight) in comparison with PBS, aPD-1, aPD1 + CDDP, and aPD-1/CDDP@NPs groups (Figure 5B and 5C). Additionally, the authors investigated body weight loss, the blood urea nitrogen (BUN) value, and total immunoglobulin G (IgG) value in the serum to assess the systemic toxicity and side effects of engineered MNs. Their results showed that the BUN values in all the MN patch groups were within the normal range (Figure 5D). Likewise, IgG values were markedly increased in the aPD-1/CDDP@NP MNs group compared to other groups (Figure 5E). Histopathological assessments using H&E staining indicated that the CDDP group and the aPD-1 plus CDDP group exhibited severe toxic tubular necrosis (the glomeruli and Bowman's capsule collapsing), while no evidence of renal damage was seen in mice treated with aPD-1, aPD-1 MNs, and aPD-1/CDDP@NP MNs.

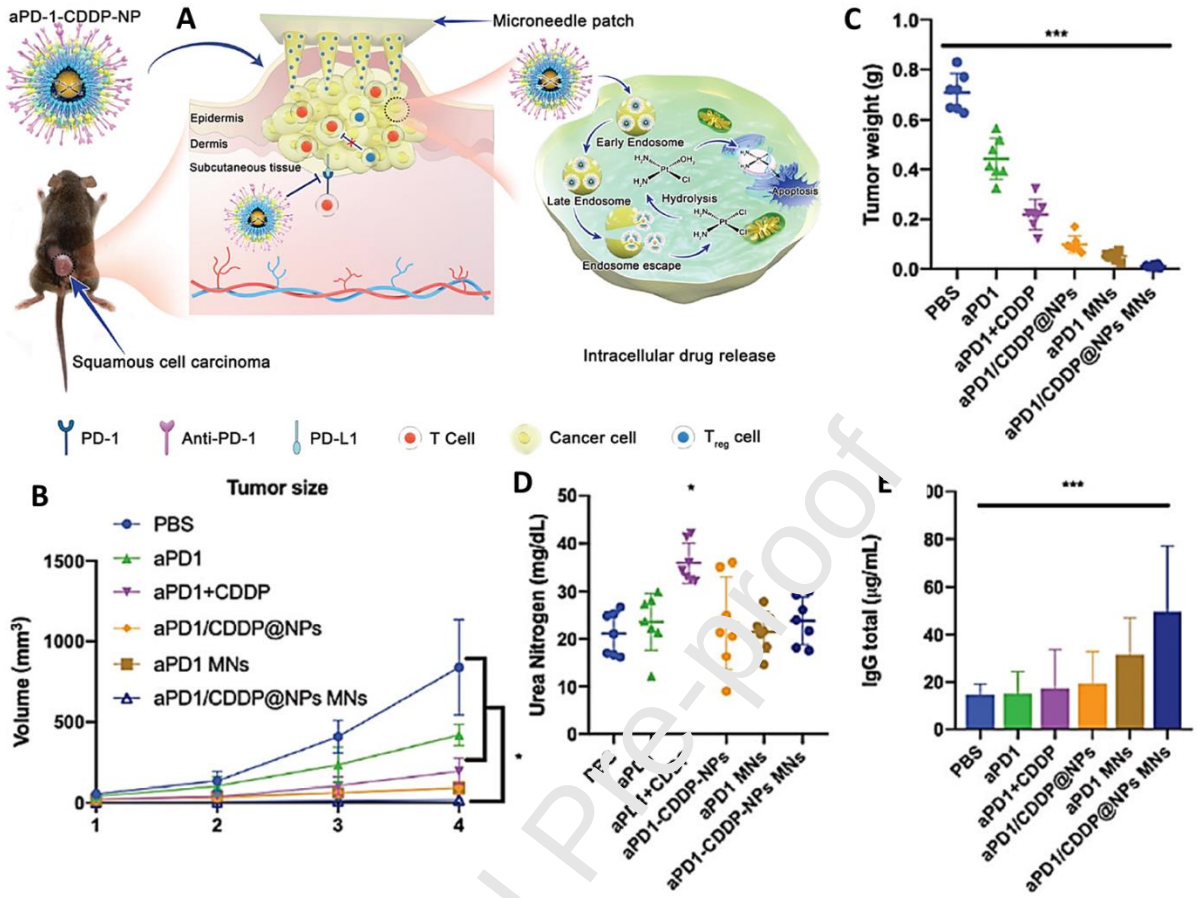

Figure 5. MNs loaded with anti-PD-1–cisplatin NPs for synergistic cancer immunochemotherapy. **A)** Schematic representation of MNs loaded with aPD-1/CDDP@NPs towards synergistic cancer immunochemotherapy. The combination of chemotherapy and immunotherapy was carried out through encapsulation of aPD-1 and CDDP into NPs and then embedding into the MNs. The aPD-1 was able to block the binding of PD-L1 to PD-1 that confers the activation of T-cells whereas intracellular release of CDDP facilitated the death of tumor cells via inducing direct cytotoxicity to them. **B)** Tumor volume and **(C)** tumor weight following sacrifice. When the tumor volume reached 10 mm^3, the treatment of each group was started (Three treatments for each group and lasted for three cycles). The measurements of tumor volume were performed before the treatment and 3 times after the treatment. **D)** The BUN value and **E)** total IgG value in the serum. Data were expressed as ± S.D (n = 7 per group). Statistical analysis was carried out based on the Mann–Whitney U test (P-value: *p < 0.05, ***p < 0.001). Reproduced with permission from ref. [107]; Copyright 2020, The Royal Society of Chemistry.

In another study by Yang *et al*., a rolling MN electrode array (RoMEA) was engineered to inhibit tumor growth in both B16F10 and CT26 xenograft murine models [108]. RoMEA was able to conduct low-voltage and large-area nucleic acid delivery (PD-L1-against siRNA (siPD-L1))

through electroporation without any noticeable damage to the skin (Figure 6A). The MN electrode array contributed to reducing the pulse voltage by penetrating via high-resistance stratum corneum layer. The penetration depth of RoMEA was about 500 μm that was larger than the epidermal skin thickness of mice (200 μm), ensuring MN entrance into subcutaneous tissue. The researchers employed anti-PD-1 monoclonal antibody or CpG oligodeoxynucleotides (CpGODNs) of CpG 2395 (immunoadjuvant) to synergistically improve the antineoplastic effects through blocking PD-L1/PD-1 recognition between tumor cells and T cells and increasing populations of $CD8^+$ T cells and $CD4^+$ T cells. For combination therapy using siPD-L1 and PD-1mAb, the antibody was infused into the tumor after siRNA electroporation to synergistically block PD-1 on lethal T cells (Figure 6B, parts a and b). *In vivo* experiments showed that siPD-L1 without electric pulse stimulation failed to create protective effects and exhibited similar tumor growth and survival profiles to PBS, all mice died within two weeks (Figure 6B, parts c-e). Although treatment with only anti-PD-1 antibody repressed tumor growth and reduced tumor volume, the differences did not reach significant levels, and the survival time was increased to 18 days. The animals treated with siPD-L1 by RoMEA or in combination with anti-PD-1 antibody injection exhibited the highest inhibition of tumor growth, survival profiles, and reducing tumor volume (Figure 6B, parts c-e).

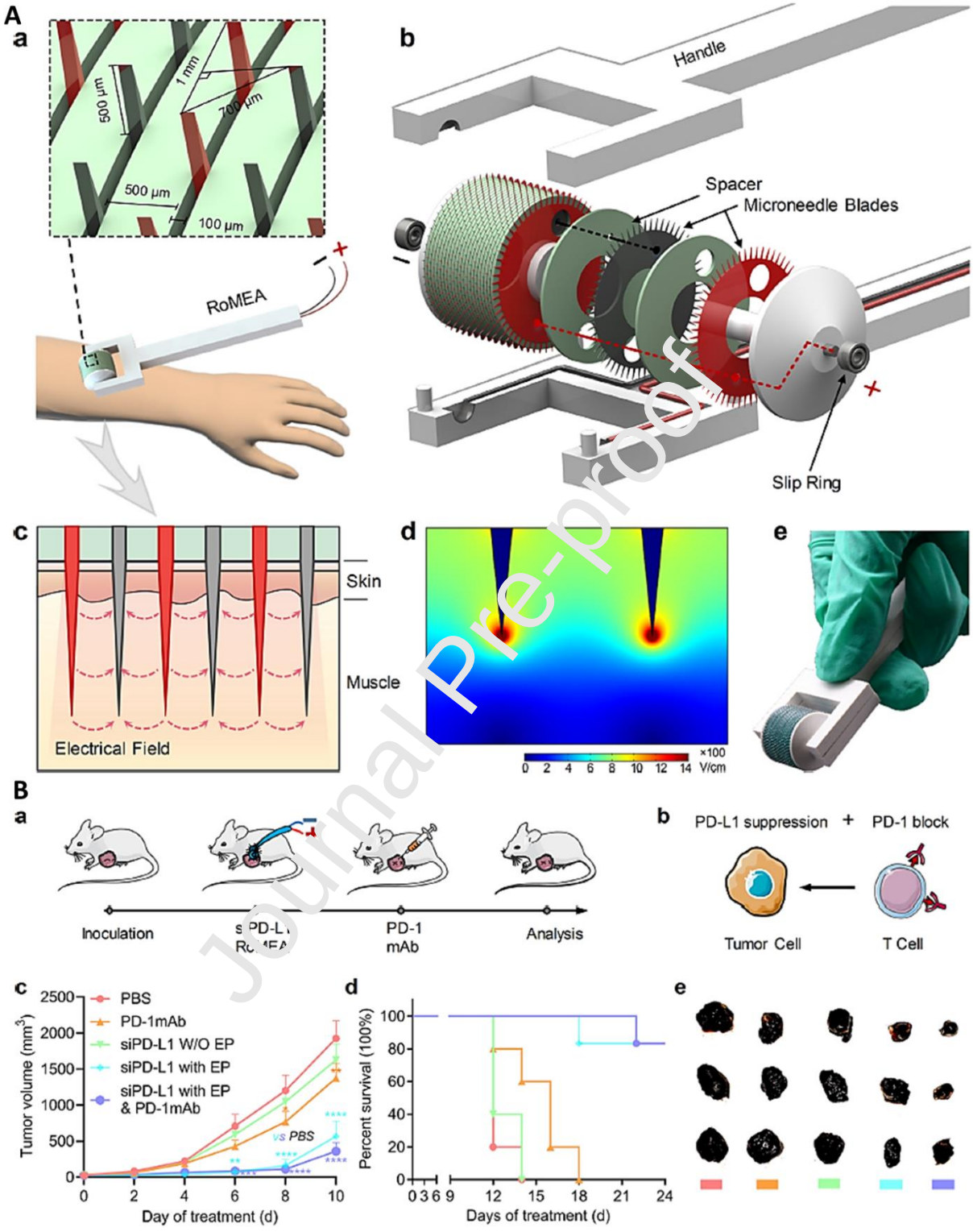

Figure 6. The design of RoMEA MN for combination therapy of tumor through large-area nucleic acid delivery (PD-L1-against siRNA (siPD-L1)) and intratumor injection of PD-1 antibody. **A)** Schematic representation of RoMEA. **(a)** Illustration of minimally invasive RoMEA that creates continuous electroporation in desired tissue. **(b)** The overall design of

RoMEA device that shows the stainless steel 316 parallel circular blades with MN arrays on edge as the electrodes. Two adjacent MN blades connect to the anode (red) and cathode (black), respectively. **(c)** Schematic representation of MN electroporation. **(d)** Simulation of electric field using the RoMEA (50 V). **(e)** The RoMEA prototype in hand. **B)** RoMEA-mediated immunotherapy in the B16F10 model and its effects on tumor growth and survival profiles. (a) Schematic representation of the experiment protocol in a melanoma tumor model in C57BL/6 mice. (b) Conceptual design of combined immunotherapy approach used in this study. (c and d) The tumor growth and survival curves of the mice during the treatment period. (e) Representative optical images of the melanoma tumors excised on day 14 post-treatment. Information about experimental groups: PBS (control without any treatment), PD-1mAb (mice treated with only PD-1mAb), siPD-L1 W/O EP (siPD-L1 without electroporation), siPD-L1 with EP (siPD-L1 electroporated with RoMEA), and siPD-L1 with EP & PD-1mAb (siPD-L1 electroporated with RoMEA plus PD-1 mAb). Data were expressed as the mean ± SEM. * $P < 0.05$; ** $P < 0.01$;*** $P < 0.001$, **** $P < 0.0001$ *vs* the control group. Reproduced with permission from ref.[108]; Copyright 2020, Elsevier B.V.

In 2020, Zhou *et al*. engineered HA MNs loaded with anti-CD40 antibody (DCs targeting antibody) and surface decorated by GMS (monostearin)-conjugated HA transfersomes co-encapsulating poly I:C adjuvant, the tumor associated antigen (tyrosinase-related protein-2), ovalbumin (OVA), and pembrolizumab (anti PD1 antibody) to improve the maturation of DCs and infiltration of effector T cells in tumor-draining lymph node (tdLN) and tumor tissue towards synergistic reinforcement of anti-PD1 immunotherapy (Figure 7A) [109]. The authors monitored intradermal fluorescence intensity to evaluate the distribution of transfersomes (DiI labeled) *in vivo*. The fluorescence distribution was investigated in lymph nodes, hearts, livers, spleens, and kidneys to ascertain tdLNs targeting capacity of transfersomes based nanovaccine- complexed MNs. At 48 h after H-αCD40 T(OVA+PolyI:C)/MNs transdermal administration, the DiI fluorescence appeared at the lymph node and reached the maximum at 96 h, indicating accumulation of the transfersomes in the lymph nodes. Likewise, a gradual increase of the fluorescence intensity was found in livers after 96 h. The highest photon quantum intensity was seen in lymph nodes (~25 × 104/g; 2-fold higher than livers at 96 h). A significant increase in the number of $CD4^+$ T or $CD8^+$ T cells was found in H-αCD40-T(PolyI:C+TAA+αPD1)/MN

compared to blank MNs (Figure 7B and 7C), indicating that the activation of effector T lymphocytes occurred by DCs mediated cascade reactions. Generally, the engineered MNs were able to activate DC maturation and improve Th1 immune responses, which, in turn, resulted in the inhibition of tumor growth and improving survival profiles.

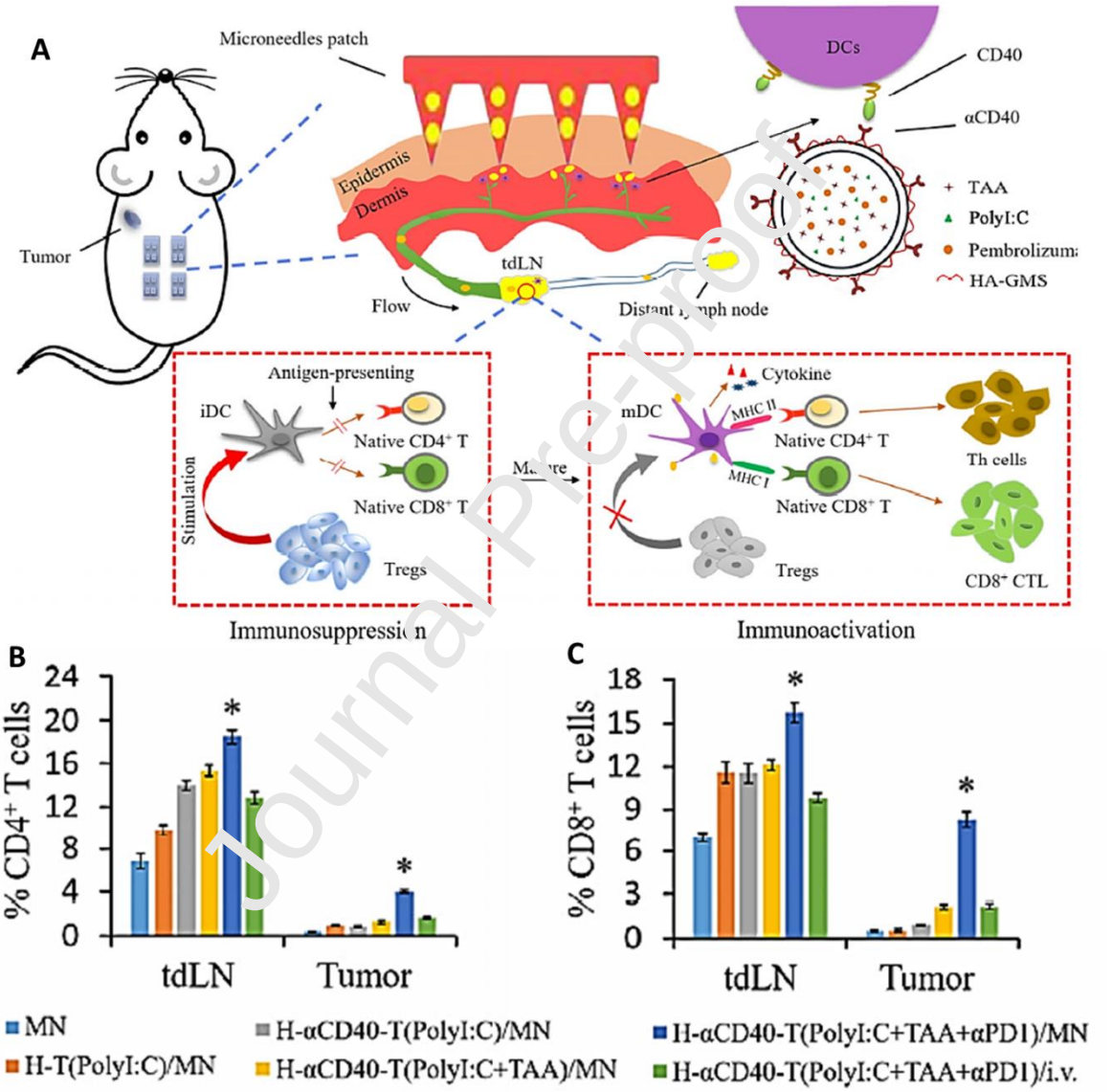

Figure 7. Combined therapy with nanovaccine complexed MNs with pembrolizumab (αPD1) for improving the maturation of DCs and infiltration of effector T cells in tdLN for tumor immunotherapy. **A)** Schematics illustration of modified transfersomes induced immune responses in tdLNs through MNs assisted transdermal immunization. Transdermal delivery resulted in accumulation in tdLN and surface decoration with αCD40 increased cellular uptake by DCs. Uptake of cargo activated DCs maturation and facilitated differentiation of naïve T-cells

into effector T lymphocyte. In the next step, reducing regulatory T lymphocytes conferred reversion of immunosuppressive microenvironment in tdLN into immune activation. **B)** Representative fluorescence images indicating retention of DiI labeled transfersomes in various tissues in vivo at 48, 96, 120, and 168 h after insertion of transfersomes complexed MNs. **C)** and **D**) Flow cytometry assay of the percentages of $CD4^+$ T or $CD8^+$ T cells among all lymph nodes or tumor tissue cells (n = 4). Data are expressed as mean ± SD. *p < 0.05, compared with MN. Reproduced with permission from ref.[109]; Copyright 2020, Springer Nature.

4.1.3. Design of MNs for cancer immunotherapy by CTLA-4 blockade

CTLA-4 is known as a protein receptor that acts as an immune checkpoint. CTLA-4 is expressed on T cells in lymph nodes, and its physiological interaction with APCs results in suppressing the activation of T-cells and the inflammatory response [82, 110]. Antibodies directed against CTLA-4 have been the first treatments in the class of immune checkpoint inhibitors to gain approval for the treatment of melanoma [111]. However, this target is systemically expressed, and the interference with this signal induces the emergence of immune-related side effects [112]. In order to improve the local delivery of anti- CTLA-4 and hinder systemic drug exposure, nanotopography-based MN array (MNA) can be applied. As an example, Kwon et al. designed a nanotopography-based MNA composed of a single-use, 66 mm^2 arrays of 100 MNs of 110 μm diameter, 350 μm long, and with a 30 μm hole located off-center (named SOFUSA^{TM}) to allow the delivery of anti- CTLA-4 into tdLN in an orthotopic mammary carcinoma murine model [113]. Repeated treatment with SOFUSA^{TM} inhibited tumor growth and metastasis development in bone, lymph nodes, and lungs better than the traditional systemic administration, an intraperitoneal administration (IP) of anti-CTLA-4 at 10 mg/kg. Moreover, the authors evaluated the transport of liquid from SOFUSA^{TM} to the brachial lymph nodes by infusing 100 μL/h of indocyanine green (ICG) into the epidermal spaces using near-infrared fluorescence imaging (NIRF). The lymphatic vessels collect the dye and transport it to the lymph nodes.

As mentioned above about cancer immunotherapy by PD-L1 blockade, a single treatment modality might be unable to efficiently treat malignant skin melanoma. To this end, Chen *et al*. designed a physiologically self-degradable MN-assisted platform to combine immunotherapy and photodynamic therapy (PDT) through controlled co-delivery of checkpoint inhibitor anti-CTLA4 antibody (aCTLA4) and photosensitizer (PS) and create synergistic effects against tumors [114]. The hydrophobic (Zinc Phthalocyanine) and hydrophilic agents (aCTLA4) were synchronically encapsulated into the pH-sensitive dextran NPs using a double emulsion water/oil/water (w/o/w) evaporation method. The acetylation of the dextran pendant hydroxyl moiety resulted in the co-loading of hydrophobic photosensitizer/hydrophilic antibodies into the NPs. UV-Vis spectra of co-encapsulated NPs showed an absorption peak around 490 nm that was an indicator of the successful encapsulation of aCTLA4-FITC. Then, the pH-sensitive dextran NPs were embedded into the biocompatible HA MNs. *In vivo* experiments in 4T1 mouse models showed that three-times of MN insertion in combination with laser resulted in sustained tumor inhibition, while other treatment groups failed to create this outcome. The authors stated that the first destroying of partial tumor by PDT resulted in the initiation of the immune response that in turn, facilitated aCTLA4-mediated immunotherapy in the next step. Additionally, preliminary systemic assessments demonstrated that the engineered MNs had favorable safety without causing any systemic immune disorder.

4.2. Design of MNs for the delivery of therapeutic cancer vaccines

4.2.1. MNs for effective delivery of DNA cancer vaccines

Unique properties of DNA vaccine technology, including stability, simplicity, and safety, make them attractive immunotherapeutic approaches to treat cancers [115]. In this technology, the resulting immune responses can be manipulated by designing genes in DNA vaccines to encode immunomodulatory molecules and various antigens [116]. Currently, several research groups loaded DNA vaccines in the MNs to treat various cancers [52, 117, 118].

The poor targeting of APCs and the lack of appropriate adjuvants have been major limitations in the transdermal delivery of a DNA vaccine for cancer immunotherapy [119]. To circumvent these shortcomings, Xu et al. fabricated a MN composed of a DNA vaccine in a polymeric nanocomplex, encapsulating a low concentration of paclitaxel (PTX) [120]. This MN patch was developed as a DC-targeted transdermal strategy for cancer immunotherapy, exploiting low-dose PTX as an adjuvant. They firstly synthesized a DNA plasmid that encodes GM-CSF, a DC chemoattractant cytokine, and a fusion protein of tyrosinase-related protein-2 (Trp-2), as a melanoma tumor antigen. In order to facilitate targeting to the mannose receptors present on DCs, the resulting plasmid was incorporated into a mannosylated N,N,N-trimethyl chitosan (mTMC) solution. At the same time, PTX at a low concentration was encapsulated in sulfobutylether-β-cyclodextrin (SBE), as a solubility enhancer and polyanionic linker. In the next step, ionic interactions between the cationic complex of mTMC/DNA and the negatively charged inclusion complex of PTX/SBE resulted in the creation of the PTX/SBE-mTMC/DNA nanocomplex. This DC-targeted nanocomplex can efficiently improve the maturation of DCs, with an increase in the secretion of IL-12p70. Furthermore, DCs pulsed with the nanocomplex enhance the proliferation of $CD4^+$ and $CD8^+$ T cells, as well as decrease the percentage of immunosuppressive FoxP3+ Tregs. The co-delivery of DNA vaccine, mannosylated chitosan, and PTX as a combination of antigen and adjuvant results in stronger suppression of tumor

growth compared to only DNA vaccine or only mannosylated chitosan/PTX in in vivo experiments in mice. It has been reported that incorporation of pH-responsive copolymers into the structure of MNs can accelerate the release of DNA vaccine in tumor acidic pH microenvironment [121]. Recently, Duong et al. designed and fabricated a smart DNA vaccine delivery system using polycarbonate MNs coated by layer-by-layer (LbL) deposition. The two layers are composed of positively charged ultra-pH-responsive oligo sulfamethazine conjugated poly(β-amino ester urethane) (OSM-(PEG-PAEU)) and a negatively charged immunostimulatory adjuvant, polyriboinosinic:polyribocytidylic (poly(I:C)), at low pH, to facilitate the controlled release of DNA vaccines and adjuvants in the immune cell-rich epidermis/dermis layer of the skin [122]. It was shown that the pH-sensitivity of OSM-(PEG-PAEU) led to the protonation of the copolymer to positively charge at pH 4.0, capable of forming a complex with poly(I:C) and hampering the release of the OVA- expressing plasmid (pOVA) and poly(I:C) from the LbL coated MNs. In addition, the presence of ionized sulfonamide moieties in the OSM oligomers resulted in the deprotonation of OSM-(PEG-PAEU) copolymer at the physiological pH (pH 7.4), resulting into a negative charge and facilitating the release of pOVA and poly(I:C) via electrostatic repulsion. The combined delivery of the DNA vaccine and adjuvant by the LbL coated MNs resulted in the induction of type I interferons followed by the production of antigen-specific antibodies by B cells and the priming of $CD8^+$ T-cell. The antigen-specific $CD8^+$ T-cells induced the production of interferon-gamma (IFN-γ) and enhanced cancer cell death. In vivo experiments showed that the LbL-coated MNs resulted in higher OVA protein expression compared to the group where the plasmid was subcutaneously injected, which may be attributed to the penetration of MNs, of ca. 600 μm height, to the dermis, and the presentation of nanoengineered DNA polyplex to antigen-presenting cells. Compared to soluble DNA vaccine

formulation, implantation of the LbL-coated MNs loaded with pOVA and poly(I:C) in mice caused a threefold increase in IFN-γ positive tumor-infiltrating $CD8^+$ T cells and threefold higher amounts of anti-OVA IgG serum antibody, indicating suitable stimulation of the humoral and cellular immune response. In another study by the same group, an array of dissolving MN was prepared using a bioresorbable polypeptide matrix (mPEG5K–PN2LG30), with nanosized polyplexes composed of pOVA and poly (I:C), which were loaded into high-transfection cationic amphiphilic conjugates (DA3) and added to the polypeptide matrix (Figure 8A) [123]. The positive charge of polyplex improved its uptake by DC 2.4 cells and RAW 264.7 macrophage cells (Figure 8B and 8C) and created a repulsive force on the other cationic copolymers, which resulted in burst release of ca. 85% of poly(I:C) and ca. 97% of pOVA within 5 min of application of the MN. This indicated the suitability of the MNs for future clinical use owing to the short treatment time with improvement of patient convenience. Additionally, the MN dissolved in the interstitial fluids of skin, mainly due to the presence of the polyethylene glycol (PEG) component in its structure. In vivo and in vitro experiments demonstrated the higher expression of OVA in the dissolving MN group compared to control and subcutaneous injection groups (Figure 8D), suggesting that the nanopolyplex can reach APCs, such as DCs and macrophage cells in the epidermis/dermis layers, and can be effectively captured by them. The administration of pOVA through dissolving MNs resulted in higher antibody titer (Figure 8E and 8F) while reducing the number of OVA-expressing metastatic foci through antibody-dependent cellular cytotoxicity (ADCC) activity, prolonging the overall survival compared to traditional vaccination.

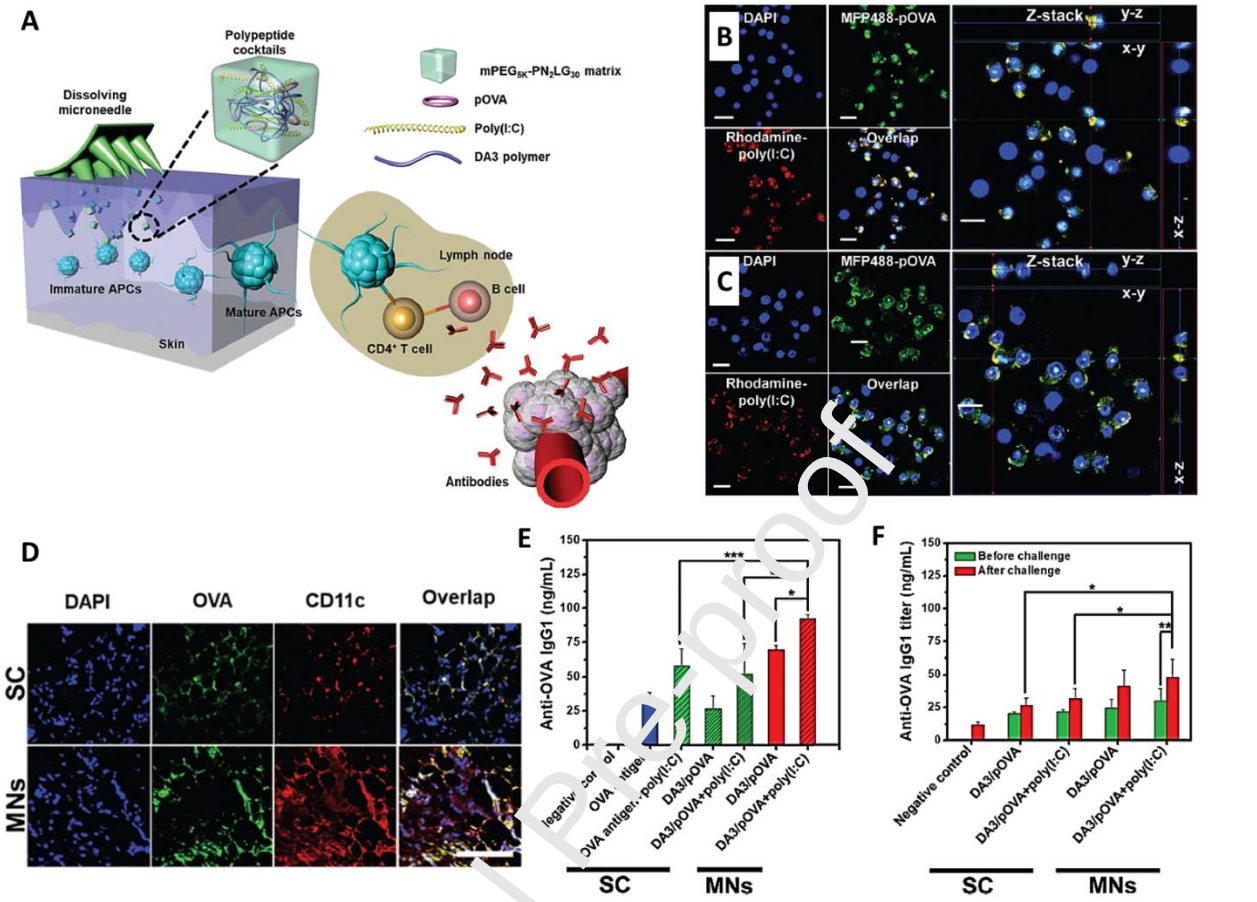

Figure 8. Dissolving MN polypeptide cocktails comprising of cationic nanopolyplex containing ovalbumin-expressing pOVA and poly(I:C) for cancer immunotherapy. **A)** A schematic representation of the proposed anticancer mechanism of dissolving MNs containing mPEG5K–PN2LG30 and the nanopolyplex (DA3 and (pOVA + poly (I:C)). The dissolving MNs interact with mature APCs followed by stimulation of antiOVA antibody production for ADCC of cancer cells. Confocal microscopy images of in vitro cellular uptake of the nanopolyplex released from dMN arrays in **B)** DC 2.4 and **C)** RAW 264.7 cells, respectively. Scale bar = 20 mm. **D)** Double immunohistofluorescence staining showing the *in vivo* OVA protein expression in DCs. **E)** Serum levels of Anti-OVA antibody IgG1 after one week in different experimental groups (*p < 0.05, **p < 0.01, ***p < 0.001, n = 3). Serum levels of Anti-OVA antibody IgG1 were markedly elevated in DA3/(pOVA + poly (I:C) compared to negative control and subcutaneous injection (SC) groups. **F)** Serum levels of Anti-OVA antibody IgG1 before and after challenge with OVA protein (*p < 0.05 and **p < 0.01, n = 5). Serum levels of Anti-OVA antibody IgG1 markedly increased in MNs compared to SC groups after challenge. Reproduced with permission from ref.[123]; Copyright 2020, Royal Society of Chemistry.

4.2.2. MNs for effective delivery of other cancer vaccines

One of the primary objectives of cancer immunotherapy is the establishment of a broad tumor-targeting T cell repertoire that is able to recognize and destroy heterogeneous tumor cell populations. One promising strategy is in situ vaccination that contributes to starting a selective and durable adaptive immune response using the diverse collection of tumor antigens within the tumor. Moreover, *in situ* vaccination plays an important role in reprogramming the TME toward an immunostimulatory state. The high interstitial fluid pressure of the TME can act as a barrier for immunotherapeutic agents to enter into the tumor. To address this limitation, Boone *et al*. developed an autonomous active MN for the direct transportation of cowpea mosaic virus NPs (CPMV) as potent immunoadjuvants towards the treatment of B16F10 melanoma in mice [124]. In this system, magnesium (Mg) microparticles were embedded into active MNs to facilitate the entrance of the NP payload into the tumor through their reaction with the interstitial fluid in the TME and creating a propulsive force. *In vivo* experiments demonstrated that active MNs strongly increased tumor regression, improved survival profiles of tumor-bearing mice, and represented enrichment in the $CD8^+$ T cell population. As mentioned in the previous section, combination therapy of cancer using immune-stimulating antigens and other techniques can be considered as a valid approach to more effectively treat cancers than monotherapy. One of the promising strategies to improve the anti-tumor immune responses is the vaccination with whole tumor antigens derived from whole cell lysates. In addition to whole tumor antigens, the whole cell lysates possess melanin that can as a photosensitizer for heat generation and subsequent PTT of cancer [125]. As an example, Ye et al. reported the design and fabrication of a transdermal cancer vaccine MN patch based on cross-linked HA materials [126]. The polymeric MNs were

loaded with B16.F10 whole tumor lysate containing melanin and granulocyte-macrophage colony-stimulating factor (GM-CSF). In addition to the sustained release of lysate into the skin, melanin can act as a photosensitizer for heat generation through localized near-infrared light (NIR) irradiation, while the presence of GM-CSF enhances the recruitment and activation of immune cells. In vitro experiments demonstrated that 10 min of NIR irradiation provided an optimal activation of matured DCs ($CD80^+/CD86^+$ cells, increasing from 36.7 ± 2.3% to 48.9 ± 3.1% after 10 min) and did not reduce their viability and functionality. In vivo experiments in a prophylactic set up in B16.F10 models indicated that the combined therapy of MNs loaded with tumor lysate and GM-CSF with NIR irradiation resulted in complete tumor rejection in 87% of the treated mice and long-term survival. Furthermore, the authors analyzed also the immunological mechanisms responsible for the vaccination efficacy by testing the MNs in animals genetically modified not to express lymphocytes (both T- and B- cells) to evaluate the contribution of the adaptive immunity, or treated with diphtheria toxin receptor to deplete DC to assess the contribution of the innate immunity and antigen processing and presentation. The results highlight the importance of both components in the instauration of an optimal immune memory against future tumor challenges. These MNs are also able to control tumor growth in a therapeutic setup after NIR irradiation. Furthermore, this immune response is systemic and able to affect distal, non-treated, or irradiated tumors.

In the case of IM or subcutaneous vaccination, patients might experience stress, fear, pain, and undesirable specific immune responses. In this regard, using MNs can be a good choice to achieve maximum delivery while limiting side effects. To this end, Lee et al. used a MN containing the antigen OVA as an immune-stimulating antigen delivery system to activate anti-tumor immunity into the skin of mice [127]. They observed that the OVA-loaded MN patch

exhibited a significantly reduced tumor size (78.75±30.1 mm^3) and weight (0.82±0.5 gr) compared to a control patch, which had a tumor size and weight of 249.67±39.1 mm^3 and 2.33±0.9 g, respectively. This observation was mainly attributed to the increased population of OVA-specific $CD8^+$ T cells and $CD4^+$ T cells. These cells were responsible for the cytotoxic effect against the graft of OVA-expressing EG7 tumor cells.

In another example, an amphiphilic triblock copolymer (Pluronic F27) was employed in constructing a dissolving MN-based cancer vaccine able to create nanomicelles (NMCs) in the intradermal fluid (Figure 9A) [128]. The amphiphilic property of the Pluronic F27 enabled the co-delivery of OVA, hydrophilic, and resiquimod (R848), hydrophobic, into in situ micelles formed after cutaneous application, contributing to the dissolution of R-848. In vitro experiments confirmed the immunostimulatory potential of R848 encapsulated within the NMCs. Furthermore, upon administration of the MN patch in vivo, the NMCs can efficiently migrate to lymph nodes and induce antigen-specific humoral and cellular immunity in EG7-OVA tumor-bearing mice (Figure 9B). Significantly increased levels of INF-γ^+CD8^+ T cells and reduction in tumor size and weight were found in mice treated with OVA/R-848 MNs compared to the mock group (Figure 9C-E).

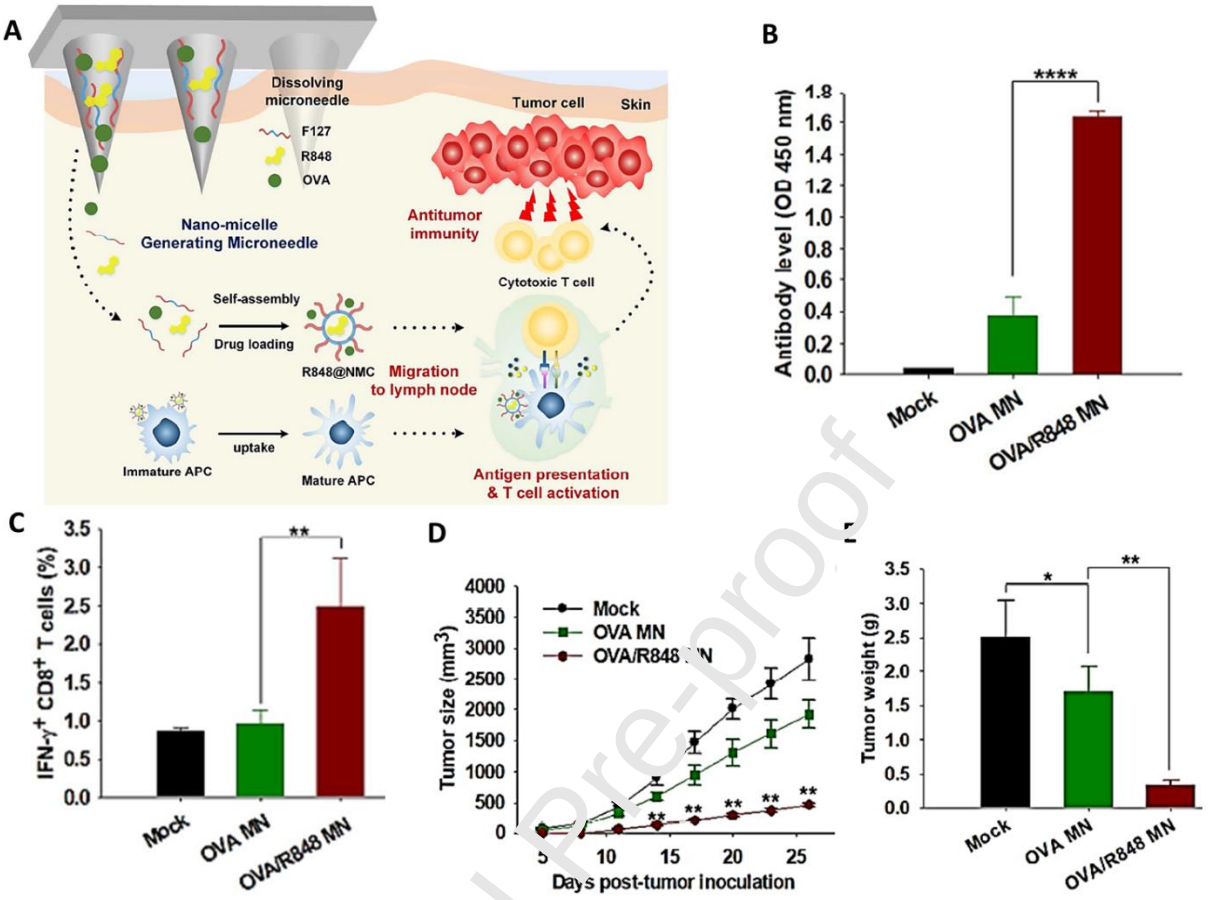

Figure 9. The amphiphilic triblock copolymer-based dissolving MNs containing OVA and R848 with the ability for in situ generation of NMCs and inhibition of tumor growth upon their dissolution after cutaneous application in EG7-OVA tumor-bearing mice. **A)** Schematic illustration of dissolving MNs for co-delivery of hydrophobic immunomodulators and tumor antigens via *in situ* formation of nanomicelles. **B)** OVA-specific IgG levels after immunization (****P<0.0001, n=5). **C)** Amount of INF-$\gamma^{+}CD8^{+}$ T cells in different experimental groups (**p < 0.01, n = 5). Co-delivery of R-848 and OVA by MNs resulted in a higher percentage of IFN-γ+CD8+ T cells compared to the mock and the MNs containing antigen only. **D)** Tumor size from the three experimental groups. The mock group only received PBS (**p < 0.01 compared to mock group, n = 5). **E)** Tumor weight in different experimental groups (*p < 0.05 and **p < 0.01, n = 5). The MNs containing antigen only (OVA) contribute to a partial control over the tumor growth, as demonstrated by the reduction of the tumor weight when compared to the mock. However, the administration of the complete formulation, antigen, and adjuvant (R-848) in the same MNs results in a higher activation of the immune system and better control over the tumor growth. Reproduced with permission from ref.[128]; Copyright 2018, American Chemical Society.

In conclusion, MN patches represent an excellent alternative to conventional cancer vaccine designs by allowing a painless administration in an area rich in APCs. Moreover, researchers

have proposed innovative formulations to allow a simple simultaneous delivery of antigens and adjuvants with opposite hydro/lipophilic characteristics or enabling efficient delivery of the payload to the draining lymph nodes. Finally, MNs can also play a role in improving the efficacy of immune checkpoint inhibitors, allowing for local delivery in the tumor area with a decrease in the immune side effect associated with systemic delivery.

5. Autoimmune diseases

Currently, MNs have been extensively investigated to precisely treat or manage autoimmune diseases, such as type 1 diabetes (T1D), alopecia areata, systemic lupus erythematosus, multiple sclerosis, and rheumatoid arthritis (RA) [129-133]. The direct administration of immunomodulatory peptides and immunosuppressive drugs to patients with the traditional techniques is no longer applicable owing to their intrinsic limitations such as poor oral bioavailability, gastrointestinal side-effects, enzymatic hydrolysis in the gastrointestinal tract, rapid plasma clearance, and poor patient compliance [134]. To address some of these limitations, Lin et al. developed dissolving MNA to deliver Thymopentin (TP5), a synthetic pentapeptide with a very short half-life in plasma (about 30 s) and immunomodulating properties for the treatment of autoimmune diseases, in immunosuppressed Sprague-Dawley rats [135]. A MN array containing TP5 was fabricated by a modified two-step molding technology using bovine serum albumin (BSA) as a mechanical strength regulator. The high-performance liquid chromatography (HPLC) chromatogram confirmed the maintenance of the integrity of TP5 after loading in the MN patch. The administration of TP5 through the MNs improved the levels of T-cells and reversed the ratio of $CD4^+/CD8^+$ 7 days after the treatment in immunosuppressed rats.

In 2020, Ahmad et al. fabricated thiolated chitosan (TCS)-based MN patch containing tacrolimus (TM), an immunosuppressant agent for the treatment of autoimmune disorders, by a mold casting method. The TCS-based MN patch was able to improve the drug bioavailability through circumvention of the hepatic first-pass metabolism and intestinal P-gp efflux and deliver the drug in a more sustained manner than oral administration [136]. Attenuated total reflectance-Fourier transform infrared (ATR-FTIR) analysis demonstrated that characteristic peaks of TM were retained in MN patches, suggesting the stability of TM during the preparation process of the patches. The author found the best tensile strength (0.05 mPa) at 2% concentration of TCS and a higher skin distribution for MN-TM ($15.34 \pm 2.4\%$) compared to ointment ($9.45 \pm 3.2\%$). Additionally, they further mentioned 84% penetration of TM with no breakage of the MNs and a sustained release (82.5%) from patches with no visible erythema or edema.

5.1. Design of MNs for immunotherapy of type 1 diabetes

The loss of T-cell-dependent immunological tolerance to β-cell autoantigens has been proposed as the most critical pathological event of T1D. A possible solution for the optimal treatment of this disease is to reverse this process [137]. Antigen-specific immunotherapy (ASI) is a promising therapeutic strategy to treat T1D through the induction of an immune regulatory response to hinder autoimmune-mediated β-cell destruction to maintain insulin production [138]. Peptide immunotherapy has been proposed as promising strategy to induce tolerance to pancreatic self-antigens. A key aspect to consider in MNs is to analyze their advantages compared to an ID injection. In a comparative study for the delivery of four different antigenic peptides, including WE 14, Insulin B9-23, Epstein–Barr virus peptide 280–288 and BDC2.5 mimotope in the non-obese diabetic (NOD) mice model, Zhao et al. found that dry-coated MN

patches consisting of methyl butanol, polyvinyl alcohol, and acetic acid exhibited a more effective delivery and prolonged antigen presentation in the skin [139]. Comparable reductions in the auto-reactive cell proliferation were observed when the authors immunized the animals with two concentrations of WE14 (6 μg of the peptide in dry-coated MNs and 50 μg of the peptide in ID injection) (Figure 10A). The results can be mainly attributed to the higher retention time of the peptide-loaded into the MN patch, which in turn resulted in providing enough time for the APCs in the skin to tender antigenic peptides to the patrolling T cells and create tolerance at lower peptide concentration. In order to minimize immune stimulation and control the localized kinetics in immunotherapy of T1D, nanomaterials with anti-inflammatory properties can be used as appropriate multi-cargo delivery platforms to present tolerogenic auto-antigens to APCs and promote a regulatory response. In another example, Dul et al. used MicronJet600, a clinically approved MN delivery system, to treat T1D through intradermal delivery of a human leukocyte antigen-DR4 (HLA-DR4)-restricted peptide epitope of proinsulin (C19-A3) tethered to gold NPs (GNPs) (Figure 10B) [140]. Ex vivo experiments showed that GNPs quickly diffused throughout human skin. Additionally, in vitro experiments indicated that uptake of GNPs - peptide complexes by DCs resulted in a reduction of their capacity to active naïve T cells.

One of the major disadvantages of the above-mentioned studies for T1D immunotherapy is the loading of a single peptide autoantigen in the MNs, which in turn can limit their applications to sub-populations of patients with a specific human leukocyte antigen (HLA) molecule [141]. It has been reported that using coated MN systems loaded with complete protein containing multiple epitopes provide high therapeutic potential for ASI of T1D because of the ability of APC to synchronically generate tolerance to a range of epitopes and be therapeutically applicable to more patients [139].

Following this concept, Arikat et al. developed Proinsulin (PI)-coated MNs to transport PI protein into the superficial layers of the skin, targeting immature epidermal Langerhans cells (LCs) and steady-state DCs, which exhibit tolerogenic functions [142]. The presence of polysorbate 80 as a non-ionic surfactant in the coating formulation resulted in the uniform coating of protein onto the outer surface of MNs. The authors found that the delivery efficiency of PI was 77.5 ± 17.3% after 1 minute of MN application and increased to 86.1 ± 4.4% after 2.5 minutes. Based on in vivo experiments in NOD female mice, significant proliferation of adoptively transferred G9 $CD8^+$ T cells was seen in the draining (axillary) lymph nodes (AxLNs) in the MN treated group (29.1%) while traditional ID PI injection failed to create this effect (4.6%).

It can be assumed that compared to conventional ID routes, delivery by coated MNs (dry coating of therapeutic antigen onto their outer surface) for treatment of T1D represents a valid method with numerous advantages, such as highly efficient antigen delivery to the dermis and epidermis, capacity for the co-delivery of multiple therapeutic agents, the prolonged retention time for therapeutic antigens in the skin, the possibility of sustained exposure of APCs to low concentrations of therapeutic antigens, less pain, no bleeding and distension of skin layer, with less skin damage and subsequent infection [143-146].

5.2. Design of MNs for Rheumatoid Arthritis immunotherapy

RA is a long-term autoimmune or chronic inflammatory disorder that can cause progressive disability of synovial joints owing to inflammation of synovial membrane, cartilage, and bone damage [147]. Glucocorticoids are frequently used in the short term to relieve pain and inflammation, but higher doses can cause serious side effects for a prolonged period.

Immunotherapy aims to reduce inflammation and protect the integrity of the joint, with manageable side effects [148]. Topical drug delivery is only able to deliver therapeutic molecules with proper oil-water partition coefficient, low molecular weight, and low melting point due to the characteristics of the stratum corneum [149].

To address these challenges, Yao et al. developed a neurotoxin (NT)-loaded dissolving MNs through two-step centrifugation, with 15.4 ± 0.5 μg of the drug-loaded in the upper part of each needle [150]. The MN exhibited good mechanical properties and less toxicity on chondrocytes. The MN could penetrate the skin at a depth higher than 70 μm. Also, the cumulative penetration of NT in MNs reached 95.8% in 4 h, whereas a NT solution could hardly penetrate the skin. After administration to animals, NT-MNs were capable of suppressing the secretion of pro-inflammatory cytokines such as the tumor necrosis factor α (TNF-α) and interleukin 1 β (IL-1β) as well as reduce the toe swelling of RA rats.

Although nonsteroidal anti-inflammatory drugs (NSAID), such as meloxicam, are widely used to reduce inflammation and protect the integrity of the joint in RA patients, their long-term use results in poor patient compliance due to their serious side effects such as hypertension, diabetes, ulceration and gastrointestinal perforation [151].

In order to highlight the compliance of MN technology, Amodwala et al. developed fast-dissolving MNs loaded with meloxicam as a patient-friendly tool to promote drug delivery to deeper layers of skin and circumvent the drug's poor patient compliance owing to gastrointestinal disturbances after oral administration [152]. They reported a 2.58-enhanced penetration, improved transdermal flux of 1.60 μg/cm^2/h, and 63.37% deposition of meloxicam in excised rat abdominal skin compared to the drug solution. Moreover, rats treated with the MN exhibited a similar anti-inflammatory activity than the existing marketed oral tablet. In another

interesting example, Chen et al. went on to address the limitations of NSAID through the design and fabrication of tip-dissolving MNs. In their study, polymer solutions containing meloxicam were added into the PDMS mold, and high pressure was exerted to drive the air bubbles out of the cavities of the mold. In the next step, the residual solutions were removed to facilitate drying the tip solutions in the cavities of mold. Finally, molten polycaprolactone (PCL) was poured into the mold, and high pressure was exerted again [153]. The author pointed out that tip-dissolving MNs exhibited burst release of the encapsulated meloxicam (91.72% within 30 min), excellent bioavailability (122.3%), favorable drug transportation to the skin (79.18%), high anti-inflammatory and analgesic activities without any adverse effects such as skin irritation. In another study, Cao *et al*. engineered dissolvable HA crosslinked MNs as the transdermal alternative to deliver etanercept (EN), a TNF- α inhibitor for RA therapy since the subcutaneous (SC) injection of EN is associated with low compliance, infection risk, and other side effects [154]. The engineered MNs exhibited good mechanical strength and excellent biocompatibility and did not reduce the bioactivity of EN. *In vivo* experiments in adjuvant-induced arthritis mice showed that treatment with both EN by SC (eSC) and EN by MN (eMN) reduced the paw swelling ratio from 1.70 to 1.48 and 1.68 to 1.44 in 10 days, respectively, indicating anti-inflammatory effects. Additionally, ELISA assay showed significantly reduced serum levels of the TNF-α and IL-6 level in both eSC and eMN mice compared to the mice that were treated with saline (SA) (Figure 10C and 10D).

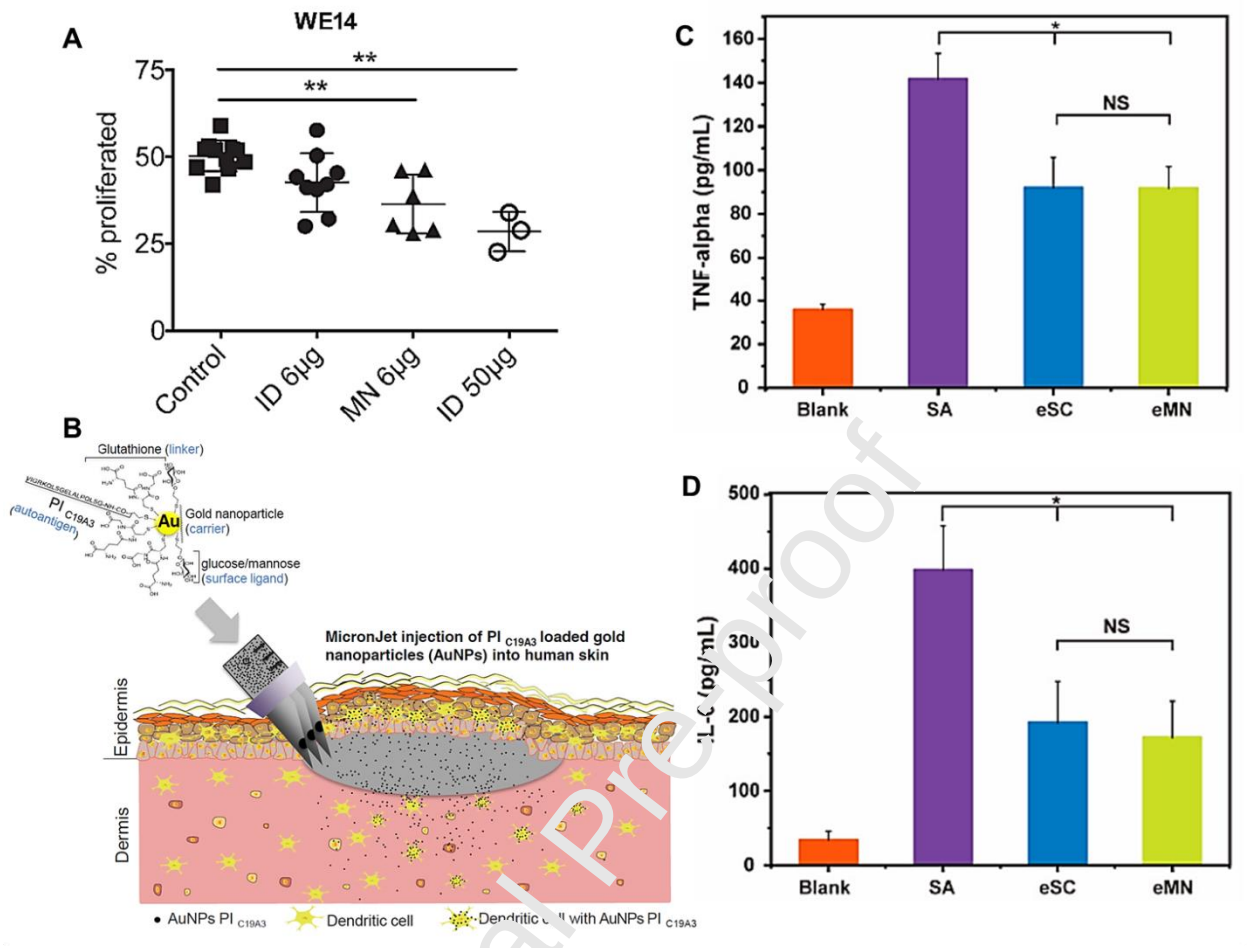

Figure 10. Comparing ASI of T1D using dry coated MNs or ID administration. **A)** Measuring the auto-reactive cell proliferation (proliferated BDC2.5 T cells) in the pancreatic lymph node after WE14 administration by ID injection or MNs. (**p<0.01). MNs with low peptide concentration (6 µg) exhibited similar efficiency to ID injection with high peptide concentration (50 µg) in reducing proliferated BDC2.5 T cells and inducing tolerance. Reproduced with permission from ref.[139] Copyright 2016, Elsevier B.V. MicronJet600 for ID delivery of proinsulin (C19-A3) tethered to GNPs towards T1D immunotherapy. **B)** Schematic representation of the delivery of AuNP-peptide complexes into the skin by MNs and their subsequent quick diffusion throughout the skin, capturing by APCs and suppressing activation of naïve T cells. Reproduced with permission from ref.[140] Copyright 2019, Elsevier B.V. **C)** the TNF-α and **D)** IL-6 serum levels in different experimental groups. * p < 0.05 vs. SA. NS represents no significance. Reproduced with permission from ref.[154]; Copyright 2019, MDPI.

In another study, Qiu *et al*. designed and prepared dissolvable MNs loaded with artemether, a drug for RA treatment, to address the poor water-solubility of this drug [155]. The dissolving MNs were capable of delivering 72.67±2.69% of the initial dose of artemether into the skin. Lower peak plasma levels but higher plasma concentrations of drug were observed for MNs at 8

h after administration compared to IM injection. The authors found an analogous reduction in total anti-CII IgG levels in collagen-induced arthritis rats compared to MI injection.

Some previous studies have shown that the combination therapy of RA possessed higher effects in reducing inflammation compared to monotherapy [156]. Yu *et al*. designed and fabricated a dissolving MN system containing immunosuppressant tacrolimus (TAC) and anti-inflammatory diclofenac (DIC) in different layers of MNs, named TD-MN (Figure 11A) [157]. The tip-layer of TD-MN was composed of a blend of dextran, HA, PVP K17 and DIC or RhB. The inter-layer was included a blend of dextran, HA, PVP K17, and TAC. *In vitro* and *in vivo* experiments for skin permeation showed that the inter-layer was able to retain TAC within the skin of ~100 μm, whereas the tip-layer transported DIC up to ~300 μm into the articular cavity. The fluorescence images of the rat knee joints punctured by the layered MNs loaded with RhB demonstrated that the RhB fluorescence quickly entered into the articular cavity. This claim was confirmed by removing treated skin after 30 min. A gradual increase of the fluorescence intensity of RhB was seen over 6 h, and remained high for 24 h (Figure 11B). compared to the layered MNs, the intra-articular injection of RhB solution showed a peak at 4 h post-injection, and a very low amount of RhB was maintained from 6 to 12 h post-injection (Figure 11C). *In vivo* experiments indicated that the TD-MN alleviated carrageenan/kaolin-induced arthritis compared to DIC injection by reducing cartilage destruction, muscle atrophy, and joint swelling. Significantly reduced levels of the serum TNF-α and IL-17A in arthritic rats treated with the TD-MN were found, while unlayered MNs loading a mixture of TAC and DIC (MIX-MN) failed to create protective effects (Figure 11D and 11E). These findings suggest that the synergistic effects highly rely on the effective integration of multiple therapeutic agents in different layers of a single platform rather than just simple mixing.

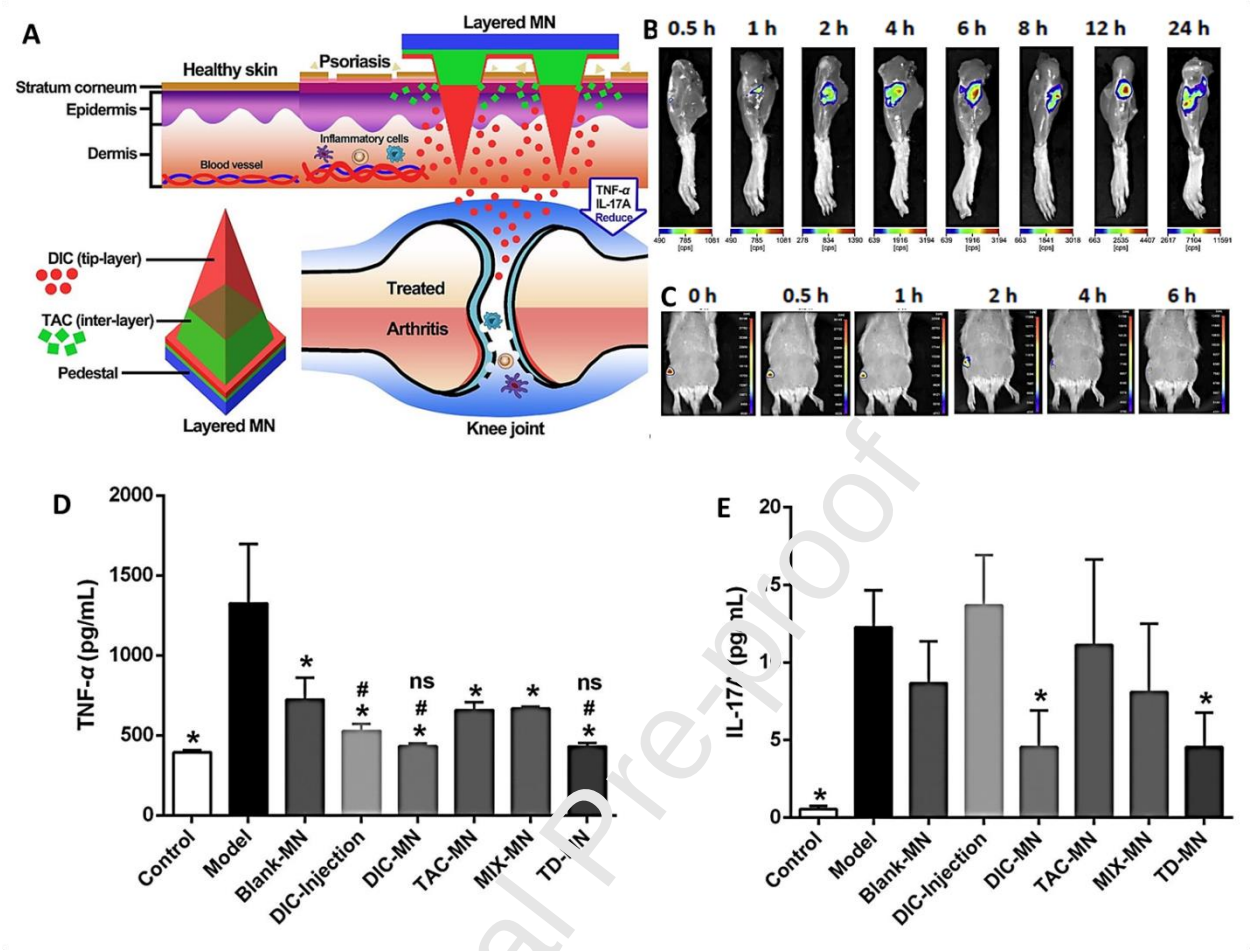

Figure 11. The TD-MN containing tacrolimus (TAC) and diclofenac sodium (DIC) in different layers for combined therapy of RA and psoriatic skin. **A)** Schematic representation of layed MNs for combined therapy of RA and psoriatic skin though modulation of inflammation. The tip-layer of TD-MN was composed from a blend of dextran, HA, PVP K17 and DIC or RhB. The inter-layer was included a blend of dextran, HA, PVP K17 and TAC. **B)** *In vivo* fluorescence images of RhB transportation of layered MNs into the articular cavity of rats at 0.5, 1, 2, 4, 6, 9, 12, and 24 h. **C)** *In vivo* fluorescence images of intra-articular injection of RhB solution at 0, 0.5, 1, 2, 4, and 6 h. Effects of various MN formulations on serum levels of **D)** TNF-α and **E)** IL-17A in arthritic rats. Data are expressed as mean ± SD (n=6 animals per group). ∗P<0.05 versus carrageenan/kaolin-induced arthritic model group; #P<0.05 versus MIX-MN group; and ns, no significant difference versus the negative group. Definition of MIX-MN group: Loading a mixture of TAC and DIC into the unlayered MNs. Reproduced with permission from ref.[157]; Copyright 2020, Elsevier B.V.

In another study, Zhao et al. used bee venom gel instead of NSAID to prevent the occurrence of gouty arthritis inflammation in rats. The authors used MNs containing bee venom gel and found that the application of the 750 μm MNs with 10N force on skin for about 3 min resulted in anti-

inflammatory effects [158]. For example, another type of hydrogel MNs encapsulated triptolide-loaded liposomes as novel systems to treat collagen-induced arthritis in rats [159]. In this study, the pharmacodynamics experiments demonstrated that the MNs attenuated the degree of joint swelling and serum levels of IL-1β and interleukin-6 (IL-6) through regulation of the balance between Th1 and Th2 pathways. In summary, the possibility to transdermally deliver therapeutic molecules using MNs for RA treatment represents a great advantage for their clinical translation since they can reduce the adverse effects of RA drugs.

6. Defeat allergy by MN patches

6.1. Design of MNs for immunotherapy of food allergies

Food allergens like peanut, milk, gluten, and aeroallergens, such as pollen and dust, can stimulate immune cells and result in the secretion of pro-inflammatory cytokines, activation of IgE antibodies, mast cells, and eosinophils [160-162]. Allergy immunotherapy promotes immunological tolerance, with a long-term effect lasting past treatment termination [163]. In a study, Shakyaa et al. used peanut protein extract (PE)-coated MNs to provide desensitization of peanut sensitized mice [164]. They firstly fabricated MNA from 50-μm thick stainless steel (304 grade) sheets through a wet etch process and then coated them by dipping in a coating solution containing PE, carboxymethyl cellulose (as a viscosity enhancer), and Lutrol F-68 NF (as a surfactant). The authors further revealed that PE-coated MN group had significant down-regulation of systemic anaphylaxis mediators like mast cell protease-1 (MCPT-1) and histamine and up-regulation of Th1 cytokines like interleukin-2 (IL-2) and IFN-γ compared to the untreated group, indicating that PE-coated MNs contributed to immune regulation by targeting the Th1 pathway. In their work, histopathological assessments of small intestinal tissues showed that PE-

coated MNs reduced the infiltration of eosinophils compared to the untreated group. It is well documented that the allergen dose delivered into the skin is a decisive factor of successful allergy immunotherapy [165]. As a result of some limitations of coated MNs, such as the difficulty of precise coating and insufficient delivery of therapeutic allergen, some researchers have used dissolvable MNA to ensure effective PE transportation into the epidermis/dermis layers. For example, Yu et al. showed that a powder-laden, dissolvable MNA (PLD-MNA) encapsulating peanut allergen (PNA)/ 1,25-dihydroxyvitamin D3 (VD3)/CpG could be used to manage IgE-mediated allergies in peanut-sensitized mice [166]. The authors revealed that the MNA was able to deliver most of its content after 1 h into the epidermis of mouse skin, with no evident skin irritation or leakage into the circulation. The intravital confocal microscopy of MHC class II–EGFP mice showed that OVA-555–laden PLD-MNA was dissolved into the mouse ears within 15 min, and the APCs were highly accumulated around each powder dot (OVA), with a peak on days 1 and 2. The emerged yellow colors of green and red on days 1 and 2 confirmed the uptake of OVA by APCs. Decreasing powder quantity in the epidermis from day 1 to day 5 resulted in the gradual reduction in the number of APCs (Figure 12). The researchers further stated that PLD-MNA encapsulating PNA/VD3/CpG reduced clinical allergy scores (from 3.5 to 1), the number of treatments, and the required dose of PNA in each treatment compared to conventional intradermal immunotherapy.

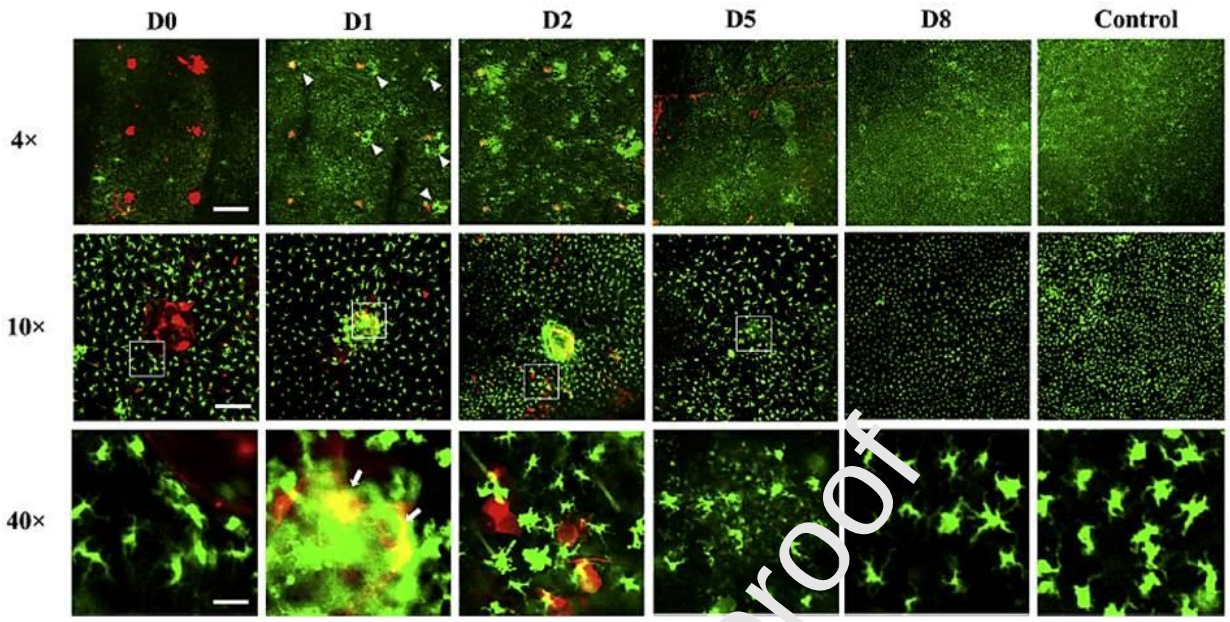

Figure 12. The ability of OVA-555–laden PLD-MNA for attracting and activating APCs and promoting antigen uptake by these cells. Two-photon confocal microscopy for tracking OVA-555 in the epidermis from day 0 to day 8. White triangles in upper panels show accumulation of APCs around each powder dot on day 1. White arrows indicate the merged yellow color of green and red owing to the uptake of OVA (red) by APCs (green). Scale bars represent 500, 200, and 50 mm in the upper, middle, and bottom panels, respectively. Reproduced with permission from ref.[166]; Copyright 2020, Elsevier B.V.

6.2. MNs for immunotherapy of allergic respiratory diseases

Airway allergies, including allergic asthma, allergic rhinitis, and allergic conjunctivitis, are common public health concerns due to their increasing prevalence worldwide [167]. The release of toxic protein granules or ROS by infiltrated eosinophils at the site of inflammation enhances the allergic immune response [168]. Moreover, mast cells are a major effector cell type in IgE-mediated hypersensitivity that induces airway allergies through releasing various inflammatory mediators, such as histamine [169]. A promising strategy for the treatment of airway allergies is allergen-specific immunotherapy (AIT). The principle of AIT is based on repeated administration of an allergen with increasing doses until the achievement of tolerance [170]. AIT is classified into two types, including sublingual allergen-specific immunotherapy (SLIT) and

subcutaneous allergen-specific immunotherapy (SCIT). SLIT is safe, but it needs high allergen doses and is not a satisfactory method for administration in kids and infants [171]. Although SCIT uses lower doses compared to SLIT, it is painful and inconvenient with other systematic side effects [172]. To overcome the limitations of SCIT, coated MNs can be applied to improve the efficiency of immunotherapy of allergic airway diseases. For example, Shakya *et al*. developed a coated MN with Ova and CpG (MNs-Ova+CpG) to evaluate its efficiency for allergen desensitization in a mouse model of Ova-induced airway allergy compared to SCIT [173]. The authors stated that treated mice were challenged with Ova through the nasal route to examine efficacy against allergen challenge. Treated mice with coated MNs demonstrated significantly increased levels of Ova specific serum IgG antibodies in comparison with SCIT-Ova+alum treated group. Likewise, up-regulation of anti-inflammatory cytokine IL-10, downregulation of pro-inflammatory cytokines, including IL-5 and IL-13, and activation of Ova specific immune response in bronchoalveolar fluid showed that (MNs-Ova+CpG have the ability to suppress the airway inflammation in allergic mice. Additionally, H&E stains for eosinophils and May-Grünwald Giemsa (MGG) stains for mast cells showed that treatment with MNs-Ova+CpG markedly reduced infiltration of these cells in lung tissues compared to the untreated and the SCIT-Ova+alum groups (Figure 13A-13D).

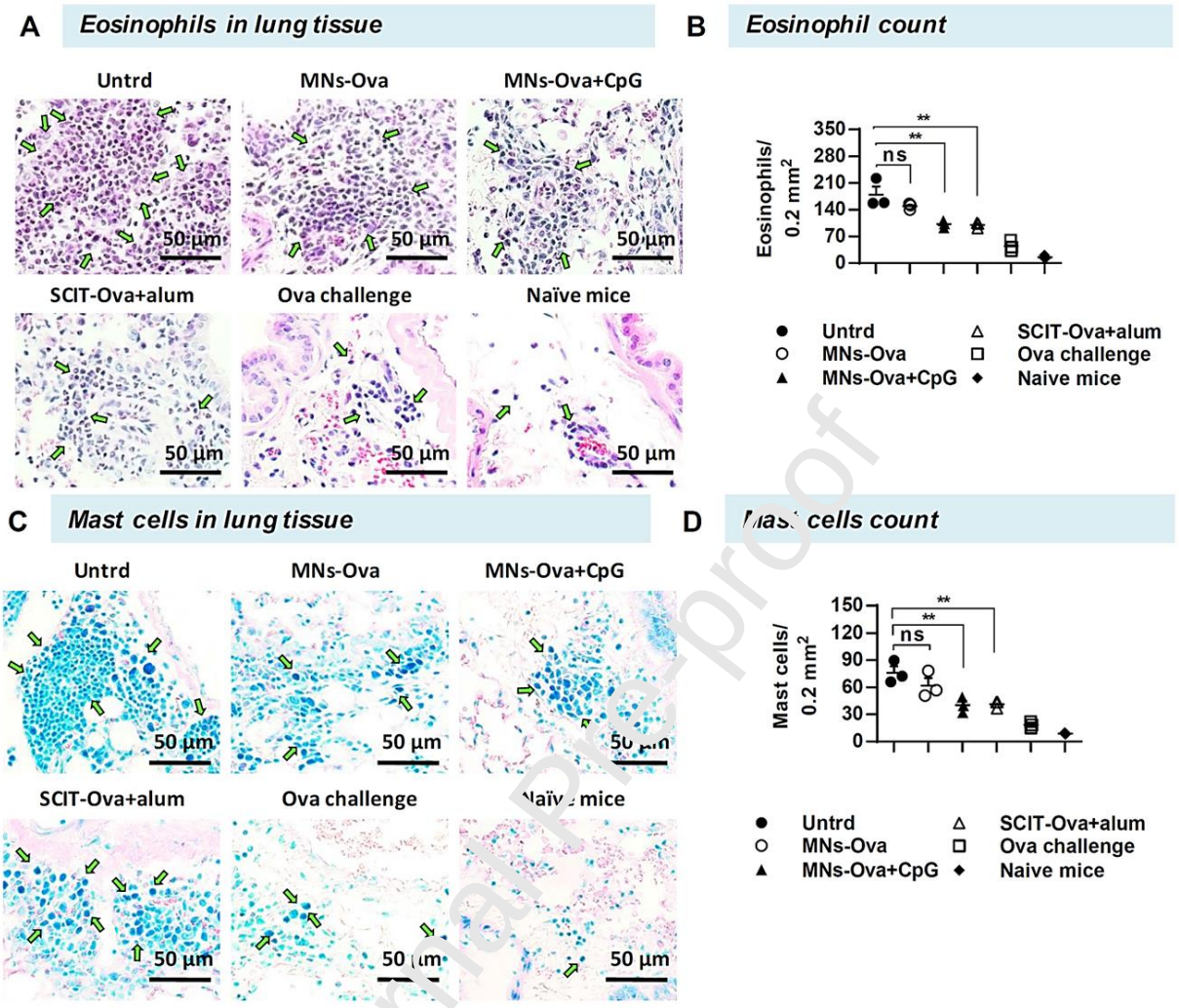

Figure 13. The effects of coated MN with Ova and CpG on the infiltration of eosinophils and mast cells in lung tissues. **A)** H&E stained lung tissue sections for evaluation of eosinophil infiltration. **B)** Eosinophil count. **C)** May-Grünwald Giemsa stained tissue sections for evaluation of mast cell infiltration. **D)** Mast cell count. Arrows show cells or mucus deposition (n = 3 animals per group). Data are expressed as mean ± SEM. ** $p \leq 0.01$, and ns: not significant. Reproduced with permission from ref.[173]; Copyright 2020, American Chemical Society.

In another interesting example, the same research group loaded Der p 1, a house dust mite allergen, onto an MN patch composed of 57 total MNs to hamper the onset and progression of Der p 1–induced airway allergy [174]. Their results by calibrated fluorescence spectroscopy demonstrated that 73.3% ± 7.4% of coated Der p 1 was transported into the skin. The authors further found that Der p 1 coated MNs created a more reliable anti–Der p 1 IgG response than

the untreated and subcutaneous immunotherapy groups. The addition of CpG as an adjuvant to Der p 1 coated MN resulted in a more significant anti–Der p 1 IgG2a response and higher IL-10 and transforming growth factor-beta (TGF-β) secretion than both the Der p 1 coated MN and subcutaneous immunotherapy.

In another example, Shakya et al. coated MNs, using an in-house micro-precision dip-coating device, in a solution containing OVA, Lutrol F-68 NF, and carboxymethylcellulose (1%, w/v) to create a preventive vaccine against airway allergy [175]. The authors stated that the coated MNs are beneficial for treating airway allergy in infants as the sublingual route is not suitable for them, and injections are painful. A strong OVA-specific systemic immune response was induced following the insertion of MN coated with OVA and CpG oligonucleotide as adjuvant into the mice's skin. The MNs modulated a variety of cytokines, including anti-inflammatory cytokines (IL-10) and Th2 cytokines (IL-13, IL-4, and IL-5) in the bronchoalveolar fluid, as well as Th1 cytokines (IFN-γ and IL-2) in re-stimulated splenocyte cultures, indicating improvement of clinical symptoms of allergy.

Owing to limitations of coated MNs, Park *et al*. developed a biodegradable MN patch (MNP) comprising of hyaluronate and Dermatophagoides farinae (D. farinae) extract (DfE) using a droplet-born air blowing method for transdermal immunotherapy (TDIT) to ameliorate airway hyperresponsiveness (AHR) and inflammation in a house dust mite (HDM) asthma model (Figure 14A and 14B) [176]. The delivery test showed that 77% and 85.4% of the allergen were absorbed after 1 and 8 h of MNP insertion, respectively. *In vivo* experiments indicated that treatment with 10 μg TDIT improved HDM-induced AHR most significantly in comparison with low-dose (10 μg) and high-dose (100 μg) SCIT. TDIT had the strongest effect in reducing the secretion of cytokines associated with the Th2 inflammatory response (IL-4, IL-5, and IL-13)

and epithelium-derived cytokines (IL-33 and TSLP) as indicators of allergic inflammation (Figure 14C). Likewise, only treatment with 10 μg TDIT markedly increased Treg-associated cytokines (IL-10 and TGF-β), which are known to be expressed following AIT (**Figure 14D**). Their results showed that treatment with 10 μg TDIT resulted in the largest decrease in D. farina-specific IgE and IgG2a. Histopathological experiments demonstrated that treatment with 10 μg TDIT reduced goblet cell hyperplasia, subepithelial fibrosis, and HDM-induced inflammation.

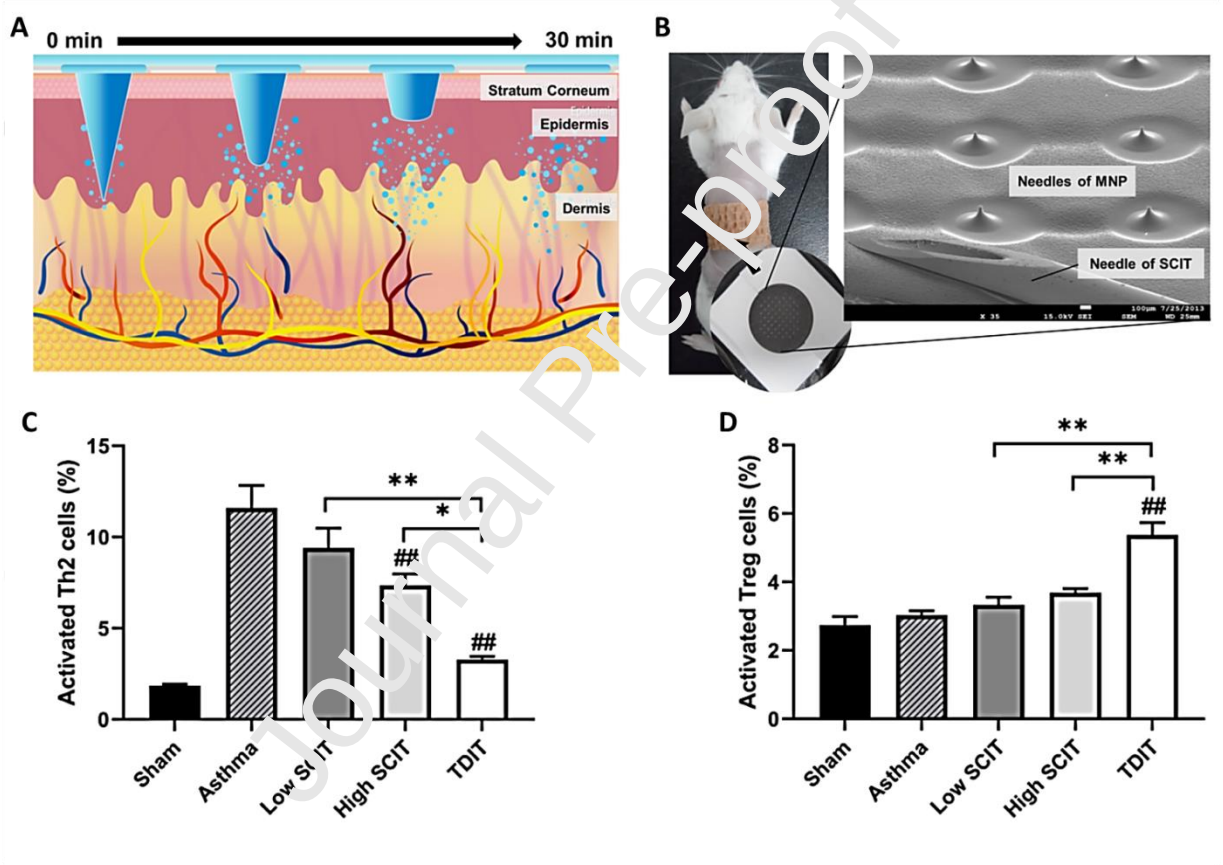

Figure 14. The effects of a biodegradable MNP loaded with D. farinae extract in reducing airway hyperresponsiveness (AHR) and inflammation. **A)** Schematic illustration of MNP loaded with DfE on the skin. MNP loaded with DfE were dissolved into the skin after insertion. **B)** MNP insertion on BALB/c female mice. Flow cytometry analysis of **C)** T helper 2 (Th2) cells and **D)** Regulatory T cells in Sham (control), Asthma (without treatment), Low SCIT (10 μg), and High SCIT (100 μg), and TDIT (MNP loaded with DfE) groups. Data are expressed as the mean ± SD. $^{\#}P < 0.05$ compared to asthma; $^{\#\#}P < 0.001$ compared to asthma; $^{*}P < 0.05$ and $^{**}P < 0.001$ between AIT modality (SCIT or TDIT). Reproduced with permission from.[176]; Copyright 2020, John Wiley & Sons Ltd.

6.3. MNs for allergen-specific immunotherapy

To compare the efficiency of MNs for cutaneous allergen-specific immunotherapy (ASIT) with other conventional routes like the IP, IM, and subcutaneous allergen immunotherapy, Shakya et al. fabricated MNs coated with OVA by a micro-precision dip coater and a coating solution containing OVA, carboxymethyl cellulose and Lutrol F-68 NF [177]. They demonstrated that most of the coating was transported into the skin following the insertion of the fluorescein-OVA coated MN patch in a mouse model. The coated MN-treated animals demonstrated an increased anti-OVA IgG response compared to IP and subcutaneous allergen immunotherapy and similar anti-OVA IgG response to IM administration at 28 days after insertion. Generally, they observed lower secretion of pro-inflammatory IL-1β, interleukin-13 (IL-13), interleukin-15 (IL-5), and IFN-γ after the insertion of OVA coated MN patches compared to the other routes of administration, as well as higher activation of the Th1 pathway, indicating their potential use for painless ASI. The authors stated that a shift from Th2 to Th1 response is thought to be beneficial for ASI.

In 2019, the same researchers coated two stimulators of interferon genes (STING) agonists, namely, cyclic diadenylate monophosphate (c-di-AMP) and cyclic diguanylate monophosphate (c-di-GMP), along with OVA as a model allergen on MN patches characterized by 57 individual micron-sized needles and transported them into mouse skin [178]. Calibrated fluorescence spectroscopy confirmed delivery of 78.8% (±4.2) of coated OVA into the skin, while 4.2% (±1.1) was seen on the skin and 17.0% (±4.0) OVA remained on the surface of MN patches. The authors showed a higher OVA-specific IgG2a antibody in serum as a surrogate marker for Th1 type immune response and higher levels of Th1 cytokines (IFN-γ and IL-2) in re-stimulation of splenocytes culture for coated MN groups compared to the approved subcutaneous hypodermic injection.

In a clinical trial conducted in Germany, Spina et al. compared MNs and adhesive-tape stripping in skin preparation for epicutaneous allergen immunotherapy [179]. They observed that MNs increased stratum corneum penetration in comparison to tape stripping and induced dendritic cell-mediated T cell responses.

Benefitting from their tailorability to the location of different subtypes of dendritic cells, such as LCs, MN patches can be designed to target LCs for allergy immunotherapy with minimal side effects. The presence of LCs in the epidermal layer makes them the first line of APCs that meet skin-invading antigens. This opens up a new avenue for immunotherapy of diseases without causing noticeable adverse effects [180]. For example, Burg et al. designed microprojection arrays (MPA) in polycarbonate material through a hot embossing procedure and coated OVA onto the surface of the MPAs [181]. In this study, they found that slit-MPAs (110 μm ± 3 μm tall projections at 7k p/cm^2) with higher tip surface areas than conical-MPAs (207 μm ± 5 μm tall projections at 10,000 (10k) projections/cm^2 (p/cm^2)) were more suitable for only epidermal delivery using low application energies. They further stated that the mouse epidermis (eMPA) delivery with larger projection tip surface areas had a lower inflammatory response and epidermal cell death, lesser erythema after 24 h, and epidermal swelling after 72 h than dermal-targeted MPAs (dMPA). Flow cytometry analysis showed that only the eMPA increased the migration of LCs with a low expression of major histocompatibility complex (MHC) II, without migration of dDCs.

Overall, the delivery of allergens by MNs to both the epidermis and the dermis can be further explored as a convenient and effective new means of allergen immunotherapy, which would encourage patient compliance and minimize side effects.

7. MN-based vaccines

The need for improvement of percutaneous vaccination arises from several major limitations of this technique, including needle phobias, the need for high doses and reconstitution of lyophilized vaccines, and the production of a huge amount of biohazardous waste, including sharp materials, such as needles that require special disposal protocol [182].

Currently, vaccine-loaded MNs have attracted tremendous attention from the scientific community as safe and dose-sparing tools to control vaccine release kinetics or improve immune response through manipulation of the composites of MNs [182, 185]. For example, DeMuth *et al*. developed layer-by-layer assembled polyelectrolyte multilayers (Poly-1/ICMV) deposited onto poly(lactic-co-glycolic acid) (PLGA) MNs, which provided a possibility to control the film thickness and dosage of immunomodulators for adjustable releasing and stabilizing goals (Figure 15A) [186]. The authros firstly synthesized nanocapsules containing interbilayer covalent cross-links among maleimide head moieties of adjacent phospholipid lamellae present in the walls of multilamellar vesicles and then deposited them onto the surface of PLGA MNs. By co-encapsulating OVA as an adjuvant and a fluorescent tracer in the structure of nanocapsules loaded into MNs, they found that OVA was taken up by the APCs into the epidermis, which, in turn, gave rise to higher serum levels of anti-OVA IgG titers and improved humoral immune response in a mice model (Figure 15B).

In another study, Boopathy *et al*. developed solid pyramidal MNs composed of silk fibroin (SF) protein tips encapsulating a stabilized HIV envelope immunogen and adjuvant to maintain drug concentrations in the skin by tailoring the speed of release [187]. It was shown that Env trimer was released over 2 weeks after immunization in the mice skin, resulting in increased germinal center (GC) B cell responses, increasing bone marrow plasma cells (16-fold), and increasing

serum IgG titers (~1,300-fold). Balmert *et al*. developed dissolving MNAs containing OVA plus Poly(I:C) via the combination of 3D laser lithography with nanoscale resolution and micromolding to compare its effects on induction of antigen-specific cellular and humoral immune responses with traditional IM [60]. The authors argued that this multi-component vaccine delivered 80.2% ± 12.5% OVA and 79.6 ± 5.0% Poly(I:C) within 10 min to murine skin (Figure 15C-15G). Likewise, epifluorescence microscopy showed penetration of MNs through the epidermis into the dermis for human skin, indicating MNs had suitable mechanical strength to penetrate into the human skin. The authors further stated that serum levels of anti-OVA IgG titers were markedly higher in immunized mice with multicomponent vaccine MNs compared to immunized mice with traditional IM injection.

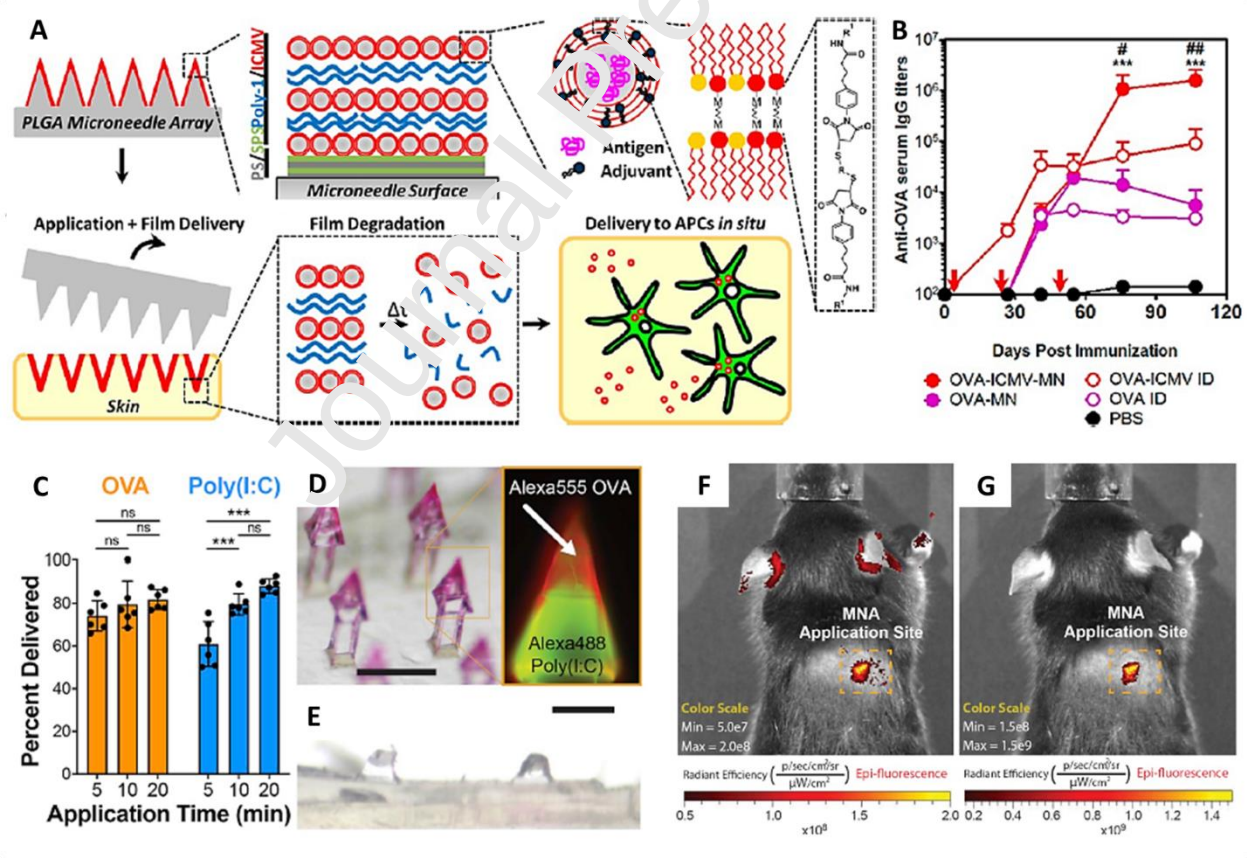

Figure 15. Transcutaneous vaccine delivery using releasable layer-by-layer assembly of stabilized lipid nanocapsules on MNs. **A**) Schematic illustration of deposition of (Poly-1/ICMV)

multilayers onto PLGA MN surfaces, transportation into the skin after insertion, and boosting immune function. **B)** Serum levels of anti-OVA IgG titers at different days after immunization ($^{\#}p < 0.05$ and $^{\#\#}p < 0.01$, and ***$p < 0.001$). Reproduced with permission from ref.[186]; Copyright 2012, American Chemical Society. **C)** Amount of OVA and poly (I:C) transported into the skin at different time points after MN insertion (***$p < 0.001$). No significant differences for delivery of OVA were seen at different times after insertion (5, 10, and 20 min), whereas the highest transportation of poly (I:C) was observed 20 min after insertion. **D)** Optical stereomicroscopy and fluorescence images of MNs containing both Alexa555-OVA (red) and Alexa488-Poly (I:C) (green). Scale bar: 500 μm. **E)** Optical stereomicroscopy photo of OVA/Poly (I:C) loaded MNs after insertion in murine skin. Scale bar: 250 μm. Effective transportation of **(F)** Alexa488-Poly (I:C) and **(G)** Alexa555-OVA into the mouse skin after MN insertion. Reproduced with permission from ref.[60]; Copyright 2019, Elsevier B.V.

7.1. Design of MNs for transdermal delivery of viral vaccines

The utility of vaccines can be improved by the use of coated and dissolving MNs since they are capable of carrying vaccines in a dried form [188]. The MNs can then release the components of the vaccine after dissolution in the epidermis/dermis, resulting in more thermostability and reducing the necessity for vaccine reconstitution as one of the steps of traditional percutaneous vaccine administration [189, 190]. The improved thermostability by coated and dissolving MNs provides the possibility to decrease or eliminate high costs relevant to the "cold chain" for storage or transportation of vaccines [191, 192]. Additionally, MNA vaccines are advantageous to create immunization against infectious diseases (SARS and COVID-19) in that they possess a high potential for self-administration without the need for any specialized equipment or an applicator [193, 194]. Although it has been reported that hollow MNs can be applied to facilitate penetration of NP loaded with therapeutic antigens into the skin and induce higher antibody response and a higher amount of interferon-γ compared to IM injection, needle clogging during piercing of skin and resistance to flow can limit their application for vaccination [195].

In the recent decade, a number of groups have used coated MNs for viral vaccinations since they are able to introduce the vaccine in a dry state (without the need for reconstitution) and improve

vaccine stability [196]. For example, Shin et al. coated 2 and 10μg of GMP with the influenza vaccine onto the stainless steel MNs using the dip-coating process before delivering them into the skin of a mice model to evaluate the reduction in influenza susceptibility [197]. In this study, mice immunized with the vaccine antigen and 2μg of GMP demonstrated the highest level of IgG at the second and fourth week after insertion (7-fold and 2.8-fold higher than the vaccine alone) while mice immunized with the vaccine antigen and 10μg of GMP did not induce a significant IgG response. Furthermore, mice immunized with 2μg GMP and the virus exhibited stronger protective immunity, while mice immunized with 10μg GMP and the virus demonstrated the lowest lung viral titer and rapid recovery rate. Thereby, the simultaneous delivery of the influenza vaccine and GMP by MNs improved both cellular and humoral immunity. In another example, Nguyen et al. designed and fabricated 800-μm-long polylactic acid MNs coated with L-HBsAg s (a third-generation hepatitis vaccine) to investigate its efficiency compared to IM immunization [198]. It was shown that the coated MNs more effectively elevated IgG1 and IgG2a titers and increased thermal and freeze-thaw stability compared to IM immunization.

Despite the potential benefits, several drawbacks of the coated MNs, such as poor coating efficiency and immunogenicity, might limit their future clinical use for viral and bacterial vaccinations [43]. The small surface area of the MNs results in delivering only small amounts of therapeutic molecules and antigens into the skin. To address this limitation, Maaden et al. coated pH-sensitive MNs with inactivated polio vaccine (IPV) particles and N-trimethyl chitosan chloride (TMC) through electrostatic interactions to achieve a sufficiently high antigen dose [199]. In their study, the MN surface was firstly decorated with pH-sensitive (pyridine) moieties and then coated with negatively charged IPV and a positively charged TMC. The authors coated ten layers of IPV alternately with TMC to achieve the required dose of antigen. With further

analysis, the authors found 45 D antigen units IPV and 700 ng TMC per MN. The ex vivo experiments demonstrated the release of both IPV and TMC into the human skin, and in vivo experiments confirmed the induction of IPV specific antibody responses. Another possible solution to overcome the limitation of coated MNs for vaccination is to use dissolvable MNs [200].

In another example, Erdos et al. developed dissolvable MNAs, consisting of trehalose and carboxymethyl cellulose, incorporating adenovirus vaccines (Ad5.OVA) with or without Poly(I:C) using a spin-casting technique to enhance the immunogenicity of skin-targeted adenovector vaccines [201]. The authors confirmed the dissolution of the MNAs upon skin insertion using optical stereomicroscopy. The multicomponent MNA vaccine platforms determined an increased OVA-specific lytic immunity compared to MNA containing adenovectors alone. In 2019, Chen et al. demonstrated that when inactivated influenza virus or OVA antigen is loaded into dissolving chitosan MNs, the delivery of inactivated influenza virus occurred in a sustained manner (up to 28 days), and induction of influenza-virus-specific IgG responses were higher than IM injection in mice (Figure 16A-C) [82].

7.2. Design of MNs for transdermal delivery of bacterial vaccines

In 2017, Pastor et al. developed outer membrane vesicle-loaded dissolving MNs to generate intradermal immunization against enteropathogens like the bacterium Shigella through induction of specific systemic IgG and mucosal IgA [202]. In 2019, Zhu et al. developed pertussis toxin (PT) vaccine MNs to transdermally target immune cells against Pertussis (whooping cough) caused by the bacterium Bordetella pertussis [203]. PT vaccine MNs released antigen in a more sustained manner (Figure 16D) and efficiently reduced the dose necessary to generate a high

level of PT-specific IgG via several pathways, mainly Th1 and Th17 pathways when compared to subcutaneous injection. In another study, Chen *et al*. designed and fabricated a MN incorporating F1 antigen-loaded liposomes (F1-liposomes) to deliver the F1 protein of *Yersinia pestis* and generate immunity against plague in a mice model [204]. Mice immunized with F1-liposome demonstrated the highest levels of the anti-F1 IgG antibody titers after 45 days compared to mice immunized with PBS buffer or F1-Alugel.

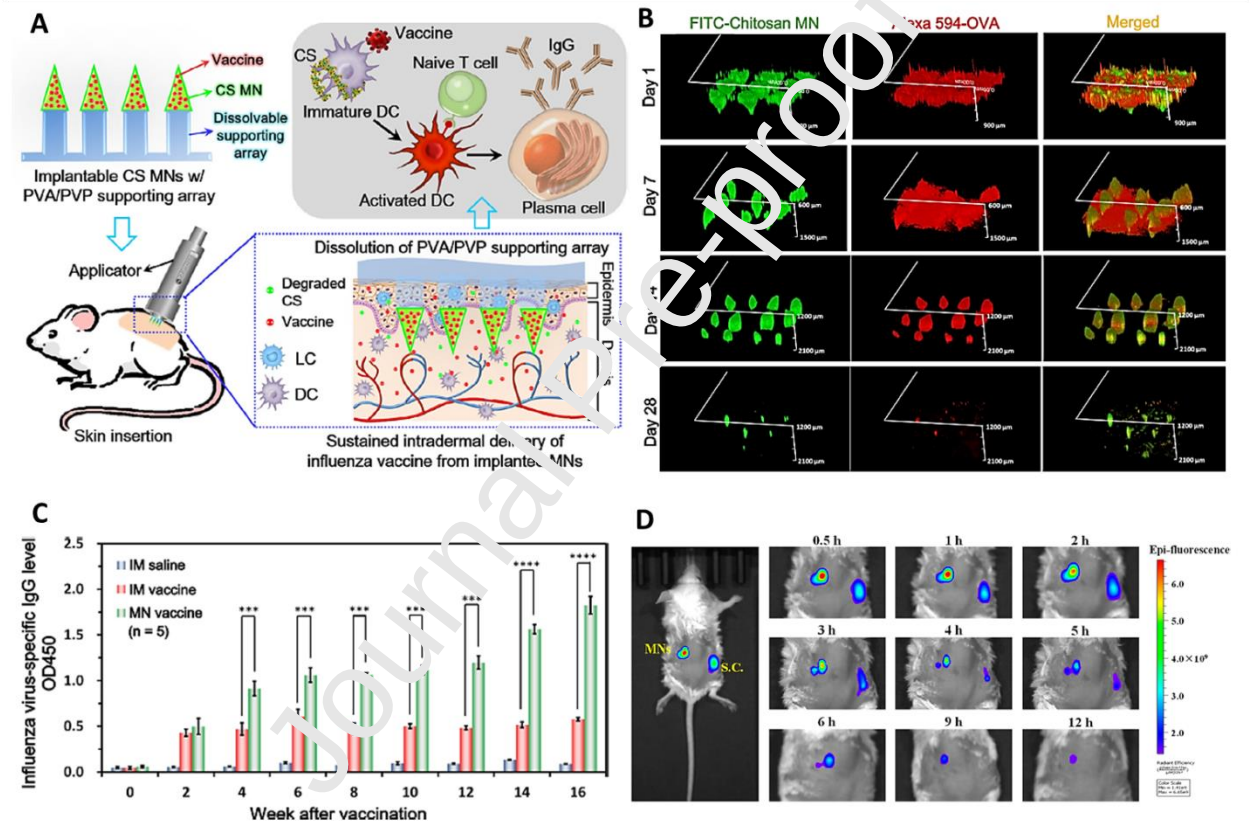

Figure 16. Immunity against influenza virus infection using patch-free chitosan MNs**. A)** Schematic illustration of the implantable chitosan (CS)-MNs with the ability to boost immune function via effective intradermal influenza vaccination through a sustained release profile. **B)** 3D reconstruction of confocal images of rat skin showing the degradation of CS-MNs and release of inactivated influenza virus in a sustained manner. FITC-Chitosan MN and Alexa 594-OVA signals were seen until 28 days after insertion of the MNs in the rat skin. **C)** Influenza-virus-specific IgG responses after IM injection of influenza vaccine or treatment using MN vaccine (***P < 0.001, n=5). Significant differences were observed between IM saline, IM vaccine, and MN vaccine. Reproduced with permission from ref.[82], Copyright 2019, Acta Materialia Inc. Published by Elsevier B.V. **D)** Fluorescent images showing the sustained release

of PT vaccine MNs compared to subcutaneous injection. No signals were seen for subcutaneous injection after 6h, while signals for MN insertion were observed until 12 h. Reproduced with permission from ref.[203]; Copyright 2019, American Chemical Society.

8. MN-mediated treatment of inflammatory diseases

MNs can reduce the required dose and adverse effects of anti-inflammatory drugs and contribute to the maintenance of the physical stability of their nanocarriers [205]. Currently, dissolving MNs have garnered much attention from the scientific community for immunotherapy of inflammatory diseases.

8.1. MN design for psoriasis treatment

Psoriasis is a chronic inflammatory disorder that is mainly characterized by vasodilation and immunological imbalance. The activation of NF-κB by some factors results in the initiation of inflammation in psoriasis [206]. The presence of T cells and DCs in the psoriatic lesions enhance the secretion of pro-inflammatory cytokines such as TNFα, IL-1β, IFNγ, IL-17, IL-22, and IL-23 [207]. Currently, evidence has shown that MNs can effectively manage psoriasis [208].

An advantage of using the dissolving MNs for immunotherapy of inflammatory diseases compared with other types of MNs and traditional needles is the dissolution of the needles within the skin and hence no requirement for proper needle disposal or the fear of needle reuse [209]. Du et al. pioneered a project using dissolving MNP composed of HA loaded with Methotrexate (MTX) using a two-step micromolding process. The aim of the study was to enhance the efficacy of psoriasis treatment by targeting inflammatory responses [210]. The release of MTX reached 52% within 10 min, 76%, and 87% at 30 and 60 min, mainly due to the water solubility of HA. In vivo experiments demonstrated a complete dissolution of MNP- MTX within 10 min resulted in a reduction in ear thickness, suppression of the IL23/IL17 axis, and imiquimod (IMQ) - induced psoriasis-like skin inflammation. They reported that both IMQ mice treated with MTX-

loaded MNs (13.8 μg) and oral administration at a double dose (27.6 μg) of MTX exhibited much milder psoriasiform dermatitis whereas oral administration at a same dose with MNs (13.8 μg) failed to exert such protective effects (Figure 17A).

In another study, Korkmaz et al. developed carboxymethyl cellulose-based dissolving MNs containing anti-TNF–α for localized ID delivery to reduce the immunosuppression associated with systemic administration of antibody and related adverse events [211]. The antibody cargo was incorporated in the needle tips using a micromilling/spin-casting fabrication method. The MNs nearly completely dissolved into the human skin explants and reduced the critical biomarkers of psoriasiform inflammation (epidermal thickness and IL-1β expression) in a psoriatic mouse model. The following year, the same group conjugated high molecular weight HA to the anti-TNF-α antibody in the same dissolving MNs to hinder the fast diffusion of antibodies from the target site to other body regions [212]. The high efficiency of this delivery method was assessed in human skin explants without antibody diffusion from the delivery site.

8.2. MN for acne treatment

One of the main causes of acne is inflammatory responses that occur in the sebaceous glands of hair follicles [213]. The proliferation of microorganisms in hair follicles in large quantities, especially *Propionibacterium acnes* (*P. acnes*), results in free fatty acid production, excessive production of reactive oxygen species (ROS), chemotaxis of inflammatory mediators, inflammatory cells, and finally the formation of acne lesions [214]. Therefore, simultaneous inhibiting bacterial growth and suppressing inflammatory responses are essential to achieve a successful acne treatment.

Excessive production of ROS under pathological conditions (more than 500 μM) in inflammatory tissues provides the possibility to design ROS-responsive MNs that are able to

release therapeutic molecules in a sustained manner based on ROS-induced degradation into the acne lesion site [215]. Based on this concept, Zhang *et al*. prepared ROS-responsive MNs containing poly(vinyl alcohol) PVA/ clindamycin (CDM) networks that were loaded into a substrate composed of HA and diatomaceous earth (DE) to improve interactions for the treatment of acne vulgaris, a common inflammatory skin disease caused by colonization of *P. acnes* (Figure 17B) [216]. The use of ROS-responsive MNs highly reduced the number of infiltrated inflammatory cells into the dermis in a P. acnes-induced mouse model while a CDM cream failed to create such protective effects (Figure 17C and 17D).

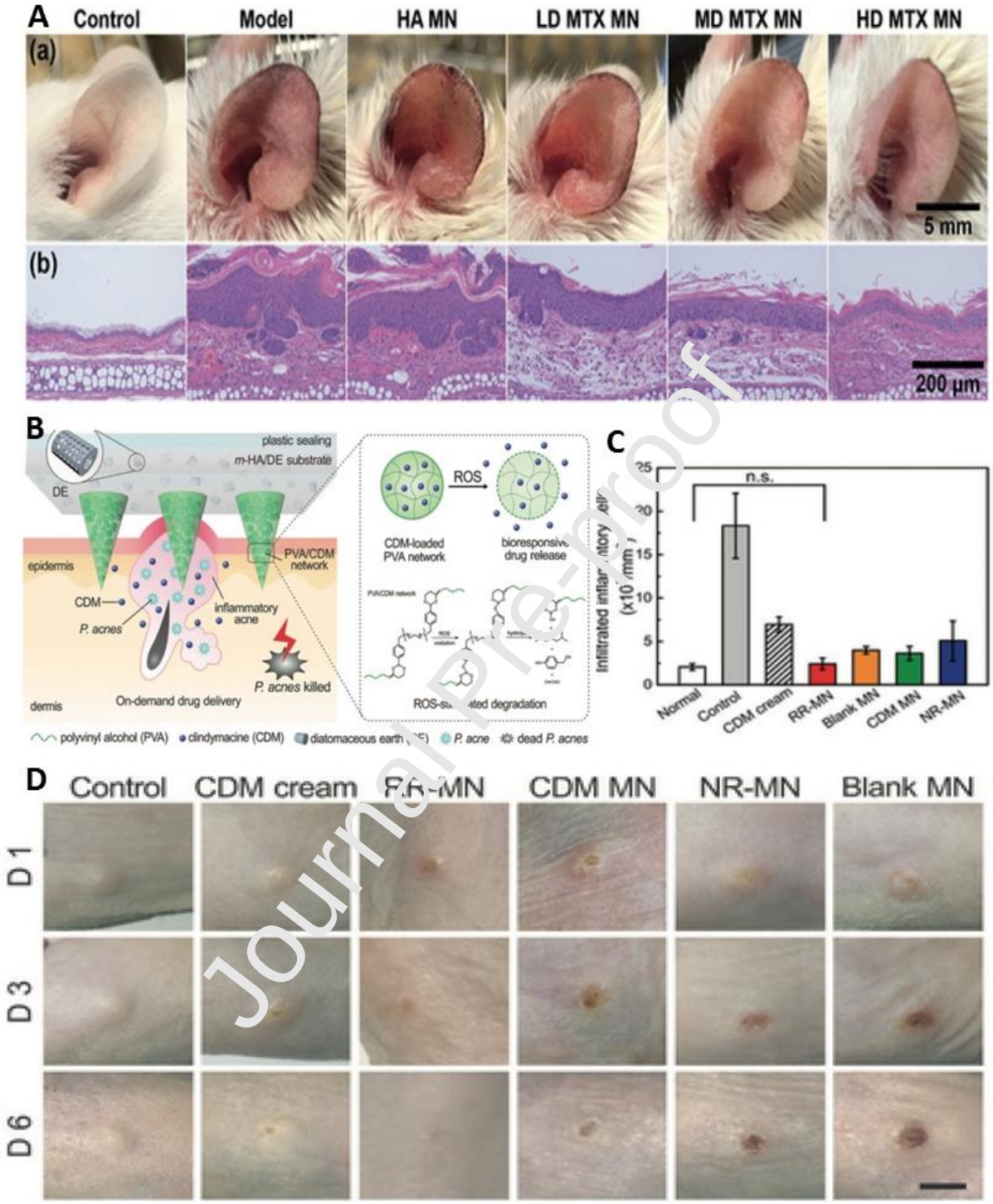

Figure 17. HA-based dissolving MNP loaded with methotrexate for psoriasis treatment. **A)** Comparison between therapeutic effects of MTX-loaded MNs (13.8 μg), oral administration of the same dose (13.8 μg), and a double dose (27.6 μg) of MTX on IMQ-induced psoriasis-like skin inflammation at day 7. **(a)** Representative images of left ear lesions, **(b)** H&E staining. Reproduced with permission from ref.[210], Copyright 2019, American Chemical Society. ROS-responsive MNP for acne vulgaris treatment. **B)** Schematic representation of the fabrication and

proposed mechanism of ROS-responsive MNs containing CDM for the treatment of inflammatory acne vulgaris. The excessive production of ROS under pathological conditions (more than 500 μM) in inflammatory tissues results in the sustained release of drug molecules. **C)** Quantitative analysis of infiltrated inflammatory cells in different groups. Control group: negative control without treatment, CDM cream: treatment with 1 wt-% CDM cream, RR-MN group: ROS-responsive PVA/CDM MN patches, CDM MN group: CDM loading HA MN patches, NR-MN group: Nonresponsive PVA/CDM MN patches and blank MN group: blank MN patches without CDM (CDM dose: 0.4 mg per mouse). There were no significant differences between RR-MN and normal groups. **D)** Representative images indicating the significant reduction in the swelling volume of the RR-MN treated back skin of P. acnes-induced mice on day 6 after MN insertion. Scale bar: 5 mm. Reproduced with permission from ref.[216]; Copyright 2018, Wiley-VCH.

In another interesting example, Zhang *et al*. designed and fabricated an active pharmaceutical ingredient poly (ionic liquid) (API PIL)-based MN patches containing salicylic acid (SA) via photo-crosslinking of an imidazolium-type ionic liquid (IL) monomer in MN micro-molds, and following by anion exchange with SA^- anions [217]. Electrostatic interactions between imidazolium cation and SA anion facilitated loading salicylic acid anions onto PIL-MN. Characterization tests showed that the cross-linked SA-PIL-MN patches possessed high strength (> 0.72 MPa), high stretchability (> 135 % strain), high compressibility (> 60 % strain) and relatively high strength (> 0.45 MPa) (Figure 18A and 18B). SEM images displayed that the bacteria (*P. acnes* and *E. coli*) were rod-like in control, and their surface remained smooth and complete, whereas culturing bacterial suspensions with the PIL-based MNs for 4 h resulted in irregular and unclear edges, atrophy, partial or complete membrane lysis or membrane perforation of the bacteria (Figure 18C). The SEM images further showed that the SA-PIL-MN patches had higher antimicrobial efficacy than only SA or only PIL-MN, mainly attributed to the synergistic activity of PIL and SA moieties against the bacteria. Histological and immunohistochemical analyses further demonstrated that expression of inflammatory cells and factors such as TNF- α, IL-8, and matrix metalloproteinase (MMP) significantly reduced in mice

treated with SA-PIL-MN while only SA or only PIL-MN groups failed to exert noticeable anti-inflammatory effects (Figure 18D and 18E).

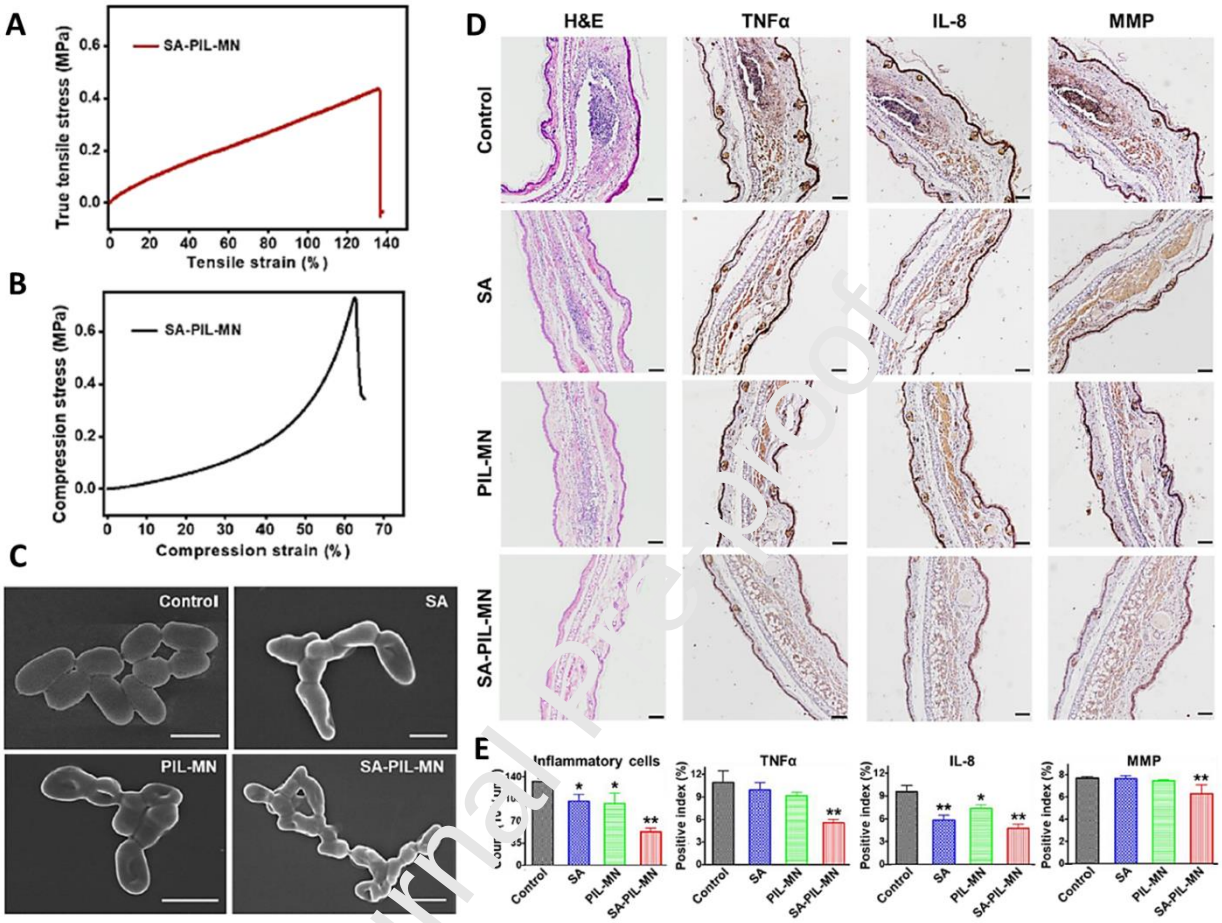

Figure 18. Anti-bacterial and anti-inflammatory effects of SA-loaded PIL-MNs in an acnes mice model. **A)** True tensile stress-strain. **B)** Compression stress-strain. **C)** SEM images showing P. acnes morphological changes in control, SA, PIL-MN, and SA- PIL-MNs for 4 h (scale bar: 1 μm). **D)** H&E and immunohistochemical images displaying tissue damage and the expression of the TNF- α, IL-8, and MMP in P. acnes -infected skin 72 h post-operation in control, SA, PIL-MN, and SA- PIL-MNs treated mice. Scale bar: 100 μm. **E)** The inflammatory cell counts and positive expression values of the TNF- α, IL-8, and MMP in control, SA, PIL-MN, and SA- PIL-MNs groups. Data are expressed as mean ± SD, (n = 3 per group); *P < 0.05, **P < 0.01. Reproduced with permission from ref. [217]; Copyright 2020, Elsevier B.V.

8.3. MN design for atopic dermatitis treatment

Atopic dermatitis (AD) is a common, chronic skin inflammatory disease that is characterized by eczematous lesions and abnormal immune responses [218]. Although detailed acknowledgments

about mechanisms of AD pathogenesis are not completely available, previous studies have shown that AD is associated with an overactive immune system, aggressive response to environmental irritants and allergens, and subsequently causing skin inflammation [219]. The onset and development of AD are associated with T helper type 2 (Th2)-polarized immune responses, including secretion of IL-4, IL-5, and IL-13 [220]. Excessive secretion of pro-inflammatory cytokines creates a sequential chain of events, including stimulating immunoglobulin (Ig) E and IgG1 production by B cells, degranulation of mast cells, histamine release, and initiation of allergic responses [221, 222]. Chen *et al.* developed dissolvable MNs composed of low- and high- molecular-weight (LMW and HMW) poly- γ- glutamate (γ-PGA) using micromolding method with immunomodulatory effects to effectively decrease abnormal immune responses and AD-like symptoms in NC/Nga mice (Figure 19A) [223]. Their results demonstrated that γ-PGA MNs were able to penetrate the epidermis easily and modulate immune responses by releasing γ-PGA into the dendritic cell-rich dermis and its interaction with DCs. Compared to AD control, noticeable reductions of clinical dermatitis scores, epidermal thickness (Figure 19B), and mast cell infiltration (Figure 19C) in treated mice with γ-PGA MNs were found. The protective effects of engineered γ-PGA MNs were attributed to downregulation of IgE and IgG1 levels (Th2-associated antibodies) (Figure 19D-19F). There was no evidence of weight loss or abnormality in the MN-treated mice during the 8-week treatment period. Additionally, the authors found that the MW of γ-PGA highly affected immunomodulatory properties of the engineered MNs.

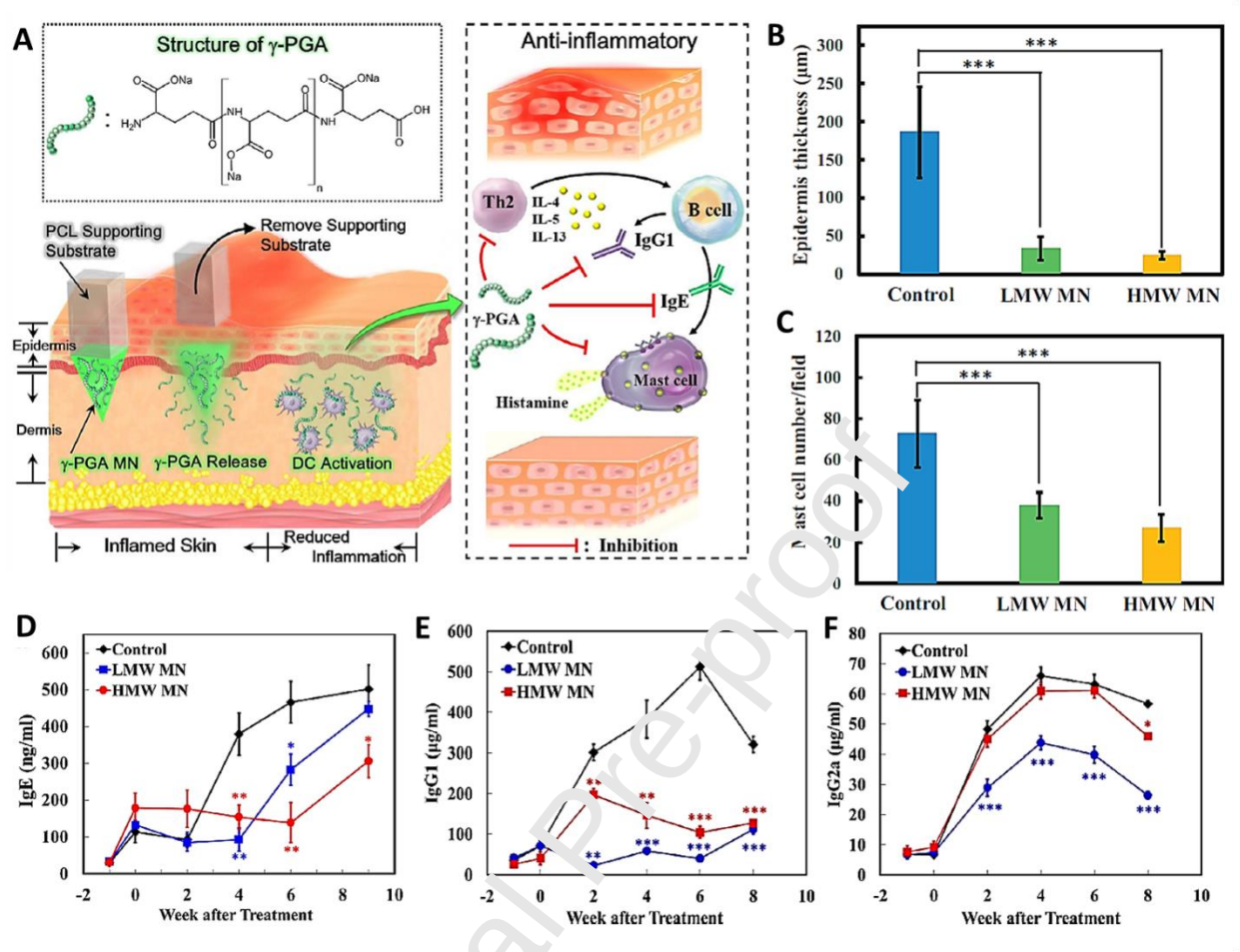

Figure 19. The γ-PGA MNs as transdermal immunomodulators for improving AD symptoms. **A)** Schematic representation of transdermal delivery of γ-PGA MNs for reducing skin inflammation through down-regulation of the IgE and IgG1 (Th2-associated antibodies) and hampering mast cell infiltration. PCL supporting substrate contributes to improving MN penetration by providing a greater length upon insertion, and then it can be quickly removed from the skin when the MN is dissolved within the skin. The dissolved γ-PGA directly confers DCs activation in the dermis, which in turn results in regulating immune responses towards ameliorating atopic dermatitis pathology. **B)** The epidermal thickness, and **C)** Mast cell number obtained from the H&E- and toluidine blue-stained skin sections at Week 8. **D)** Serum IgE, **E)** IgG1, and **F)** IgG2a. The serum levels were measured using ELISA. Data are expressed as the mean ± SD (n = 4 animals per group). *P < 0.05, **P < 0.01, ***P < 0.005 compared with the control group. Reproduced with permission from ref.[223]; Copyright 2020, Elsevier B.V.

A recent study has shown the superiority of AD immunotherapy using MN technology compared to other routes of administration (IM, IP, oral, and SCIT). Kim *et al*. have evaluated the ability of DfE-loaded sodium hyaluronate-based MN patches for the establishment of immunotherapy in

coping with AD [224]. The researchers found that an antigen extract's concentration of 10 μg into the MN patches created similar efficiency to subcutaneous immunotherapy with 100 μg of the antigen extract, as quantified by the improvement of clinical appearance and reduction of eosinophil cell counts, indicating that MN patches possess more substantial immunological efficacy and safety. Thereby, MN patches could be considered as potential candidates for the treatment of AD as they can transport antigen straightly into the epidermis and dermis at a lower dose, hence reducing the risk of anaphylaxis.

8.4. MN for modulation of inflammation during the wound healing process

Inflammation displays a powerful role during the wound healing process. In the first hours after injury, recruitment of inflammatory cells, and releasing different molecules by them contributes to matrix remodeling and keratinocyte migration towards promoting the healing process. After this initial response, which is mainly mediated by neutrophils, elimination of inflammation is essential to accelerate the healing process [225]. To this end, Jeon *et al*. developed a hydrogel-forming double-layered adhesive MN patch comprising of a non-swellable SF-based core (for effective tissue fixation without delamination) and a swellable mussel adhesive protein (MAP)-based shell that was able to improve wound sealing capacity through reduction of inflammatory responses [226]. In this system, in-situ rigid base was comprised of the regenerated SF with improved water solubility that was able to support effective tissue insertion of the adhesive MN patch. The hydrogel-forming adhesive MN patches exhibited good adhesion on wet and dynamic biological surfaces via both MAP-derived surface adhesive and swelling-mediated mechanical interlocking (Figure 20A). Monitoring time-dependent shape changes of various DL-MN patches demonstrated that water absorption of the 20% and 40% DL-MN patches was confined to only

the end of tip region while the base region of 80% DL-MN patches began to swell up due to high amounts of hydrophilic materials (Figure 20B). The authors reported the 80% DL-MN patch for surgical closure owing to detachment of the swollen shell from the core that hampered stable interfacial adhesion. A bud-like shaped MN structure was found for the 60% DL-MN patch at a maximum swollen state that provided the possibility of physical interlocking with surrounding tissues without delamination. *In vivo* experiments in a full-thickness incision of rat skin showed that the strip-type of 60% DL-MN patch showed excellent adhesion liquid absorption ability, which in turn resulted in good wound closure at days 4 and 7 compared to non-treatment and suture (Figure 20C and 20D). Histological examination with H&E-staining indicated that the 60% DL-MN patch contributed to wound closure, re-epithelialization, and reducing inflammation and inflammatory cells into the wound site, whereas prolonged intense inflammation, delayed re-epithelialization, and impaired dermal healing over 21 days was seen for non-treatment group (Figure 20E). Masson's Trichrome staining further confirmed fast deposition of produced collagen at the junction site and reducing inflammatory cells at days 4, 7, 14, and 21 (Figure 20F). The *ex vivo* experiments demonstrated that hydrogel-forming adhesive MN patches had superior wound sealing capacity against luminal leaks (139.7 ± 14.1 mmHg) in comparison with suture (151.0 ± 23.3 mmHg).

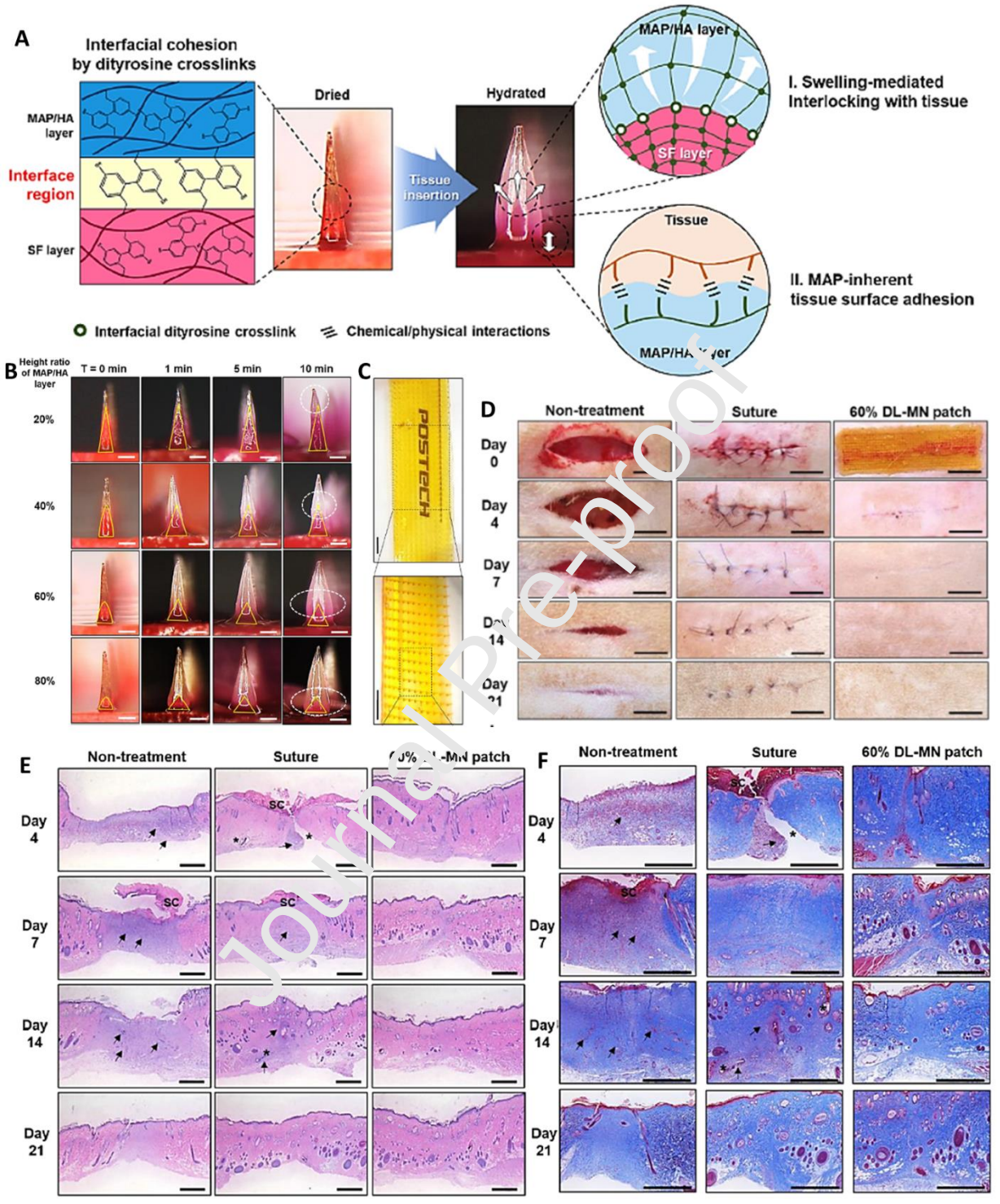

Figure 20. The bioinspired adhesive MN patch for regenerative internal/external surgical closure by modulation of inflammation. **A)** Schematic representation for the proposed working mechanisms of a hydrogel-forming double-layered adhesive MN protein patch comprising of a non-swellable silk fibroin (SF)-based core (for effective tissue fixation without delamination) and a swellable mussel adhesive protein (MAP)-based shell. **B)** Merged images from

fluorescence and bright-field micrographs for investigation of time-dependent shape change of various DL-MN patches with different height ratios of the swellable MAP/HA layer after incubation in PBS at 0, 1, 5, and 10 min. White dashed circles show radial expansion by water absorption, and yellow triangles demonstrate the stiff core layer (scale bar=250 μm). **C)** Photographs of the transparent strip-type 60% DL-MN patch. Scale bar = 2 mm. **D)** Macroscopic photographs for wound healing of full-thickness incisions in rats following after non-treatment, suture treatment, and 60% DL-MN patch treatment at 0,4,7,14, and 21 days. **E)** H&E staining **and F)** Masson's trichrome staining of skin wounds after non-treatment, suture treatment, and 60% DL-MN patch treatment. Scabs are indicated as sc. Black arrows show inflammation, and black stars indicate defects. Scale bar = 500 μm. Reproduced with permission from ref.[226]; Copyright 2019 Elsevier B.V.

In another interesting example, Gao *et al*. engineered an intelligent origami SF MN-structured dressing (i-SMD) with a smart drug release system and capability for epidermal sensing and wound healing (Figure 21A). The authors used temperature-responsive N-isopropylacrylamide (NIPAM) hydrogel and inverse opal (IO) photonic crystals (PCs) to obtain a controllable release of VEGF on the i-SMD. In order to improve the mechanical properties of SF membranes, the SF solution was mixed with PVA solution. Patterned SF-based MNs were fabricated using the micromolding technique. Microfluidic channels and electro circuits were first patterned on the same SF MN and then origami to prepare multifunctional integrated i-SMD. In vivo experiments showed that general wound closure rates were markedly higher in treated mice with VEGF i-SMD than i-SMD and control (without treatment) groups (Figure 21B). Additionally, immunohistochemistry (IHC) staining showed that the secretion of inflammatory factors including IL-6 and TNF-α significantly reduced in VEGF i-SMD group compared to i-SMD and control (without treatment) groups (Figure 21C and 21D).

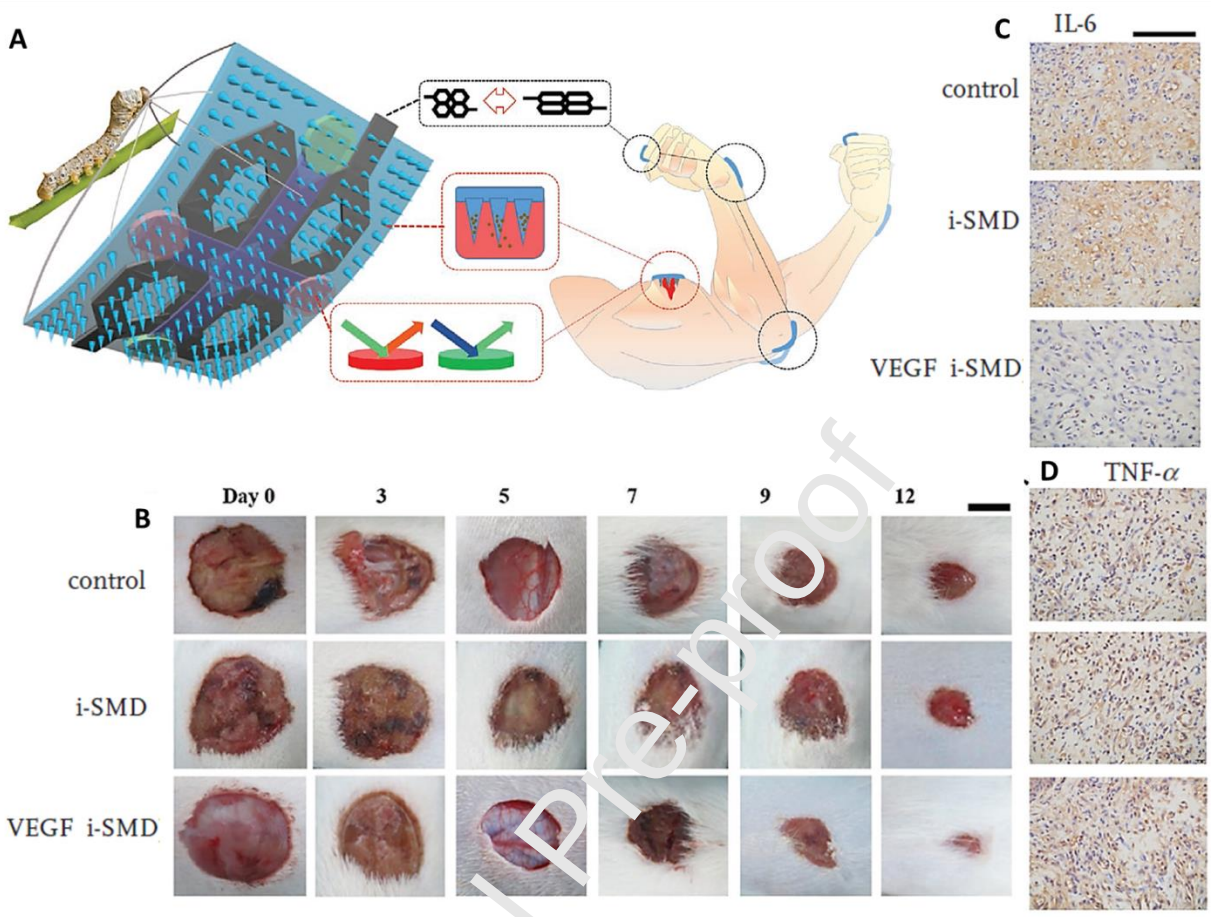

Figure 21. Intelligent SF based MNs dressing (i-SMD) for epidermal sensing and wound healing through modulation of inflammation. **A)** Schematic illustration of intelligent, biocompatible, stretchable, and highly integrated i-SMD for biochemical sensing and wound healing by modulation of inflammation. **B)** Representative images of wound closure rate in the diabetic mice treated with no therapy (control), blank i-SMD, and drug-loaded i-SMD (VEGF i-SMD). Scale bar = 1 cm. **C)** Immunohistochemistry staining of TNF-α and **D)** IL-6. The scale bar = 100μm. Reproduced with permission from ref [227]; Copyright 2020, Wiley-VCH.

10. Conclusions and future perspectives

Although immunotherapy has been proposed as a clinical revolution, it still remains in its infancy. Detailed knowledge about its mechanistic intricacies is still not completely available, limiting the effective treatment of diseases in a safe, potent, and durable fashion by immunoengineering. In addition, the poor biodistribution of many immunotherapies can cause toxicity and adverse effects in off-target tissues. To address these challenges, great efforts have

been made to design MN transdermal delivery systems to locally deliver immunotherapeutic with the highest efficiency and minimal invasiveness. Nevertheless, Concerns regarding the future success of MNs for clinical immunotherapy is totally dependent on FDA approval for novel biomaterials used in this delivery system for MN fabrication. In addition, future developments should take into account some of the current challenges, including the difficulty of precise coating of biomolecules on the MNs and insufficient delivery of therapeutic antigens, allergens, or immunotherapeutic drugs to the desired site.

The improvement of the mechanical properties of MNs is another decisive factor for successful clinical translation and future commercialization. The mechanical characteristics of MN must meet two properties to ensure successful immunotherapy. First, the insertion force should be enough to neglect the skin friction force for the insertion of the MNs before puncturing the skin. Second, the insertion force must be higher than the skin force in order to perforate the skin and create holes in the epidermis/dermis layer. The insertion force strongly depends on thickness, the wall angle, and tip radius. Up to now, in vivo performance and efficiency of MN technology for immunotherapies have been mainly investigated on small animals, such as mice, rats, and rabbits, while the physiology, anatomy, and biomechanics of these animals' skins are different from the human's skin. Future evaluations of MN technology for immunotherapies should be implemented on the body of large animals (e.g., dogs and monkeys), on the excised human's skin models, or even human volunteers. However, the skin properties of each person and even of various parts of the body are different; thereby additional investigation is required to determine the best application areas. Another concern regarding the wide clinical use of MNs is their large-scale production in sterile conditions, which needs a carefully thought setting. The material type for the fabrication of MNs is another substantial issue that needs much attention. Although

hollow and solid MNs fabricated by metals and silicon have mainly been applied in the clinical trial setup to deliver various immunotherapeutic molecules for immunotherapy, the lack of approval for silicon and the possibility of sharp hazardous tip wastes limit their clinical applications. Owing to the increasing interest in the design of biocompatible systems, researchers have recently focused on polymer science to fabricate biocompatible or dissolvable polymeric MNs with minimum side effects. Therefore, it is expected to see a tremendous interest in designing biocompatible and dissolvable MN systems in the near future with current advances in polymer science. We believe future researches should focus on the scaling up of sterile MNs with adequate loading capacity and minimal defects for clinical translation.

Conflict of interest

The authors declare no conflict of interest in the present study.

Acknowledgments

M.-A. Shahbazi acknowledges the financial support from the Academy of Finland (grant no. 317316). H. A. Santos acknowledges the financial support from the HiLIFE Research Funds, the Sigrid Jusélius Foundation, and the Academy of Finland (grant no. 317042).

References

[1] G. Ma, C. Wu, Microneedle, bio-microneedle and bio-inspired microneedle: A review, J Control Release, 251 (2017) 11-23.
[2] S. Bhatnagar, K. Dave, V.V.K. Venuganti, Microneedles in the clinic, J Control Release, 260 (2017) 164-182.
[3] K. van der Maaden, W. Jiskoot, J. Bouwstra, Microneedle technologies for (trans) dermal drug and vaccine delivery, J Control Release, 161 (2012) 645-655.
[4] J. Zhu, X. Zhou, H.J. Kim, M. Qu, X. Jiang, K. Lee, L. Ren, Q. Wu, C. Wang, X. Zhu, Gelatin Methacryloyl Microneedle Patches for Minimally Invasive Extraction of Skin Interstitial Fluid, Small, 16 (2020) 1905910.
[5] A. Ramalheiro, J.L. Paris, B.F. Silva, L.R. Pires, Rapidly dissolving microneedles for the delivery of cubosome-like liquid crystalline nanoparticles with sustained release of rapamycin, Int. J. Pharm. 591 (2020) 119942.
[6] M.S. Arshad, S. Fatima, K. Nazari, R. Ali, M. Farhan, S.A. Muhammad, N. Abbas, A. Hussain, I. Kucuk, M.-W. Chang, Engineering and characterisation of BCG-loaded polymeric microneedles, J Drug Target. (2019) 1-8.
[7] C.B. Chesson, S. Ekpo-Otu, J.J. Endsley, J.S. Rudra, Biomaterials-based vaccination strategies for the induction of CD8+ T cell responses, ACS Biomater. Sci. Eng. 3 (2017) 126-143.
[8] Y.-C. Kim, J.-H. Park, M.R. Prausnitz, Microneedles for drug and vaccine delivery, Adv. Drug Deliv. Rev. 64 (2012) 1547-1568.
[9] H. Chang, M. Zheng, S.W.T. Chew, C. Xu, Advances in the Formulations of Microneedles for Manifold Biomedical Applications, Adv. Mater. Technol. 5 (2020) 1900552.
[10] H.L. Quinn, M.-C. Kearney, A.J. Courtenay, M.T. McCrudden, R.F. Donnelly, The role of microneedles for drug and vaccine delivery, Expert Opin Drug Deliv. 11 (2014) 1769-1780.
[11] J.J. Norman, J.M. Arya, M.A. McClain, P.M. Frew, M.I. Meltzer, M.R. Prausnitz, Microneedle patches: usability and acceptability for self-vaccination against influenza, Vaccine, 32 (2014) 1856-1862.
[12] L. Milling, Y. Zhang, D.J. Irvine, Delivering safer immunotherapies for cancer, Adv. Drug Deliv. Rev. 114 (2017) 79-101.
[13] M.L. Bookstaver, S.J. Tsai, J.S. Bromberg, C.M. Jewell, Improving vaccine and immunotherapy design using biomaterials, Trends Immunol. 39 (2018) 135-150.
[14] R. Zhang, M.M. Billingsley, M.J. Mitchell, Biomaterials for vaccine-based cancer immunotherapy, J Control Release, 292 (2018) 256-276.
[15] M.O. Dellacherie, B.R. Seo, D.J. Mooney, Macroscale biomaterials strategies for local immunomodulation, Nat. Rev. Mater. 4 (2019) 379-397.
[16] M. Rescigno, F. Avogadri, G. Curigliano, Challenges and prospects of immunotherapy as cancer treatment, Biochim Biophys Acta Rev Cancer. 1776 (2007) 108-123.
[17] D.G. McNeel, Prostate cancer immunotherapy, Curr Opin Urol, 17 (2007) 175-181.
[18] R.S. Riley, C.H. June, R. Langer, M.J. Mitchell, Delivery technologies for cancer immunotherapy, Nat. Rev. Drug Discov. 18 (2019) 175-196.
[19] C. Anfray, F. Mainini, F.T. Andón, Nanoparticles for immunotherapy, in: Front. Nanosci. Elsevier, 2020, pp. 265-306.
[20] M. Leone, J. Mönkäre, J. Bouwstra, G. Kersten, Dissolving microneedle patches for dermal vaccination, Pharm. Res. 34 (2017) 2223-2240.

[21] L. Klimek, O. Pfaar, Asher, I.P.T.S. Group, Björkstén, I.P.I.S. Group, Maurer, Jacobsen, P.i. group, Calderon, A comparison of immunotherapy delivery methods for allergen immunotherapy, Expert Rev. Clin. Immunol. 9 (2013) 465-475.
[22] E. Maggi, T cell responses induced by allergen-specific immunotherapy, Clin. Exp. Immunol. 161 (2010) 10-18.
[23] S. Park, Y. Lee, Y.-M. Kwon, Y.-T. Lee, K.-H. Kim, E.-J. Ko, J.H. Jung, M. Song, B. Graham, M.R. Prausnitz, Vaccination by microneedle patch with inactivated respiratory syncytial virus and monophosphoryl lipid A enhances the protective efficacy and diminishes inflammatory disease after challenge, PloS one, 13 (2018) e0205071.
[24] Y.-C. Kim, F.-S. Quan, R.W. Compans, S.-M. Kang, M.R. Prausnitz, Formulation and coating of microneedles with inactivated influenza virus to improve vaccine stability and immunogenicity, J Control Release, 142 (2010) 187-195.
[25] H.W. Yang, L. Ye, X.D. Guo, C. Yang, R.W. Compans, M.R. Prausnitz, Ebola vaccination using a DNA vaccine coated on PLGA-PLL/γPGA nanoparticles administered using a microneedle patch, Adv.Healthcare Mater. 6 (2017) 1600750
[26] W. Li, Z. Liu, F. Fontana, Y. Ding, D. Liu, J.T. Hirvonen, H.A. Santos, Tailoring porous silicon for biomedical applications: from drug delivery to cancer immunotherapy, Adv. Mater. 30 (2018) 1703740.
[27] Y. Li, H. Zhang, R. Yang, Y. Laffitte, U. Schmill, W. Hu, M. Kaddoura, E.J. Blondeel, B. Cui, Fabrication of sharp silicon hollow microneedles by deep-reactive ion etching towards minimally invasive diagnostics, Microsyst. Nanoeng. 5 (2019) 1-11.
[28] M. Rajabi, N. Roxhed, R.Z. Shafagh, T. Haraldson, A.C. Fischer, W.v.d. Wijngaart, G. Stemme, F. Niklaus, Flexible and stretchable microneedle patches with integrated rigid stainless steel microneedles for transdermal biointerfacing, PloS one, 11 (2016) e0166330.
[29] E. Parker, M. Rao, K. Turner, C. Meinhart, N. MacDonald, Bulk micromachined titanium microneedles, J Microelectromech Syst. 16 (2007) 289-295.
[30] S. Lee, W. Jeong, D.J. Beebe, Microfluidic valve with cored glass microneedle for microinjection, Lab Chip. 3 (2003) 164-167.
[31] S. Olhero, E. Lopes, J. Ferreira, Fabrication of ceramic microneedles–The role of specific interactions between processing additives and the surface of oxide particles in Epoxy Gel Casting, J. Eur. Ceram. Soc. 36 (2016) 4131-4140.
[32] S.P. Sullivan, N. Murthy, M.R. Prausnitz, Minimally invasive protein delivery with rapidly dissolving polymer microneedles, Adv. Mater. 20 (2008) 933-938.
[33] P.C. DeMuth, Y. Min, D.J. Irvine, P.T. Hammond, Implantable silk composite microneedles for programmable vaccine release kinetics and enhanced immunogenicity in transcutaneous immunization, Adv.Healthcare Mater. 3 (2014) 47-58.
[34] H. Kathuria, D. Lim, J. Cai, B.G. Chung, L. Kang, Microneedles with Tunable Dissolution Rate, ACS Biomater. Sci. Eng. 6 (2020) 5061-5068.
[35] A.M. Rodgers, A.J. Courtenay, R.F. Donnelly, Dissolving microneedles for intradermal vaccination: manufacture, formulation, and stakeholder considerations, in, Taylor & Francis, 2018. Volume 15, 2018 - Issue 11.
[36] L.Y. Chu, S.-O. Choi, M.R. Prausnitz, Fabrication of dissolving polymer microneedles for controlled drug encapsulation and delivery: bubble and pedestal microneedle designs, J. Pharm. Sci. 99 (2010) 4228-4238.

[37] A. Vrdoljak, M.G. McGrath, J.B. Carey, S.J. Draper, A.V. Hill, C. O'Mahony, A.M. Crean, A.C. Moore, Coated microneedle arrays for transcutaneous delivery of live virus vaccines, J Control Release, 159 (2012) 34-42.
[38] J.B. Carey, F.E. Pearson, A. Vrdoljak, M.G. McGrath, A.M. Crean, P.T. Walsh, T. Doody, C. O'Mahony, A.V. Hill, A.C. Moore, Microneedle array design determines the induction of protective memory CD8+ T cell responses induced by a recombinant live malaria vaccine in mice, PloS one, 6 (2011) e22442.
[39] J.B. Carey, A. Vrdoljak, C. O'mahony, A.V. Hill, S.J. Draper, A.C. Moore, Microneedle-mediated immunization of an adenovirus-based malaria vaccine enhances antigen-specific antibody immunity and reduces anti-vector responses compared to the intradermal route, Sci. Rep. 4 (2014) 6154.
[40] K. Ita, Transdermal delivery of drugs with microneedles: Strategies and outcomes, J Drug Deliv Sci Technol, 29 (2015) 16-23.
[41] K. van der Maaden, H. Yu, K. Sliedregt, R. Zwier, R. Lebeux, M. Oguri, A. Kros, W. Jiskoot, J.A. Bouwstra, Nanolayered chemical modification of silicon surfaces with ionizable surface groups for pH-triggered protein adsorption and release: application to microneedles, J Mater Chem B, 1 (2013) 4466-4477.
[42] R.F. Donnelly, D.I. Morrow, F. Fay, C.J. Scott, S. Abdelghany, R.R.T. Singh, M.J. Garland, A.D. Woolfson, Microneedle-mediated intradermal nanoparticle delivery: potential for enhanced local administration of hydrophobic pre-formed photosensitisers, Photodiagnosis Photodyn Ther, 7 (2010) 222-231.
[43] D. Jung, N.S. Rejinold, J.-E. Kwak, S.-H. Park, Y.-C. Kim, Nano-patterning of a stainless steel microneedle surface to improve the dip-coating efficiency of a DNA vaccine and its immune response, Colloids Surf. B, 159 (2017) 54-61.
[44] H.S. Gill, M.R. Prausnitz, Coated microneedles for transdermal delivery, J Control Release, 117 (2007) 227-237.
[45] H.-J. Choi, B.J. Bondy, D.-G. Yoo, R.W. Compans, S.-M. Kang, M.R. Prausnitz, Stability of whole inactivated influenza virus vaccine during coating onto metal microneedles, J Control Release, 166 (2013) 159-171.
[46] B. Cai, W. Xia, S. Bredenberg, H. Li, H. Engqvist, Bioceramic microneedles with flexible and self-swelling substrate, Eur J Pharm Biopharm, 94 (2015) 404-410.
[47] B. Cai, W. Xia, S. Bredenberg, H. Engqvist, Self-setting bioceramic microscopic protrusions for transdermal drug delivery, J. Mater. Chem. B, 2 (2014) 5992-5998.
[48] M. Verhoeven, S. Bystrova, L. Winnubst, H. Qureshi, T.D. De Gruijl, R.J. Scheper, R. Luttge, Applying ceramic nanoporous microneedle arrays as a transport interface in egg plants and an ex-vivo human skin model, Microelectron. Eng. 98 (2012) 659-662.
[49] H. Vallhov, W. Xia, H. Engqvist, A. Scheynius, Bioceramic microneedle arrays are able to deliver OVA to dendritic cells in human skin, J. Mater. Chem. B, 6 (2018) 6808-6816.
[50] K. Ita, Ceramic microneedles and hollow microneedles for transdermal drug delivery: Two decades of research, J Drug Deliv Sci Technol, 44 (2018) 314-322.
[51] K.A. Moga, L.R. Bickford, R.D. Geil, S.S. Dunn, A.A. Pandya, Y. Wang, J.H. Fain, C.F. Archuleta, A.T. O'Neill, J.M. DeSimone, Rapidly–dissolvable microneedle patches via a highly scalable and reproducible soft lithography approach, Adv. Mater. 25 (2013) 5060-5066.
[52] A.A. Ali, C.M. McCrudden, J. McCaffrey, J.W. McBride, G. Cole, N.J. Dunne, T. Robson, A. Kissenpfennig, R.F. Donnelly, H.O. McCarthy, DNA vaccination for cervical cancer; a novel

technology platform of RALA mediated gene delivery via polymeric microneedles, Nanomedicine, 13 (2017) 921-932.
[53] K.J. Koh, Y. Liu, S.H. Lim, X.J. Loh, L. Kang, C.Y. Lim, K.K. Phua, Formulation, characterization and evaluation of mRNA-loaded dissolvable polymeric microneedles (RNApatch), Sci. Rep. 8 (2018) 1-11.
[54] G. Cole, J. McCaffrey, A.A. Ali, J.W. McBride, C.M. McCrudden, E.M. Vincente-Perez, R.F. Donnelly, H.O. McCarthy, Dissolving microneedles for DNA vaccination: Improving functionality via polymer characterization and RALA complexation, Hum Vaccin Immunother, 13 (2017) 50-62.
[55] Y. Li, X. Hu, Z. Dong, Y. Chen, W. Zhao, Y. Wang, L. Zhang, M. Chen, C. Wu, Q. Wang, Dissolving Microneedle Arrays with Optimized Needle Geometry for Transcutaneous Immunization, Eur J Pharm Sci, (2020) 105361.
[56] J. Mönkäre, M.R. Nejadnik, K. Baccouche, S. Romeijn, W. Jiskoot, J.A. Bouwstra, IgG-loaded hyaluronan-based dissolving microneedles for intradermal protein delivery, J Control Release, 218 (2015) 53-62.
[57] M.-C. Chen, S.-F. Huang, K.-Y. Lai, M.-H. Ling, Fully embeddable chitosan microneedles as a sustained release depot for intradermal vaccination, Biomaterials, 34 (2013) 3077-3086.
[58] M. Zaric, O. Lyubomska, O. Touzelet, C. Poux, S. Al-Zahrani, F. Fay, L. Wallace, D. Terhorst, B. Malissen, S. Henri, Skin dendritic cell targeting via microneedle arrays laden with antigen-encapsulated poly-D, L-lactide-co-glycolide nanoparticles induces efficient antitumor and antiviral immune responses, ACS nano, 7 (2013) 2042-2055.
[59] S. Kommareddy, B.C. Baudner, S. Oh, S.-y. Kwon, M. Singh, D.T. O'hagan, Dissolvable microneedle patches for the delivery of cell-culture-derived influenza vaccine antigens, J. Pharm. Sci. 101 (2012) 1021-1027.
[60] S.C. Balmert, C.D. Carey, G.D. Falo, S.K. Sethi, G. Erdos, E. Korkmaz, L.D. Falo Jr, Dissolving undercut microneedle arrays for multicomponent cutaneous vaccination, J Control Release, 317 (2020) 336-346.
[61] J.W. Lee, J.-H. Park, M.R. Prausnitz, Dissolving microneedles for transdermal drug delivery, Biomaterials, 29 (2008) 2113-2124.
[62] M.S. Arshad, S. Fatima, K. Nazari, R. Ali, M. Farhan, S.A. Muhammad, N. Abbas, A. Hussain, I. Kucuk, M.-W. Chang, Engineering and characterisation of BCG-loaded polymeric microneedles, J Drug Target, 28 (2020) 525-532.
[63] Y.K. Demir, Z. Akan, O. Kerimoglu, Characterization of polymeric microneedle arrays for transdermal drug delivery, PloS one, 8 (2013) e77289.
[64] P.C. DeMuth, W.F. Garcia-Beltran, M.L. Ai-Ling, P.T. Hammond, D.J. Irvine, Composite dissolving microneedles for coordinated control of antigen and adjuvant delivery kinetics in transcutaneous vaccination, Adv. Funct. Mater. 23 (2013) 161-172.
[65] H.-J. Choi, D.-G. Yoo, B.J. Bondy, F.-S. Quan, R.W. Compans, S.-M. Kang, M.R. Prausnitz, Stability of influenza vaccine coated onto microneedles, Biomaterials, 33 (2012) 3756-3769.
[66] Y.-C. Kim, D.-G. Yoo, R.W. Compans, S.-M. Kang, M.R. Prausnitz, Cross-protection by co-immunization with influenza hemagglutinin DNA and inactivated virus vaccine using coated microneedles, J Control Release, 172 (2013) 579-588.
[67] P.C. DeMuth, Y. Min, B. Huang, J.A. Kramer, A.D. Miller, D.H. Barouch, P.T. Hammond, D.J. Irvine, Polymer multilayer tattooing for enhanced DNA vaccination, Nat. Mater. 12 (2013) 367-376.

[68] G.J. Fernando, J. Hickling, C.M.J. Flores, P. Griffin, C.D. Anderson, S.R. Skinner, C. Davies, K. Witham, M. Pryor, J. Bodle, Safety, tolerability, acceptability and immunogenicity of an influenza vaccine delivered to human skin by a novel high-density microprojection array patch (Nanopatch™), Vaccine, 36 (2018) 3779-3788.
[69] P. Griffin, S. Elliott, K. Krauer, C. Davies, S.R. Skinner, C.D. Anderson, A. Forster, Safety, acceptability and tolerability of uncoated and excipient-coated high density silicon micro-projection array patches in human subjects, Vaccine, 35 (2017) 6676-6684.
[70] G. Icardi, A. Orsi, A. Ceravolo, F. Ansaldi, Current evidence on intradermal influenza vaccines administered by Soluvia™ licensed micro injection system, Hum. Vaccines Immunother. 8 (2012) 67-75.
[71] Y. Levin, E. Kochba, I. Hung, R. Kenney, Intradermal vaccination using the novel microneedle device MicronJet600: Past, present, and future, Hum. Vaccines Immunother. 11 (2015) 991-997.
[72] S.B. Troy, D. Kouiavskaia, J. Siik, E. Kochba, H. Beydoun, O. Mirochnitchenko, Y. Levin, N. Khardori, K. Chumakov, Y. Maldonado, Comparison of the immunogenicity of various booster doses of inactivated polio vaccine delivered intradermally versus intramuscularly to HIV-infected adults, J. Infect. Dis. 211 (2015) 1969-1976.
[73] L.Y. Chu, M.R. Prausnitz, Separable arrowhead microneedles, J Control Release, 149 (2011) 242-249.
[74] T. Liu, G. Luo, M. Xing, Biomedical Applications of Polymeric Microneedles for Transdermal Therapeutic Delivery and Diagnosis. Current Status and Future Perspectives, Adv. Ther. 3 (2020) 1900140.
[75] N.G. Rouphael, M. Paine, R. Mosley, S. Henry, D.V. McAllister, H. Kalluri, W. Pewin, P.M. Frew, T. Yu, N.J. Thornburg, The safety, immunogenicity, and acceptability of inactivated influenza vaccine delivered by microneedle patch (TIV-MNP 2015): a randomised, partly blinded, placebo-controlled, phase 1 trial, The Lancet, 390 (2017) 649-658.
[76] S. Hirobe, H. Azukizawa, K. Matsuo, Y. Zhai, Y.-S. Quan, F. Kamiyama, H. Suzuki, I. Katayama, N. Okada, S. Nakagawa, Development and clinical study of a self-dissolving microneedle patch for transcutaneous immunization device, Pharm. Res. 30 (2013) 2664-2674.
[77] S. Hirobe, H. Azukizawa, T. Hanafusa, K. Matsuo, Y.-S. Quan, F. Kamiyama, I. Katayama, N. Okada, S. Nakagawa, Clinical study and stability assessment of a novel transcutaneous influenza vaccination using a dissolving microneedle patch, Biomaterials, 57 (2015) 50-58.
[78] J. Arya, S. Henry, H. Kalluri, D.V. McAllister, W.P. Pewin, M.R. Prausnitz, Tolerability, usability and acceptability of dissolving microneedle patch administration in human subjects, Biomaterials, 128 (2017) 1-7.
[79] A.S. Rzhevskiy, T.R.R. Singh, R.F. Donnelly, Y.G. Anissimov, Microneedles as the technique of drug delivery enhancement in diverse organs and tissues, J Control Release, 270 (2018) 184-202.
[80] S. Mitragotri, P.A. Burke, R. Langer, Overcoming the challenges in administering biopharmaceuticals: formulation and delivery strategies, Nat. Rev. Drug Discov. 13 (2014) 655-672.
[81] A.P. Chapman, PEGylated antibodies and antibody fragments for improved therapy: a review, Adv. Drug Deliv. Rev. 54 (2002) 531-545.
[82] Y.-H. Chen, K.-Y. Lai, Y.-H. Chiu, Y.-W. Wu, A.-L. Shiau, M.-C. Chen, Implantable microneedles with an immune-boosting function for effective intradermal influenza vaccination, Acta Biomater. 97 (2019) 230-238.

[83] D. Mittal, M.M. Gubin, R.D. Schreiber, M.J. Smyth, New insights into cancer immunoediting and its three component phases—elimination, equilibrium and escape, Curr. Opin. Immunol. 27 (2014) 16-25.
[84] J. Liu, R. Zhang, Z.P. Xu, Nanoparticle-Based Nanomedicines to Promote Cancer Immunotherapy: Recent Advances and Future Directions, Small, 15 (2019) 1900262.
[85] Y. Cao, X. Wang, T. Jin, Y. Tian, C. Dai, C. Widarma, R. Song, F. Xu, Immune checkpoint molecules in natural killer cells as potential targets for cancer immunotherapy, Signal Transduct Target Ther, 5 (2020) 1-19.
[86] H.Y. Yoon, S.T. Selvan, Y. Yang, M.J. Kim, D.K. Yi, I.C. Kwon, K. Kim, Engineering nanoparticle strategies for effective cancer immunotherapy, Biomaterials, 178 (2018) 597-607.
[87] G. Prendergast, Immune escape as a fundamental trait of cancer: focus on IDO, Oncogene, 27 (2008) 3889-3900.
[88] P. Terness, J.-J. Chuang, G. Opelz, The immunoregulatory role of IDO-producing human dendritic cells revisited, Trends Immunol. 27 (2006) 68-73.
[89] A.L. Mellor, D.H. Munn, IDO expression by dendritic cells: tolerance and tryptophan catabolism, Nat. Rev. Immunol. 4 (2004) 762-774.
[90] B. Ricciuti, G.C. Leonardi, P. Puccetti, F. Fallarino, V. Bianconi, A. Sahebkar, S. Baglivo, R. Chiari, M. Pirro, Targeting indoleamine-2, 3-dioxygenase in cancer: Scientific rationale and clinical evidence, Pharmacol. Ther. 196 (2019) 105-116.
[91] G.C. Prendergast, W.P. Malachowski, J.B. DuHadaway, A.J. Muller, Discovery of IDO1 inhibitors: from bench to bedside, Cancer Res. 77 (2017) 6795-6811.
[92] M. Chen, G. Quan, T. Wen, P. Yang, W. Qin, H. Mai, Y. Sun, C. Lu, X. Pan, C. Wu, Cold to Hot: Binary Cooperative Microneedle Array Amplified Photo-Immunotherapy for Eliciting Antitumor Immunity and Abscopal Effect, ACS Appl. Mater.Interfaces. 12 (2020) 32259–32269.
[93] N. Frydenlund, M. Mahalingam, PD-L1 and immune escape: insights from melanoma and other lineage-unrelated malignancies, Hum. Pathol. 66 (2017) 13-33.
[94] J.A. Seidel, A. Otsuka, K. Kabashima, Anti-PD-1 and anti-CTLA-4 therapies in cancer: mechanisms of action, efficacy, and limitations, Front. oncol. 8 (2018) 86.
[95] H.O. Alsaab, S. Sau, R. Alzhrani, K. Tatiparti, K. Bhise, S.K. Kashaw, A.K. Iyer, PD-1 and PD-L1 checkpoint signaling inhibition for cancer immunotherapy: mechanism, combinations, and clinical outcome, Front. Pharmacol. 8 (2017) 561.
[96] L. Spain, S. Diem, J. Larkin, Management of toxicities of immune checkpoint inhibitors, Cancer Treat Rev, 44 (2016) 51-60.
[97] R.W. Jenkins, D.A. Barbie, K.T. Flaherty, Mechanisms of resistance to immune checkpoint inhibitors, Br J Cancer, 118 (2018) 9-16.
[98] C. Wang, Y. Ye, G.M. Hochu, H. Sadeghifar, Z. Gu, Enhanced cancer immunotherapy by microneedle patch-assisted delivery of anti-PD1 antibody, Nano Lett. 16 (2016) 2334-2340.
[99] G. Chen, Z. Chen, D. Wen, Z. Wang, H. Li, Y. Zeng, G. Dotti, R.E. Wirz, Z. Gu, Transdermal cold atmospheric plasma-mediated immune checkpoint blockade therapy, Proc. Natl. Acad. Sci. U.S.A. 117 (2020) 3687-3692.
[100] W. Fan, B. Yung, P. Huang, X. Chen, Nanotechnology for multimodal synergistic cancer therapy, Chem. Rev. 117 (2017) 13566-13638.
[101] Y. Ye, J. Wang, Q. Hu, G.M. Hochu, H. Xin, C. Wang, Z. Gu, Synergistic transcutaneous immunotherapy enhances antitumor immune responses through delivery of checkpoint inhibitors, ACS nano, 10 (2016) 8956-8963.

[102] E. Bracho-Sanchez, A. Hassanzadeh, M.A. Brusko, M.A. Wallet, B.G. Keselowsky, Dendritic Cells Treated with Exogenous Indoleamine 2,3-Dioxygenase Maintain an Immature Phenotype and Suppress Antigen-specific T cell Proliferation, J Immunol Regen Med, 5 (2019) 100015.
[103] L. Brochez, I. Chevolet, V. Kruse, The rationale of indoleamine 2,3-dioxygenase inhibition for cancer therapy, Eur J Cancer, 76 (2017) 167-182.
[104] G. Yao, G. Quan, S. Lin, T. Peng, Q. Wang, H. Ran, H. Chen, Q. Zhang, L. Wang, X. Pan, Novel dissolving microneedles for enhanced transdermal delivery of levonorgestrel: In vitro and in vivo characterization, Int. J. Pharm. 534 (2017) 378-386.
[105] Q. Wang, G. Yao, P. Dong, Z. Gong, G. Li, K. Zhang, C. Wu, Investigation on fabrication process of dissolving microneedle arrays to improve effective needle drug distribution, Eur J Pharm Sci, 66 (2015) 148-156.
[106] P. Yang, C. Lu, W. Qin, M. Chen, G. Quan, H. Liu, L. Wang, X. Bai, X. Pan, C. Wu, Construction of a Core-shell Microneedle System to Achieve Targeted Co-delivery of Checkpoint Inhibitors for Melanoma Immunotherapy, Acta Biomater.104 (2020) 147-157.
[107] X. Lan, W. Zhu, X. Huang, Y. Yu, H. Xiao, L. Jin, J. Fu, X. Xie, J. She, V.W.Y. Lui, Microneedles loaded with anti-PD-1–cisplatin nanoparticles for synergistic cancer immuno-chemotherapy, Nanoscale, 12 (2020) 18885-18898.
[108] T. Yang, D. Huang, C. Li, D. Zhao, J. Li, M. Zhang, Y. Chen, Q. Wang, Z. Liang, X.-J. Liang, Rolling microneedle electrode array (RoMEA) empowered nucleic acid delivery and cancer immunotherapy, Nano Today, 36 (2021) 101017.
[109] Z. Zhou, J. Pang, X. Wu, W. Wu, X. Chen, M. Kong, Reverse immune suppressive microenvironment in tumor draining lymph nodes to enhance anti-PD1 immunotherapy via nanovaccine complexed microneedle, Nano Res. (2020) 1-10.
[110] Z.S. Dunn, J. Mac, P. Wang, T Cell Immunotherapy Enhanced by Designer Biomaterials, Biomaterials, (2019) 119265.
[111] N.L. Syn, M.W. Teng, T.S. Mok, R.A. Soo, De-novo and acquired resistance to immune checkpoint targeting, Lancet Oncol. 18 (2017) e731-e741.
[112] D.Y. Oh, J. Cham, L. Zhang, G. Fong, S.S. Kwek, M. Klinger, M. Faham, L. Fong, Immune Toxicities Elicted by CTLA-4 Blockade in Cancer Patients Are Associated with Early Diversification of the T-cell Repertoire, Cancer Res, 77 (2017) 1322-1330.
[113] S. Kwon, F.C. Velasquez, J.C. Rasmussen, M.R. Greives, K.D. Turner, J.R. Morrow, W.-J. Hwu, R.F. Ross, S. Zhang, E.M. Sevick-Muraca, Nanotopography-based lymphatic delivery for improved anti-tumor responses to checkpoint blockade immunotherapy, Theranostics, 9 (2019) 8332.
[114] S.-X. Chen, M. Ma, F. Xue, S. Shen, Q. Chen, Y. Kuang, K. Liang, X. Wang, H. Chen, Construction of microneedle-assisted co-delivery platform and its combining photodynamic/immunotherapy, J Control Release, 324 (2020) 218-227.
[115] B. Yang, J. Jeang, A. Yang, T.C. Wu, C.-F. Hung, DNA vaccine for cancer immunotherapy, Hum. Vaccines Immunother. 10 (2014) 3153-3164.
[116] M. Lim, A.Z.M. Badruddoza, J. Firdous, M. Azad, A. Mannan, T.A. Al-Hilal, C.-S. Cho, M.A. Islam, Engineered Nanodelivery Systems to Improve DNA Vaccine Technologies, Pharmaceutics, 12 (2020) 30.
[117] G. Cole, A.A. Ali, E. McErlean, E.J. Mulholland, A. Short, C.M. McCrudden, J. McCaffrey, T. Robson, V.L. Kett, J.A. Coulter, DNA vaccination via RALA nanoparticles in a

microneedle delivery system induces a potent immune response against the endogenous prostate cancer stem cell antigen, Acta Biomater. 96 (2019) 480-490.
[118] G. Cole, A.A. Ali, C.M. McCrudden, J.W. McBride, J. McCaffrey, T. Robson, V.L. Kett, N.J. Dunne, R.F. Donnelly, H.O. McCarthy, DNA vaccination for cervical cancer: Strategic optimisation of RALA mediated gene delivery from a biodegradable microneedle system, Eur J Pharm Biopharm, 127 (2018) 288-297.
[119] T.L. Nguyen, Y. Yin, Y. Choi, J.H. Jeong, J. Kim, Enhanced Cancer DNA Vaccine via Direct Transfection to Host Dendritic Cells Recruited in Injectable Scaffolds, ACS nano, 14 (2020) 11623-11636.
[120] J. Xu, B. Xu, J. Tao, Y. Yang, Y. Hu, Y. Huang, Microneedle-Assisted, DC-Targeted Codelivery of pTRP-2 and Adjuvant of Paclitaxel for Transcutaneous Immunotherapy, Small, 13 (2017) 1700666.
[121] H.T.T. Duong, N.W. Kim, T. Thambi, V.G. Phan, M.S. Lee, Y. Yin, J.H. Jeong, D.S. Lee, Microneedle arrays coated with charge reversal pH-sensitive copolymers improve antigen presenting cells-homing DNA vaccine delivery and immune responses, J Control Release, 269 (2018) 225-234.
[122] H.T.T. Duong, Y. Yin, T. Thambi, T.L. Nguyen, V.G. Phan, M.S. Lee, J.E. Lee, J. Kim, J.H. Jeong, D.S. Lee, Smart vaccine delivery based on microneedle arrays decorated with ultra-pH-responsive copolymers for cancer immunotherapy, Biomaterials, 185 (2018) 13-24.
[123] H.T.T. Duong, Y. Yin, T. Thambi, B.S. Kim, J.H. Jeong, D.S. Lee, Highly potent intradermal vaccination by an array of dissolving microneedle polypeptide cocktail for cancer immunotherapy, J. Mater. Chem. B, 8 (2020) 1171-1181.
[124] C.E. Boone, C. Wang, M.A. Lopez-Ramirez, V. Beiss, S. Shukla, P.L. Chariou, D. Kupor, R. Rueda, J. Wang, N.F. Steinmetz, Active Microneedle Administration of Plant Virus Nanoparticles for Cancer In Situ Vaccination Improves Immunotherapeutic Efficacy, ACS Appl. Nano Mater. 3 (2020) 8037-8051.
[125] L.L. Colombo, S.I. Vanzulli, A. Blázquez-Castro, C.S. Terrero, J.C. Stockert, Photothermal effect by 808-nm laser irradiation of melanin: a proof-of-concept study of photothermal therapy using B16-F10 melanotic melanoma growing in BALB/c mice, Biomed. Opt. Express, 10 (2019) 2932-2941.
[126] Y. Ye, C. Wang, X. Zhang, Q. Hu, Y. Zhang, Q. Liu, D. Wen, J. Milligan, A. Bellotti, L. Huang, A melanin-mediated cancer immunotherapy patch, Sci. Immunol, 2 (2017) eaan5692.
[127] S.-J. Lee, H.-S. Lee, Y.-H. Hwang, J.-J. Kim, K.-Y. Kang, S.J. Kim, H.K. Kim, J.D. Kim, D.H. Jeong, M.-J. Paik, Enhanced anti-tumor immunotherapy by dissolving microneedle patch loaded ovalbumin, PloS one, 14 (2019) e0220382.
[128] N.W. Kim, S.-Y. Kim, J.E. Lee, Y. Yin, J.H. Lee, S.Y. Lim, E.S. Kim, H.T.T. Duong, H.K. Kim, S. Kim, Enhanced cancer vaccination by in situ nanomicelle-generating dissolving microneedles, ACS nano, 12 (2018) 9702-9713.
[129] N. Kohli, P. Sawadkar, S. Ho, V. Sharma, M. Snow, S. Powell, M.A. Woodruff, L. Hook, E. García-Gareta, Pre-screening the intrinsic angiogenic capacity of biomaterials in an optimised ex ovo chorioallantoic membrane model, J. Tissue Eng. 11 (2020) 2041731420901621-2041731420901621.
[130] R. Fertig, A. Gamret, J. Cervantes, A. Tosti, Microneedling for the treatment of hair loss?, J Eur Acad Dermatol Venereol, 32 (2018) 564-569.

[131] P. Shende, M. Salunke, Transepidermal microneedles for co-administration of folic acid with methotrexate in the treatment of rheumatoid arthritis, Biomed. Phys. Eng. Express, 5 (2019) 025023.
[132] D.M. Goldenberg, W.A. Wegener, Subcutaneous administration of anti-CD74 antibody for systemic lupus erythematosus, in, Google Patents, 2019.
[133] C. Giorgio, G. Babino, S. Caccavale, T. Russo, A. De Rosa, R. Alfano, E. Fulgione, G. Argenziano, Combination of photodynamic therapy with 5-aminolaevulinic acid and microneedling in the treatment of alopecia areata resistant to conventional therapies: our experience with 41 patients, Clin Exp Dermatol, 45 (2020) 323-326.
[134] T. Zhang, X.-y. Qin, X. Cao, W.-h. Li, T. Gong, Z.-r. Zhang, Thymopentin-loaded phospholipid-based phase separation gel with long-lasting immunomodulatory effects: in vitro and in vivo studies, Acta Pharmacol. Sin. 40 (2019) 514-521.
[135] S. Lin, B. Cai, G. Quan, T. Peng, G. Yao, C. Zhu, Q. Wu, H. Ran, X. Pan, C. Wu, Novel strategy for immunomodulation: Dissolving microneedle array encapsulating thymopentin fabricated by modified two-step molding technology, Eur J Pharm Biopharm, 122 (2018) 104-112.
[136] Z. Ahmad, M.I. Khan, M.I. Siddique, H.S. Sarwar, G. Shahnaz, S.Z. Hussain, N.I. Bukhari, I. Hussain, M.F. Sohail, Fabrication and Characterization of Thiolated Chitosan Microneedle Patch for Transdermal Delivery of Tacrolimus, AAPS PharmSciTech, 21 (2020) 1-12.
[137] B.O. Roep, D.C. Wheeler, M. Peakman, Antigen-based immune modulation therapy for type 1 diabetes: the era of precision medicine, Lancet Diabetes Endocrinol. 7 (2019) 65-74.
[138] R.J. Creusot, J. Postigo-Fernandez, N. Teteloshvili, Altered function of antigen-presenting cells in type 1 diabetes: a challenge for antigen-specific immunotherapy?, Diabetes, 67 (2018) 1481-1494.
[139] X. Zhao, J.C. Birchall, S.A. Coulman, D. Tatovic, R.K. Singh, L. Wen, F.S. Wong, C.M. Dayan, S.J. Hanna, Microneedle delivery of autoantigen for immunotherapy in type 1 diabetes, J Control Release, 223 (2016) 178-187.
[140] M. Dul, T. Nikolic, M. Stefanidou, M. McAteer, P. Williams, J. Mous, B. Roep, E. Kochba, Y. Levin, M. Peakman, Conjugation of a peptide autoantigen to gold nanoparticles for intradermally administered antigen specific immunotherapy, Int. J. Pharm. 562 (2019) 303-312.
[141] M. So, C.M. Elso, F. Tresoldi, M. Pakusch, V. Pathiraja, J.M. Wentworth, L.C. Harrison, B. Krishnamurthy, H.E. Thomas, C. Rodda, Proinsulin C-peptide is an autoantigen in people with type 1 diabetes, Proc. Natl. Acad. Sci. U.S.A. 115 (2018) 10732-10737.
[142] F. Arikat, S.J. Hanna, R.K. Singh, L. Vilela, F.S. Wong, C.M. Dayan, S.A. Coulman, J.C. Birchall, Targeting proinsulin to local immune cells using an intradermal microneedle delivery system; a potential antigen-specific immunotherapy for type 1 diabetes, J Control Release, 322 (2020) 593-601.
[143] R.F. Donnelly, T.R.R. Singh, M.M. Tunney, D.I. Morrow, P.A. McCarron, C. O'Mahony, A.D. Woolfson, Microneedle arrays allow lower microbial penetration than hypodermic needles in vitro, Pharm. Res. 26 (2009) 2513-2522.
[144] J. Gupta, H.S. Gill, S.N. Andrews, M.R. Prausnitz, Kinetics of skin resealing after insertion of microneedles in human subjects, J Control Release, 154 (2011) 148-155.
[145] L. Wei-Ze, H. Mei-Rong, Z. Jian-Ping, Z. Yong-Qiang, H. Bao-Hua, L. Ting, Z. Yong, Super-short solid silicon microneedles for transdermal drug delivery applications, Int. J. Pharm. 389 (2010) 122-129.

[146] S. Li, W. Li, M. Prausnitz, Individually coated microneedles for co-delivery of multiple compounds with different properties, Drug Deliv. Transl. Res. 8 (2018) 1043-1052.
[147] G.S. Firestein, I.B. McInnes, Immunopathogenesis of rheumatoid arthritis, Immunity, 46 (2017) 183-196.
[148] F.M. Meier, M. Frerix, W. Hermann, U. Muller-Ladner, Current immunotherapy in rheumatoid arthritis, Immunotherapy, 5 (2013) 955-974.
[149] E. Larraneta, R.E. Lutton, A.D. Woolfson, R.F. Donnelly, Microneedle arrays as transdermal and intradermal drug delivery systems: Materials science, manufacture and commercial development, Mater. Sci. Eng. R Rep. 104 (2016) 1-32.
[150] W. Yao, C. Tao, J. Zou, H. Zheng, J. Zhu, Z. Zhu, J. Zhu, L. Liu, F. Li, X. Song, Flexible two-layer dissolving and safing microneedle transdermal of neurotoxin: A biocomfortable attempt to treat Rheumatoid Arthritis, Int. J. Pharm. 563 (2019) 91-100.
[151] S. Thakur, B. Riyaz, A. Patil, A. Kaur, B. Kapoor, V. Mishra, Novel drug delivery systems for NSAIDs in management of rheumatoid arthritis: An overview, Biomed. Pharmacother. 106 (2018) 1011-1023.
[152] S. Amodwala, P. Kumar, H.P. Thakkar, Statistically optimized fast dissolving microneedle transdermal patch of meloxicam: a patient friendly approach to manage arthritis, Eur J Pharm Sci, 104 (2017) 114-123.
[153] J. Chen, W. Huang, Z. Huang, S. Liu, Y. Ye, G. Li, M. Huang, Fabrication of tip-dissolving microneedles for transdermal drug delivery of meloxicam, AAPS PharmSciTech, 19 (2018) 1141-1151.
[154] J. Cao, N. Zhang, Z. Wang, J. Su, J. Yang, J. Han, Y. Zhao, Microneedle-Assisted Transdermal Delivery of Etanercept for Rheumatoid Arthritis Treatment, Pharmaceutics, 11 (2019) 235.
[155] Y. Qiu, C. Li, S. Zhang, G. Yang, M. He, Y. Gao, Systemic delivery of artemether by dissolving microneedles, Int. J. Pharm. 508 (2016) 1-9.
[156] X. Chen, X. Zhu, T. Xu, M. Xu, Y. Wen, Y. Liu, J. Liu, X. Qin, Targeted hexagonal Pd nanosheet combination therapy for rheumatoid arthritis via the photothermal controlled release of MTX, J. Mater. Chem. B, 7 (2019) 112-122.
[157] K. Yu, X. Yu, S. Cao, Y. Wang, Y. Zhai, F. Yang, X. Yang, Y. Lu, C. Wu, Y. Xu, Layered dissolving microneedles as a seed-based delivery system to simultaneously alleviate skin and joint lesions in psoriatic arthritis, Acta Pharm. Sin. B. (2020).
[158] M. Zhao, J. Bai, Y. Lu, S. Du, K. Shang, P. Li, L. Yang, B. Dong, N. Tan, Anti-arthritic effects of microneedling with bee venom gel, J. Tradit. Chinese Medical Sci. 3 (2016) 256-262.
[159] G. Chen, B. Hao, D. Ju, M. Liu, H. Zhao, Z. Du, J. Xia, Pharmacokinetic and pharmacodynamic study of triptolide-loaded liposome hydrogel patch under microneedles on rats with collagen-induced arthritis, Acta Pharm. Sin. B. 5 (2015) 569-576.
[160] H. Renz, K.J. Allen, S.H. Sicherer, H.A. Sampson, G. Lack, K. Beyer, H.C. Oettgen, Food allergy, Nat. Rev. Dis. Primers. 4 (2018) 1-20.
[161] R. Valenta, A. Karaulov, V. Niederberger, P. Gattinger, M. van Hage, S. Flicker, B. Linhart, R. Campana, M. Focke-Tejkl, M. Curin, Molecular aspects of allergens and allergy, in: Advances in immunology, Elsevier, 2018, pp. 195-256.
[162] S. Ito, S. Hirobe, Y. Kuwabara, M. Nagao, M. Saito, Y.-S. Quan, F. Kamiyama, T. Fujisawa, N. Okada, Immunogenicity of Milk Protein-Containing Hydrophilic Gel Patch for Epicutaneous Immunotherapy for Milk Allergy, Pharm. Res. 37 (2020) 35.

[163] J.N. Larsen, L. Broge, H. Jacobi, Allergy immunotherapy: the future of allergy treatment, Drug Discov. Today, 21 (2016) 26-37.
[164] A.K. Shakya, R.S. Ingrole, G. Joshi, M.J. Uddin, S. Anvari, C.M. Davis, H.S. Gill, Microneedles coated with peanut allergen enable desensitization of peanut sensitized mice, J Control Release, 314 (2019) 38-47.
[165] H.A. Sampson, W.G. Shreffler, W.H. Yang, G.L. Sussman, T.F. Brown-Whitehorn, K.C. Nadeau, A.S. Cheema, S.A. Leonard, J.A. Pongracic, C. Sauvage-Delebarre, Effect of varying doses of epicutaneous immunotherapy vs placebo on reaction to peanut protein exposure among patients with peanut sensitivity: a randomized clinical trial, Jama, 318 (2017) 1798-1809.
[166] Y. Yu, M.N.K. Kumar, M.X. Wu, Delivery of allergen powder for safe and effective epicutaneous immunotherapy, J. Allergy Clin. Immunol. 145 (2020) 597-609.
[167] N.L. Krupp, S. Sehra, J.E. Slaven, M.H. Kaplan, S. Gupta, R.S. Tepper, Increased prevalence of airway reactivity in children with eosinophilic esophagitis, Pediatr. Pulmonol. 51 (2016) 478-483.
[168] S.S. Possa, E.A. Leick, C.M. Prado, M.A. Martins, I.F.L.C. Tibério, Eosinophilic inflammation in allergic asthma, Front. Pharmacol. 4 (2013) 46.
[169] S.I. Wasserman, Mast cells and airway inflammation in asthma, Am. J. Respir. Crit. Care Med. 150 (1994) S39.
[170] C.A. Akdis, M. Akdis, Mechanisms of immune tolerance to allergens: role of IL-10 and Tregs, J. Clin. Investig. 124 (2014) 4678-4680.
[171] P.G. Holt, P.D. Sly, H.A. Sampson, P. Robinson, R. Loh, H. Lowenstein, A. Calatroni, P. Sayre, Prophylactic use of sublingual allergen immunotherapy in high-risk children: a pilot study, J. Allergy Clin. Immunol. 132 (2013) 991-993. e991.
[172] M.H. Sohn, Efficacy and safety of subcutaneous allergen immunotherapy for allergic rhinitis, Allergy Asthma Immunol. Res. 10 (2018) 1-3.
[173] A.K. Shakya, C.H. Lee, H.S. Gill, Microneedle-Mediated Allergen-Specific Immunotherapy for the Treatment of Airway Allergy in Mice, Mol. Pharm. 17 (2020) 3033-3042.
[174] A.K. Shakya, C.H. Lee, H.S. Gill, Coated microneedle-based cutaneous immunotherapy prevents Der p 1–induced airway allergy in mice, J. Allergy Clin. Immunol. 142 (2018) 2007-2011. e2003.
[175] A.K. Shakya, C.H. Lee, H.S. Gill, Cutaneous vaccination with coated microneedles prevents development of airway allergy, J Control Release, 265 (2017) 75-82.
[176] K.H. Park, E.Y. Oh, H. Han, J.D. Kim, S.J. Kim, K.Y. Jeong, J.H. Kim, C.O. Park, S.R. Kim, J.H. Lee, Efficacy of transdermal immunotherapy with biodegradable microneedle patches in a murine asthma model, Clin. Exp. Allergy, 50 (2020) 1084-1092.
[177] A.K. Shakya, H.S. Gill, A comparative study of microneedle-based cutaneous immunization with other conventional routes to assess feasibility of microneedles for allergy immunotherapy, Vaccine, 33 (2015) 4060-4064.
[178] A.K. Shakya, C.H. Lee, M.J. Uddin, H.S. Gill, Assessment of Th1/Th2 Bias of sting agonists coated on microneedles for possible use in skin allergen immunotherapy, Mol. Pharm. 15 (2018) 5437-5443.
[179] L. Spina, M. Weisskopf, S. von Moos, N. Graf, T.M. Kündig, G. Senti, Comparison of microneedles and adhesive-tape stripping in skin preparation for epicutaneous allergen delivery, Int. Arch. Allergy Immunol. 167 (2015) 103-109.

[180] J. Pielenhofer, J. Sohl, M. Windbergs, P. Langguth, M.P. Radsak, Current Progress in Particle-Based Systems for Transdermal Vaccine Delivery, Front. Immunol. 11 (2020) 266.
[181] N.M. van der Burg, A.C. Depelsenaire, M.L. Crichton, P. Kuo, S. Phipps, M.A. Kendall, A low inflammatory, Langerhans cell-targeted microprojection patch to deliver ovalbumin to the epidermis of mouse skin, J Control Release, 302 (2019) 190-200.
[182] M. Kermode, Unsafe injections in low-income country health settings: need for injection safety promotion to prevent the spread of blood-borne viruses, Health Promot. Int. 19 (2004) 95-103.
[183] Z. Li, Y. He, L. Deng, Z.-R. Zhang, Y. Lin, A fast-dissolving microneedle array loaded with chitosan nanoparticles to evoke systemic immune responses in mice, J. Mater. Chem. B, 8 (2020) 216-225.
[184] A.P. Raphael, T.W. Prow, M.L. Crichton, X. Chen, C.J. Fernando, M.A. Kendall, Targeted, needle-free vaccinations in skin using multilayered, densely-packed dissolving microprojection arrays, Small, 6 (2010) 1785-1793.
[185] S. Moon, Y. Wang, C. Edens, J.R. Gentsch, M.R. Prausnitz, B. Jiang, Dose sparing and enhanced immunogenicity of inactivated rotavirus vaccine administered by skin vaccination using a microneedle patch, Vaccine, 31 (2013) 3396-3402.
[186] P.C. DeMuth, J.J. Moon, H. Suh, P.T. Hammond, D.J. Irvine, Releasable layer-by-layer assembly of stabilized lipid nanocapsules on microneedles for enhanced transcutaneous vaccine delivery, ACS nano, 6 (2012) 8041-8051.
[187] A.V. Boopathy, A. Mandal, D.W. Kulp, S. Menis, N.R. Bennett, H.C. Watkins, W. Wang, J.T. Martin, N.T. Thai, Y. He, Enhancing humoral immunity via sustained-release implantable microneedle patch vaccination, Proc. Natl. Acad. Sci. U.S.A. 116 (2019) 16473-16478.
[188] Q. Yan, H. Liu, Z. Cheng, Y. Xue, Z. Cheng, X. Dai, W. Shan, F. Chen, Immunotherapeutic effect of BCG-polysaccharide nucleic acid powder on Mycobacterium tuberculosis-infected mice using microneedle patches, Drug Deliv. 24 (2017) 1648-1653.
[189] M.J. Mistilis, A.S. Bommarius, M.R. Prausnitz, Development of a thermostable microneedle patch for influenza vaccination, J. Pharm. Sci. 104 (2015) 740-749.
[190] J. Arya, M.R. Prausnitz, Microneedle patches for vaccination in developing countries, J Control Release, 240 (2016) 135-141.
[191] V. Bachy, C. Hervouet, P.D. Becker, L. Chorro, L.M. Carlin, S. Herath, T. Papagatsias, J.-B. Barbaroux, S.-J. Oh, A. Benlahrech, Langerin negative dendritic cells promote potent CD8+ T-cell priming by skin delivery of live adenovirus vaccine microneedle arrays, Proc. Natl. Acad. Sci. U.S.A. 110 (2013) 3041-3046.
[192] C. Edens, M.L. Collins, J.L. Goodson, P.A. Rota, M.R. Prausnitz, A microneedle patch containing measles vaccine is immunogenic in non-human primates, Vaccine, 33 (2015) 4712-4718.
[193] E. Kim, G. Erdos, S. Huang, T.W. Kenniston, S.C. Balmert, C.D. Carey, V.S. Raj, M.W. Epperly, W.B. Klimstra, B.L. Haagmans, Microneedle array delivered recombinant coronavirus vaccines: Immunogenicity and rapid translational development, EBioMedicine, (2020) 102743.
[194] K.J. McHugh, L. Jing, S.Y. Severt, M. Cruz, M. Sarmadi, H.S.N. Jayawardena, C.F. Perkinson, F. Larusson, S. Rose, S. Tomasic, Biocompatible near-infrared quantum dots delivered to the skin by microneedle patches record vaccination, Sci. Transl. Med. 11 (2019).
[195] L. Niu, L.Y. Chu, S.A. Burton, K.J. Hansen, J. Panyam, Intradermal delivery of vaccine nanoparticles using hollow microneedle array generates enhanced and balanced immune response, J Control Release, 294 (2019) 268-278.

[196] Q. Zhu, V.G. Zarnitsyn, L. Ye, Z. Wen, Y. Gao, L. Pan, I. Skountzou, H.S. Gill, M.R. Prausnitz, C. Yang, Immunization by vaccine-coated microneedle arrays protects against lethal influenza virus challenge, Proc. Natl. Acad. Sci. U.S.A. 106 (2009) 7968-7973.
[197] J.-H. Shin, J.-H. Lee, S.D. Jeong, J.-Y. Noh, H.W. Lee, C.-S. Song, Y.-C. Kim, C-di-GMP with influenza vaccine showed enhanced and shifted immune responses in microneedle vaccination in the skin, Drug Deliv. Transl. Res. (2020) 1-11.
[198] T.T. Nguyen, J.-a. Choi, J.S. Kim, H. Park, E. Yang, W.J. Lee, S.-K. Baek, M. Song, J.-H. Park, Skin immunization with third-generation hepatitis B surface antigen using microneedles, Vaccine, 37 (2019) 5954-5961.
[199] K. van der Maaden, E. Sekerdag, P. Schipper, G. Kersten, W. Jiskoot, J. Bouwstra, Layer-by-layer assembly of inactivated poliovirus and N-trimethyl chitosan on pH-sensitive microneedles for dermal vaccination, Langmuir, 31 (2015) 8654-8660.
[200] S.P. Sullivan, D.G. Koutsonanos, M. del Pilar Martin, J.W. Lee, V. Zarnitsyn, S.-O. Choi, N. Murthy, R.W. Compans, I. Skountzou, M.R. Prausnitz, Dissolving polymer microneedle patches for influenza vaccination, Nat. Med. 16 (2010) 915.
[201] G. Erdos, S.C. Balmert, C.D. Carey, G.D. Falo, N.A. Patel, J. Zhang, A. Gambotto, E. Korkmaz, L.D. Falo Jr, Improved cutaneous genetic immunization by microneedle array delivery of an adjuvanted adenovirus vaccine, J. Invest. Dermatol, 140 (2020) 2528–2531.e2.
[202] Y. Pastor, E. Larrañeta, Á. Erhard, G. Quincoces, I. Peñuelas, J.M. Irache, R. Donnelly, C. Gamazo, Dissolving Microneedles for Intradermal Vaccination against Shigellosis, Vaccines, 7 (2019) 159.
[203] D.D. Zhu, X.L. Wang, X.P. Zhang, J.J. Ma, D.L. Kong, M.M. Zhang, X.D. Guo, C. Wang, A Dissolvable Microneedle Formulation of Bordetella pertussis Subunit Vaccine: Translational Development and Immunological Evaluation in Mice, ACS Appl. Bio Mater. 2 (2019) 5053-5061.
[204] Y.-C. Chen, S.-J. Chen, H.-F. Cheng, M.-K. Yeh, Development of Yersinia pestis F1 antigen-loaded liposome vaccine against plague using microneedles as a delivery system, J Drug Deliv Sci Technol, 55 (2020) 101143.
[205] T. Guo, N. Cheng, J. Zhao, X. Hou, Y. Zhang, N. Feng, Novel nanostructured lipid carriers-loaded dissolving microneedles for controlled local administration of aconitine, Int. J. Pharm. 572 (2019) 118741.
[206] J. Ye, H. Huang, G. Luo, L. Yin, B. Li, S. Chen, H. Li, Y. Yang, X. Yang, NB-UVB irradiation attenuates inflammatory response in psoriasis, Dermatol Ther.33 (2020) e13626.
[207] S.K. Mahil, F. Capon, J.N. Barker, Update on psoriasis immunopathogenesis and targeted immunotherapy, in: Seminars in immunopathology, Springer, 2016, pp. 11-27.
[208] S.N. Bodkhe, R. Kale, K. Biyani, A Review of Microneedles–Elevation to TDDS Approach and Function in Management of Psoriasis, AJPRD, 8 (2020) 114-122.
[209] A.M. Rodgers, A.S. Cordeiro, A. Kissenpfennig, R.F. Donnelly, Microneedle arrays for vaccine delivery: the possibilities, challenges and use of nanoparticles as a combinatorial approach for enhanced vaccine immunogenicity, Expert Opin Drug Deliv. 15 (2018) 851-867.
[210] H. Du, P. Liu, J. Zhu, J. Lan, Y. Li, L. Zhang, J. Zhu, J. Tao, Hyaluronic acid-based dissolving microneedle patch loaded with methotrexate for improved treatment of psoriasis, ACS Appl. Mater.Interfaces, 11 (2019) 43588-43598.
[211] E. Korkmaz, E.E. Friedrich, M.H. Ramadan, G. Erdos, A.R. Mathers, O.B. Ozdoganlar, N.R. Washburn, L.D. Falo Jr, Therapeutic intradermal delivery of tumor necrosis factor-alpha antibodies using tip-loaded dissolvable microneedle arrays, Acta Biomater. 24 (2015) 96-105.

[212] E. Korkmaz, E.E. Friedrich, M.H. Ramadan, G. Erdos, A.R. Mathers, O.B. Ozdoganlar, N.R. Washburn, L.D. Falo Jr, Tip-loaded dissolvable microneedle arrays effectively deliver polymer-conjugated antibody inhibitors of tumor-necrosis-factor-alpha into human skin, J. Pharm. Sci. 105 (2016) 3453-3457.
[213] H.-J. Lim, Y.-D. Jeon, S.-H. Kang, M.-K. Shin, K.-M. Lee, S.-E. Jung, J.-Y. Cha, H.-Y. Lee, B.-R. Kim, S.-W. Hwang, Inhibitory effects of Euphorbia supina on Propionibacterium acnes-induced skin inflammation in vitro and in vivo, BMC Compl Alternative Med, 18 (2018) 263.
[214] L.-T. Chuang, T.-H. Tsai, T.-J. Lien, W.-C. Huang, J.-J. Liu, H. Chang, M.-L. Chang, P.-J. Tsai, Ethanolic extract of origanum vulgare suppresses propionibacterium acnes-induced inflammatory responses in human monocyte and mouse ear edema models, Molecules, 23 (2018) 1987.
[215] S.H. Lee, M.K. Gupta, J.B. Bang, H. Bae, H.J. Sung, Current progress in reactive oxygen species (ROS)-responsive materials for biomedical applications, Adv. Healthcare Mater. 2 (2013) 908-915.
[216] Y. Zhang, P. Feng, J. Yu, J. Yang, J. Zhao, J. Wang, Q. Shen, Z. Gu, ROS-Responsive Microneedle Patch for Acne Vulgaris Treatment, Adv. Ther. 1 (2018) 1800035.
[217] T. Zhang, B. Sun, J. Guo, M. Wang, H. Cui, N. Mao, B. Wang, F. Yan, Active pharmaceutical ingredient poly (ionic liquid)-based microneedles for the treatment of skin acne infection, Acta Biomater. 115 (2020) 136-147.
[218] J.E. Kim, J.S. Kim, D.H. Cho, H.J. Park, Molecular mechanisms of cutaneous inflammatory disorder: atopic dermatitis, Int. J. Mol. Sci. 17 (2016) 1234.
[219] T. Werfel, J.-P. Allam, T. Biedermann, K. Eyerich, S. Gilles, E. Guttman-Yassky, W. Hoetzenecker, E. Knol, H.-U. Simon, A. Wollenberg, Cellular and molecular immunologic mechanisms in patients with atopic dermatitis, J. Allergy Clin. Immunol. 138 (2016) 336-349.
[220] S.H. Park, J.E. An, S. Jang, J.Y. Kim, J.W. Lee, H.K. Kim, Gardenia jasminoides extract without crocin improved atopic dermatitis-like skin lesions via suppression of Th2-related cytokines in Dfe-induced NC/Nga mice, Journal of ethnopharmacology, 241 (2019) 112015.
[221] H.-Y. Jang, J.-H. Koo, S.-M. Lee, B.-H. Park, Atopic dermatitis-like skin lesions are suppressed in fat-1 transgenic mice through the inhibition of inflammasomes, Exp. Mol. Med. 50 (2018) 1-9.
[222] K. Amin, The role of mast cells in allergic inflammation, Respir. Med. 106 (2012) 9-14.
[223] M.-C. Chen, C.-S. Chen, Y.-W. Wu, Y.-Y. Yang, Poly-γ-Glutamate microneedles as transdermal immunomodulators for ameliorating atopic dermatitis-like skin lesions in Nc/Nga mice, Acta Biomater. 114 (2020) 183-192.
[224] J.H. Kim, J.U. Shin, S.H. Kim, J.Y. Noh, H.R. Kim, J. Lee, H. Chu, K.Y. Jeong, K.H. Park, J.D. Kim, Successful transdermal allergen delivery and allergen-specific immunotherapy using biodegradable microneedle patches, Biomaterials, 150 (2018) 38-48.
[225] A. Gutiérrez-Fernández, M. Inada, M. Balbín, A. Fueyo, A.S. Pitiot, A. Astudillo, K. Hirose, M. Hirata, S.D. Shapiro, A. Noël, Increased inflammation delays wound healing in mice deficient in collagenase-2 (MMP-8), FASEB J. 21 (2007) 2580-2591.
[226] E.Y. Jeon, J. Lee, B.J. Kim, K.I. Joo, K.H. Kim, G. Lim, H.J. Cha, Bio-inspired swellable hydrogel-forming double-layered adhesive microneedle protein patch for regenerative internal/external surgical closure, Biomaterials, 222 (2019) 119439.
[227] B. Gao, M. Guo, K. Lyu, T. Chu, B. He, Intelligent Silk Fibroin Based Microneedle Dressing (i-SMD), Adv. Funct. Mater. (2020) 2006839.

Table 1. A summary of various materials used into the structure of MNs towards immunotherapy, as well as a comparison of their advantages and limitations.

Category	Material	Fabrication methods	Advantages	Limitations	Ref.
Silicon MNs	Silicon	Wet etch technology	- Ability for coating of the viable virus in a dry form around the shaft of needles - Elimination of cold chain storage	----	[37]
	Silicon	Wet etch technology	- Successful delivery of liquid vaccinia virus Ankara (MVA) vaccine - Eliminating the skin inflammatory response	-----	[38]
	Silicon	Wet etch technology	Decreasing the anti-vector antibody response	------	[39]
	Silicon	-Photolithography -Thin-film deposition - Microelectromechanical systems (MEMS)	Easily fabrication using existing MEMS technologies	Easy breaking and subsequent creation of biohazardous waste	[40]
	Silicon	-----	- Capability of surface decoration of silicon with pH-sensitive groups towards burst release of antigen within 15s	Suitability for delivering only ovalbumin (OVA) antigen (no for all the antigens)	[41]
	Silicon	------	------	-Lack of FDA approval for silicon - Requiring extensive processing and clean-room facilities for fabricating silicon MNs	[42]
Metal MNs	- Stainless steel - Titanium	- Micromachining - Laser ablation -Photochemical etching	Adequate mechanical strength for penetration into the skin	Possibility of creating a potential biohazardous waste	[40]
	Stainless steel	----------	Capability for creating the nano-patterning on the surface of stainless MNs	Poor coating efficiency of DNA-based immunotherapeutic agents owing to low hydrophilic nature of stainless steel	[43]
	Stainless steel	Laser cutting	Cost-effective and FDA approval for stainless MNs	-----	[44]

	Titanium	Lithographic masking followed by wet etching	Facile adsorption of Vaccine to the titanium surface via electrostatic/hydrophobic interactions due to high dielectric constant (ε ~ 114) and isoelectric point (3.5–6.7) of titanium oxide	------	[45]
Ceramic MNs	Alpha calcium sulfate hemihydrate	Micromolding process	Higher mechanical strength and better stability at high temperature and humidity than most polymeric MNs	Possibility of contamination during production and risk of microbial spoilage	[46]
	- β-Tricalcium phosphate ($Ca_3(PO_4)_2$) - Monocalcium phosphate monohydrate ($Ca(H_2PO_4)_2 \cdot H_2O$) - Calcium sulfate alpha hemihydrates ($CaSO_4 \cdot 0.5H_2O$)	Micromolding process	Capability for controlling drug release by changing the bulk surface area, porosity and resorbability of the ceramics	Low drug loading capability	[47]
	Al_2O_3	Micromolding process	Capability for creating nanoporous MNs for both delivery of substances, and the extraction of compounds	----	[48]
	- Alumina - Alpha calcium sulfate hemihydrate	- Micromolding process - Sintering technique	- Good in vivo resorbability (micromolding process) - Adjustable porosity	Non-resorbability of sintered ceramic MNs	[49]
	Alumina	- Sintering technique	good mechanical strength in comparison with monocrystalline silicon	Poor loading efficiency for thermo-labile medications into sintered ceramic MNs due to the high temperature treatment during the fabrication process	[50]
	polyvinylpyrrolidone (PVP)	Soft lithography	Highly water solubility, high tensile strength, and FDA approval of PVP	-----	[51]
	PVP	Micromolding process	safely clearance of PVP via the kidneys within a few days	----	[52]
	PVP	Micromolding process	Low likelihood of RNase contamination of PVP	-Poor solubility of mRNA vaccine in	[53]

				concentrated PVP solutions - Inhibitory effect of concentrated PVP solutions on mRNA transfection due to steric hindrance.	
	PVP	In situ micromolding process	Good mechanical strength of PVP due to the presence of a ring in the chemical backbone structure of the vinyl pyrrolidone monomer		[32]
dissolvable Polymeric MNs	PVP	Micromolding process	-----	Possibility for the DNA vaccine degradation in PVP matrices	[54]
	PVP/ dextran	two-step molding process	the adjuvant effects of PVP and dextran	-----	[55]
	hyaluronan	Micromolding process	FDA approval and biodegradability of hyaluronan	Possibility for insoluble particle formation and entrapment of vaccine antigens into them during MN preparation	[56]
	chitosan	Micromolding process	- Excellent biodegradability - Noncytotoxicity - Ability of chitosan for improving both humoral and cell-mediated immune responses - creating an antigen depot by the viscous chitosan solution	- Requiring supporting arrays for insertion owing to weak mechanical strength of chitosan	[57]
	Gantrez	Micromolding process	Highly water solubility and biodegradability of Gantrez	----	[58]
	Trehalose and sodium carboxymethyl cellulose (CMC)	Theraject's microneedle technology	-------	The difficulty of analysis of the samples by single radial immunodiffusion (SRID) with increasing the viscosity of Trehalose and sodium carboxymethyl cellulose	[59]
	Trehalose and CMC		- FDA approval for both trehalose and CMC - Increasing antigen stability by trehalose - water-solubility and mechanical strength of CMC	-------	[60]

	CMC and amylopectin	Micromolding process	---	Producing deformed microneedles with weak mechanical strength at high viscosity of CMC	[61]
	Sodium Alginate	Micromold casting technique	- Adjuvant properties of sodium alginate - Good biocompatibility and biodegradability - Utilizing sodium alginate as a permeation enhancer	----	[62]
	Sodium Alginate	Spin-casting approach	----	Less physical robustness than biodegradable polylactic-co-glycolic acid MN	[63]
	Silk fibroin /poly(acrylic acid)	Micromolding process	- Good Biocompatibility and Biodegradability of silk fibroin - Simple one-step process for loading antigens in silk protein matrices - Facile stabilization of immunotherapeutic agents and vaccines in silk at room temperature for more than two months - Rapid dissolution of PPA in the skin - Sustained vaccine release from silk protein matrices (over 1–2 weeks)	- The high brittleness of silk fibroin	[33]
	poly(lactide-coglycolide) (PLGA)/PPA	Micromolding process	- Rapid dissolution of PPA in the skin - Adjustable sustained release of encapsulated vaccines based on the PLGA molecular weight	- Complexity of the vaccine loading process in PLGA polymer	[64]
	Carboxymethylcellulose and trehalose as coating	Dip-coating	- Improving antigen stability during drying by trehalose disaccharide - Improving the retention of Hemagglutination activity of influenza vaccine after drying by trehalose	Loss of Hemagglutination (HA) activity at high concentrations of CMC (1wt%)	[24]
	Carboxymethylcellulose and trehalose as coating	Dip-coating	---	Increasing trehalose crystallization and vaccine separation from the trehalose crystal matrix during crystallization result in	[65]

				denaturation of antigenic proteins	
Coated MNs	Carboxymethylcellulose and trehalose as coating	Dip-coating	Reducing virus aggregation at 3% concentration of trehalose	Reduced delivery efficiency of the inactivated virus at a high concentration of trehalose	[66]
	Poly(o-nitrobenzyl-methacrylate-comethylmethacrylate-copoly(ethylene-glycol)-methacrylate) (PNMP)/ polyelectrolyte multilayers as coating	Layer by layer assembly	- Ability for the preparation of bioresponsive MNs due to photo-sensitive and pH-responsive properties of PNMP polymer - Delivery of antigens in a sustained manner after photoswitching PNMP polymer through ultraviolet irradiation (254 nm, 2.25 mW cm^{-2}) for 15 min during coating	The need for reformulation of vaccine components for their coating	[67]

Highlights

- Microneedles are promising devices for painless drug delivery with high bioavailability.
- Transdermal microneedle can improve the biological effect of drugs through adjustable drug release.
- Facile fabrication and versatility have caused high attraction towards microneedle-based drug delivery.
- Microneedles are suggested for immunotherapy due to the high abundance of immune cells under the skin.